UTRECHT UNIVERSITY, FACULTY OF GEOSCIENCES

The effects of river regulation on global river flood risk assessments

---

A study in the Mississippi River Watershed

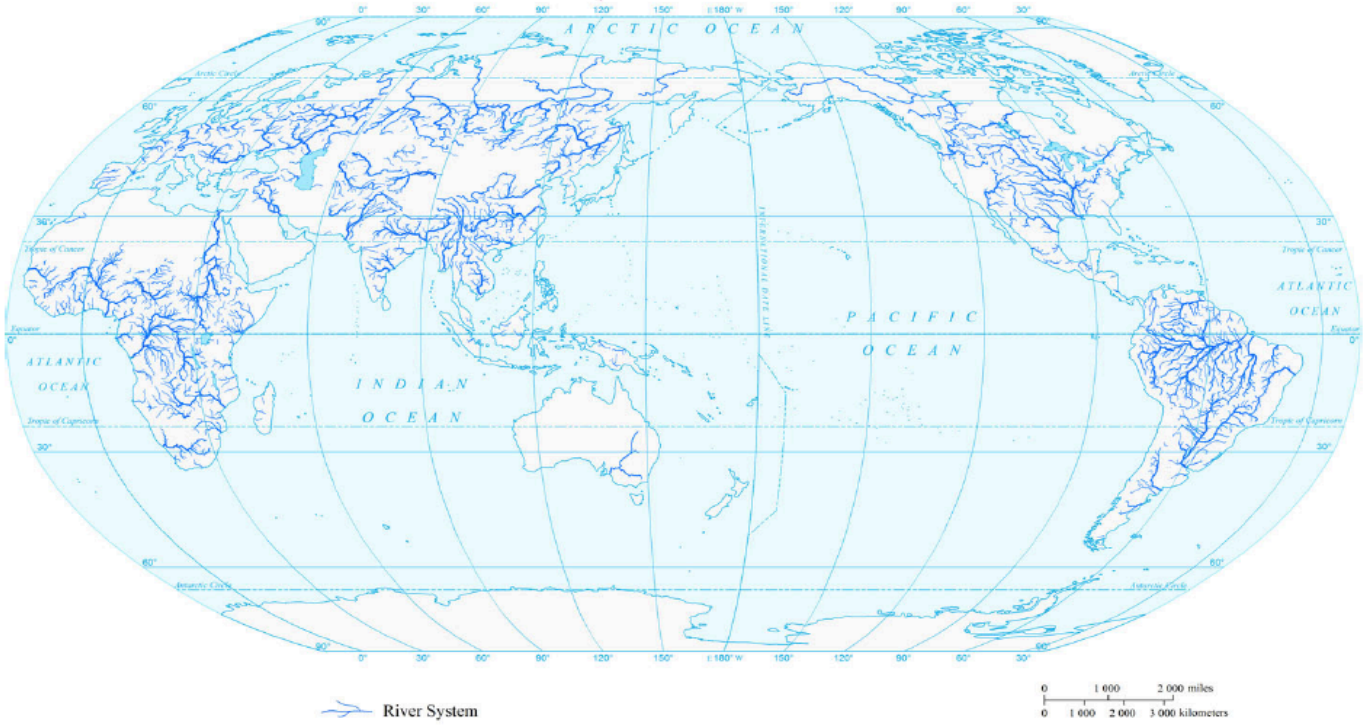

K. Mooij

The effects of river regulation on global river flood risk assessments – A study in the Mississippi River Watershed

Master of Science Thesis

Koen Mooij

Water Science and Management

Earth Sciences

30 ECTs

October 27th 2015

Cover Photo: World Atlas of Natural Disaster Risk by P. Shi and R. Kasperson

Supervision:

Dr. L. P. H. van Beek – Utrecht University

Dr. Ir. R. J. van der Ent – Witteveen+Bos

Witteveen+Bos

Universiteit Utrecht

Preface

This report is the final product of my Master Water Science and Management at the Utrecht University. The actual study started on the 6th of April and after 6 months I finally finished it. This means that from primary school until the end of my Master I have been a "student" for a period of 7.158 days (including a 1-year sabbatical). Naturally, I am better in the practical side of work and study and therefore the past two years at the University of Utrecht were a challenge after my more practical study bachelor "Watermanagement" at the University of Applied Sciences in Rotterdam. This thesis was an interesting study for finishing my Master and therefore I want to thank Witteveen+Bos for providing me the opportunity to work on this.

Additionally, I would like to thank my supervisors Ruud van der Ent and Rens van Beek for making time in their busy schedules and their vacation periods to guide me and answer my questions. Rens van Beek helped me a lot with his ideas about this study and with understanding the processes in PCR-GLOBWB and Ruud van der Ent of Witteveen+Bos helped me during the thesis by giving me ideas, discussing all kinds of matters related to this study and provided me useful feedback. In addition, I want to thank my unofficial supervisor Edwin Sutanudjaja for helping me with understanding PCR-GLOBWB and my brother Bart Mooij for providing ideas about analyzing the final data outcomes.

This thesis is a way to show my close friends what I was actually doing in the past years, instead of becoming a millionaire by designing large waterslides. Furthermore, I want to thank my girlfriend for being interested and for providing me shelter in the last difficult financial period of a student ;). Finally, I am very grateful that my parents and little brother have supported me over the years and showed interest in the different subjects I was dealing with.

I hope you find it an interesting study.

Koen Mooij

Rotterdam, October 27th 2015

Abstract

Due to large worldwide economic losses due to flooding and the lack of data in developing countries global river flood risk assessments are developed to be able to estimate the potential economic risk of floods. The potential impacts of these assessments are based on Global Hydrological Models (GHMs), which are being used in studies related to land surface hydrology.

In this study the GHM PCRaster GLOBal Water Balance model (PCR-GLOBWB) is used, which is already successfully used in riverine flood assessments. However, river regulation (dikes and floodways) is not yet explicitly included in the model. Other studies included dikes implicitly by neglecting flooding for certain return periods. This is mainly because PCR-GLOBWB operates on a much larger scale than required for accurately including dikes or floodways. As a case the Mississippi watershed is used to analyze the impact of including dike heights from the National Levee Database of the U.S. Army Corps of Engineers by pre-processing the channel dimensions and therewith the channel capacity. The response of the model to the changes in channel capacity due to increasing dike heights and the inclusion of floodplains and the response to floodways is analyzed during this study.

The model was tested for several flood events in the period between 1980 and 2010, to allow for a comparison between the modeled discharges from PCR-GLOBWB and observed discharges from the Global Runoff Data Centre (GRDC). The comparison shows that peak discharges are reproduced correctly, but in the overall pattern larger gaps occur between modeled and simulated discharges. This results from the differences in reproducing floods and droughts with PCR-GLOBWB. The influence of the Manning coefficient is mainly noticeable in the height of peak discharges, since peaks reduce as the Manning coefficient increases. This effect becomes larges as the width and depth of the channel increase. Besides the effects on the height of the peak, it also results in a shift of the peak over time, in terms of a few days. The Manning coefficient increases in this study since the capacity of the channel and the floodplains are combined and therewith only one Manning coefficient can be used.

Two different methods are used to translate the flood outcomes of the PCR-GLOBWB model to economic damage. The urban damage method is based on a depth-damage relationship, which is applied on a total GDP distribution based on nightlight intensity. The agricultural damage method is based on a duration-damage relationship that is applied on the most common crop, soybeans. Based on the average price per bushel, bushel per ha, vegetation fraction and month of flooding the economic damage is determined. The two methods have large differences between them due to the fact that there are significant differences in the way economic values are determined. The simulated economic damage is validated by comparing it with observed damage from the international disaster database, EM-DAT. Results show large differences between simulated and observed economic damages. This is the result of errors from the global hydrological model and therefore, despite large uncertainties in economic damage methods, the focus for further studies is improving the hydrological model.

Overall, it can be concluded that the impact of including river regulation on extreme river discharges is small, when considering an increasing Manning coefficient. However, the impact on flooding is large and therewith it has a considerable impact on resulting damages.

Contents

List of Figures

1 Introduction

1.1 Background

Over the last decades, the number of fatalities and economic damage caused by river floods worldwide has increased considerably. In the Global Assessment Report on Disaster Risk Reduction of 2015 The United Nations Office for Disaster Risk Reduction (UNISDR) mentioned that the economic losses from natural hazards such as cyclones, earthquakes, tsunamis and flooding reached an average between $250-300 billion each year and are expected to increase to $314 billion in the built environment alone (UNISDR, 2015). Average annual global economic losses due to river flooding represent a third of the total amount, $104 billion. Flood risk is determined based on probability that a flood occurs, the exposure and vulnerability. UNISDR defines flood risk as the combination of the probability of a flood and its negative consequences, where negative consequences are described by exposure and vulnerability. Exposure refers to people, property, systems or other elements present in flood zones that are thereby subject to potential losses and vulnerability refers to the characteristics and circumstances of a community, system or asset that makes it susceptible to the damaging effects of a flood. Furthermore, international loss databases with global coverage show an increase in reported flood disasters and flood losses through time (Kundzewicz et al., 2013). Besides the large economic losses, floods affect more people worldwide than any other hazard. A new analysis of the World Resources Institute (WRI) shows that on average 21 million people are affected by river flooding each year and that these numbers could increase to 54 million in 2030, due to socio-economic development and climate change (Luo et al., 2015).

Possible flood protection measures to invest in are increasing dike heights or creating floodways along the river. The Netherlands is an example of a country that has made major investments in dikes. This led to low exceedance probabilities and therewith the flood risk has been reduced. However, high quality flood defenses might encourage further development of floodplains and flood-prone areas. This could results in devastating consequences if a flood exceeds the threshold level. Furthermore, the consequences of measures for down- and upstream areas should also be considered. Conflicts might arise when upstream countries reduce their risk to flooding, while the risk in downstream areas increases. Floodways are used to diverse the water flow and therewith reduce the discharge in downstream areas. Therewith, the impact of downstream areas is being reduced. However, due to the diversion of water, other areas will be affected and therefore a trade-off has to be made between the different impacts. Mostly, floodwaters are diverted away from urban areas to less developed lands, such as agricultural lands.

1.1.1 Previous flood regulation studies

The Joint Research Centre (JRC) used the LISFLOOD model (Van der Knijff & de Roo, 2008), which simulates hydrological processes in large European river basins, to analyze the impacts of reservoirs, dike-breaks, dike-shifts and retentions polders during Elbe Flood in 2002 (Gierk & de Roo, 2008). Changes in water storage in two reservoirs (Bleiloch and Hohenwarte reservoir) resulted in a minimal impact (-4-8 m^3/s, with $25*10^6$ m^3 extra storage) on the discharge in the river Elbe. However, excluding and including the Vltava cascade, Czech Republic, resulted in a reduction between 84 and 171 m^3/s in the German part of the river Elbe. The exclusion of dike-breaks resulted in 2.6-9.1% higher peak discharges with the largest increase in downstream areas. Including planned dike-shifts would have resulted in a decrease of 1.3-4.6% (58-202 m^3/s) and including both dike-shifts and retention polders would have resulted in a decrease of 3.9-10.8% (178-469 m^3/s). However, the impact of these measures also depends on the flood characteristics. During the flood in spring 2006 the flood wave was

longer, but less extreme in maximum peak. The impact of the latter scenario on the flood in 2006 was considerably lower (1.2-3.3%, 31-121 m^3/s).

1.1.2 Previous economic impact studies

The quantitative assessment of flood damage models of Jongman et al. (2012) showed that model outcomes are very sensitive to uncertainties in both exposure and vulnerability. In their research exposure was expressed in asset values and vulnerability in depth-damage functions. Depth-damage functions describe the mathematical relationship between the total damage of an asset with increasing inundation depth. Furthermore, sensitivity analysis of Jongman et al. (2012) and de Moel et al. (2012) shows that uncertainties in depth-damage functions have a larger impact on damage estimates compared to uncertainty in exposure and applied maximum damage values.

In most risk assessments the estimation of assets is not explained, which might be caused by the fact that no quantitative risk indicators are used or because absolute damage functions are used (Merz et al., 2010). Jongman et al. (2012) used two methods to be able to estimate global exposure to river flooding. The first method is based on population and the second method is based on land use. In the population method exposure is determined based on the population living within in the flood hazard areas. The exposed assets are a function of exposed population and GDP per capita, multiplied by a factor 5. They assume that GDP per capita is homogenous within a country and therefore this method should only be applied on larger scales. In the land-use method a distinction is made between different types of land use within the flood prone area and based on depth-damage functions per type of land use the maximum damage per unit or surface area is determined. Also, in their method a uniform value of all exposed urban area in a country is chosen, but in reality this would depend on several factors, such as land use function and economic activity (Merz et al., 2010).

Vulnerability is the degree of loss to a community, system or asset at risk resulting from a flood of a given magnitude, where 0% is no damage and 100% is total loss. Damage due to flooding depends on several factors, such as water depth, duration of flooding, flow velocity, sediment concentration, pollution, the existence of a flood warning system and the effectiveness of emergency responses (Merz et al., 2010; Pistrika et al., 2014). Most studies only focuses on the relation between damage to buildings and floodwater depth. Therefore, the method of depth-damage functions is mainly used to estimate direct tangible flood damage. Direct damage is described as damage that occurs due to physical contact of floodwater with humans, property or any other objects. Tangible damage is described as damage to manmade capital or resource flows which can be easily specified in monetary terms, e.g. private buildings and contents and destruction of harvest (Merz et al., 2010). However, depth-damage functions differ per type of building or type of land use and also per region or country (Jongman et al., 2012). Therefore, local information is required to adjust depth-damage functions per area, but this is a time consuming process. Also, Bremond et al. (2013) noted that the duration of flooding is a necessary parameter in determining the agricultural losses and in the HAZUS-MH flood loss estimation methodology (Scawthorn et al., 2006) only the timing and duration of flooding is taken into account to determine the agricultural losses and inundation depth is excluded.

1.2 Problem description

Due to large worldwide economic annual losses as a result of flooding, the large size of watersheds and the lack of data in developing countries global river flood risk assessments are developed to be able to estimate the potential economic risk of floods (Winsemius et al, 2013). Based on these findings, International Financial Institutions (IFIs), such as the World Bank, can prioritize areas that require investments in reducing flood risk.

Global river flood risk assessments consist of different parts, i.e. global meteorological forcing datasets, a global hydrological model (GHM), a global flood routing model and an impact model. The explosion of global data availability from satellites in the last two decades has had an positive influence on meteorological data in GHMs (Tang et al., 2009). Currently, most of the variables, e.g. precipitation, evapotranspiration, snow and ice, soil moisture and terrestrial water storage variations, are now observable at varying spatial and temporal resolutions and accuracy. GHMs are used to simulate land surface dynamics of the hydrological cycle on a global scale, in which they mainly focus on modeling the terrestrial hydrological processes, runoff and streamflow. Global flood routing models are used to predict changes in the shape of flood waves as it moves through a channel. Results can be used to predict flooding and determine flood protection levels. Impact models use the results of GHMs to predict the damage that will occur during an event based on exposure and vulnerability. Where, vulnerability is described with depth-damage or duration-damage functions. These functions describe the mathematical relationship between floodwater depth or duration of the flood and the damage to e.g. buildings and crops. Based on the outcomes of both GHMs and impact models organizations can prioritize investments.

Section 1.1 described the importance of dikes and floodways along rivers with respect to reducing the flood risk. Not including dikes and floodways might have resulted in higher economic losses than expected. Also, difference in dike height might result in variety of protection levels along rivers and therewith different locations of flooding and different types of damage (USACE, 2014c). In current assessments dikes are not included explicitly, but instead they included dikes implicitly by neglecting flooding for certain return periods. However, the spatial resolution of GHMs is based on the available global climatological input data. The data is available on a low spatial resolution (e.g. 30 arc-min, approximately 50*50 km) and therefore GHMs are mainly used in global-scale studies and are not recommended in basin-scale studies. On the other hand, some databases of dike-heights have a high resolution and thus a problem arises when including them in GHMs.

1.3 Research aim and questions

The aim of this research is to include flood regulation measures and evaluate its impact on the outcomes of global river flood risk assessments. In this study the implementation of dikes and floodways will be considered as flood regulation measures. The outcome of this study may serve as an improvement of the current risk assessments and therewith it supports international decision-making in disaster management and it could support the development of informed adaptation strategies. The **PCR**aster **GLOB**al **W**ater **B**alance model (PCR-GLOBWB) (Van Beek & Bierkens, 2008) will be used to model scenarios with each different type of river regulation measures and the impact method used in the **Clim**ate **ada**ptation model (Climada) (Bresch, 2015) will be used to determine the economic losses in these scenarios. The method in Climada is used for determining economic exposure, because it uses a different approach compared to the framework of Winsemius et al. (2013), section 1.1.2. The method in Climada uses nightlight intensity, instead of population density or land use, to determine exposure. This can be used to determine if this method could give a better estimate of economic damage compared to currently used methods (WRI, 2015).

The main research question of this thesis is:

What are the impacts of taking into account dikes as flood protection standards on extreme river discharges and the resulting damages in global river flood risk assessments?

Different sub-questions are formulated to be able to give answer on the main question:

- What are the impacts of river regulation on discharge and flooding in global hydrological modeling?
    - How does river regulation influence discharge and flood wave propagation?
    - How does river regulation influence flooding in terms of flood extent, flood depth and time of occurrence?
    - Does the inclusion of river regulation improve the model performance in reproducing discharge (GRDC), compared to the original settings?
- How does river regulation influence expected damage?
    - What is the difference in economic damage, while including river regulation, based on the method used in Climada?
    - What is the difference in expected damage between urban flooding (depth-damage functions) and agricultural flooding (duration-damage functions)?
    - To what extent can historical economic damages (EM-DAT) be reproduced with the method used in Climada?

1.4 Outline Thesis

In Chapter 2 a description of the study area the Mississippi watershed is presented. Here, the main characteristics and information about the area is shown. Chapter 3 describes the methodology and data that have been used during the study. The chapter starts with a description of the PCR-GLOBWB model, followed by the Climada model. Moreover, a description of the different scenarios given and the chapter ends with the data that has been used to validate the results of the model. The results of the different scenarios are treated in Chapter 4. The report ends with a discussion and conclusion in chapter 5 and 6.

2 Study Area: Mississippi River

In this study floods in the Mississippi watershed are analysed, because of the available data of dikes and damage functions. Because the Mississippi watershed is of a large size, a conceptual and parsimonious model such as a GHM is required and in order to simulate the propagation of the floodwave truthfully information on dike heights and channel and floodplain properties are required. Although a wealth of data for the Mississippi can be found in publicly accessible sources, these data still require interpretation and processing before meaningful results can be obtained and the impact of floods assessed. The Mississippi allows one to analyse this processes in detail and formulate procedures and recommendations that will be advantageous when applying the model to this end in data poor environments where information is urgently required to design informed adaptation strategies.

2.1 Introduction

The Mississippi River watershed is located in the North America and it drains parts of 31 states in the U.S. and 2 Canadian provinces and totals 3.28 million km^2 (Cai et al., 2014) (Figure 1). The river is about 3.766 km long from its source to the Gulf of Mexico (Kammerer, 1990) and in combination with the Missouri River it has a total length of approximately 5.970 km, which makes it one of the longest rivers in the world (Leopold, 1994). The source of the Mississippi River starts at Lake Itasca, Minnesota, at an elevation of 450 m above sea level and it falls to 220 meter below the Saint Anthony Falls, Minneapolis, and it ends in the Gulf of Mexico just below New Orleans (New World Encyclopedia, 2014). The average discharge of the Mississippi River together with its largest distributary, the Atchafalaya River (Figure 5), is equal to 18.392 m^3/s (Meade, 1995).

Figure 1. Mississippi watershed with gauging stations of the Global Runoff Data Centre (National Park Service, 2015)

The Mississippi River watershed covers multiple climate zones, which influences both timing and amounts of runoff. In the eastern half of the watershed a humid subtropical climate generates large amounts of runoff over the Tennessee, Ohio and Mississippi River. From north to south in the center there are sub humid regions that are

neither fully humid nor semiarid and to the west semiarid climates arise in the Great Plains and an alpine climate prevails in the Rocky Mountains (Severin et al., 2015). Across the climate zones a large temperature gradient occurs between north and south. A minimum average of -3°C in the Rocky Mountains and a maximum average in the most southern area of 22.9°C (Cai et al., 2014). In the southern part in the Appalachian Mountains and the Gulf Coast annual average precipitation values range between 1.5 m/year or more to 0.25-0.38 m/year in the westernmost regions and annual rates of evaporation vary between 0.60-0.75 m/year in the north to 1.5 m/year in the south (National Research Council, 2008).

2.2 Land Use

In this study the differences between the economic impact of riverine flooding on urban areas and agricultural businesses will be analyzed. Therefore, the different types of land use are described in this section.

In the Mississippi watershed the land use is drastically converted from the former riparian forests to primarily agriculture (USGS, 2010). Over the years more than 75% of riparian forest has been converted and nowadays forests and croplands are the most common type of land use in the Mississippi watershed (Figure 2).

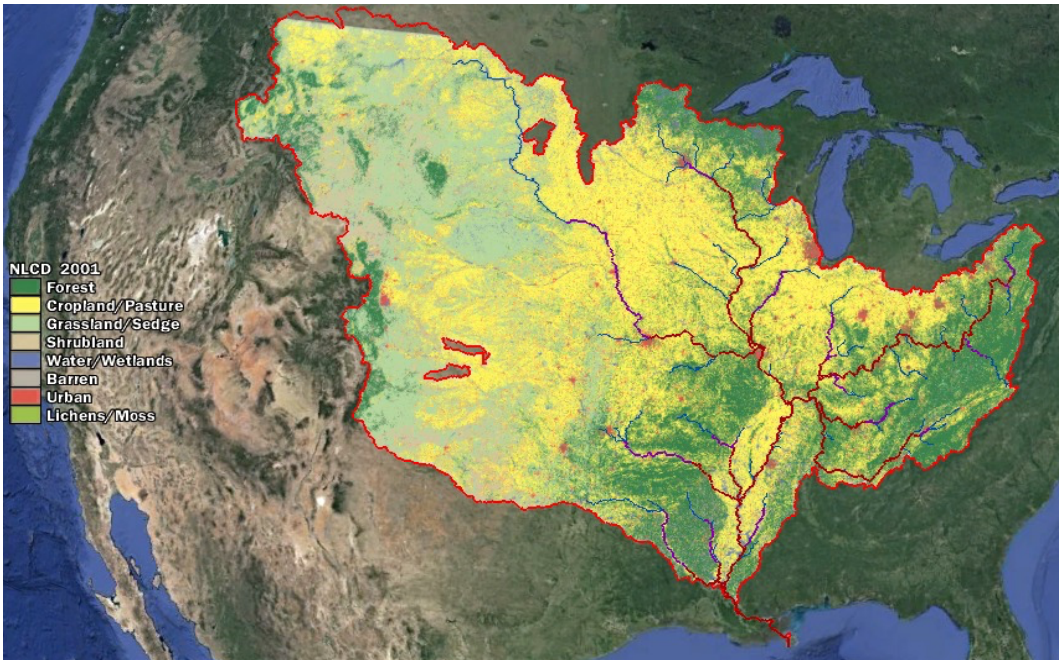

Figure 2. Geographic extent, land use and land cover of the Mississippi watershed in 2001, retrieved from USGS and Google Earth (USGS, 2010)

The three most valuable commodities are in the first place poultry, followed by forestry and soybean crops (Coblentz, 2014). Soybeans are the most valuable part of the agricultural sector and therefore they are used in this study to describe the economic impact on the agricultural sector as a result of flooding. Furthermore, soybeans are mainly located along the main river (Figure 3).

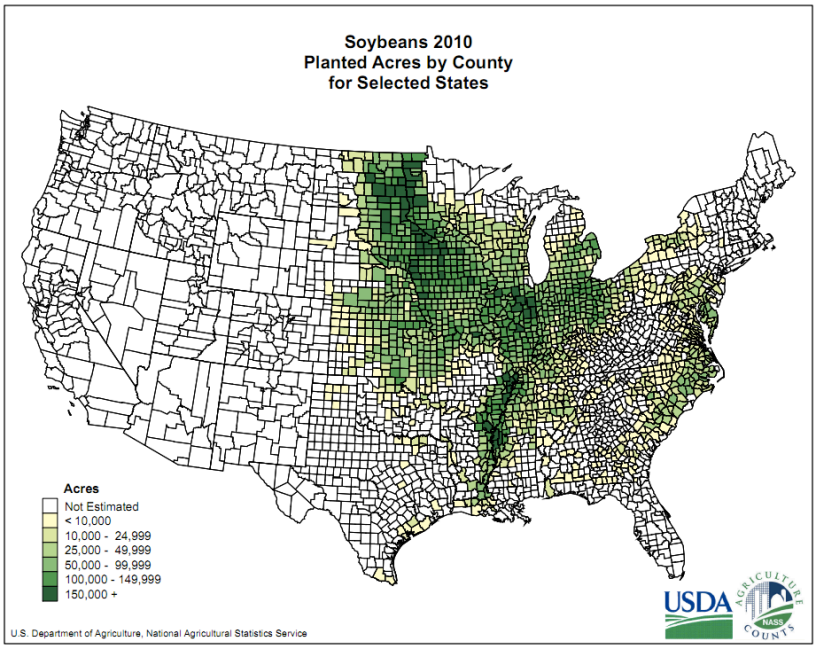

Figure 3. Planted Acres of Soybeans by County in 2010 in the Mississippi watershed (NASS, 2015)

Analyzing the population density in the Mississippi watershed clearly reveals the locations of the largest urban areas (Figure 4). The method used to describe the economic impact on these urban areas as a result of flooding is described in more detail in in section 3.2.3.

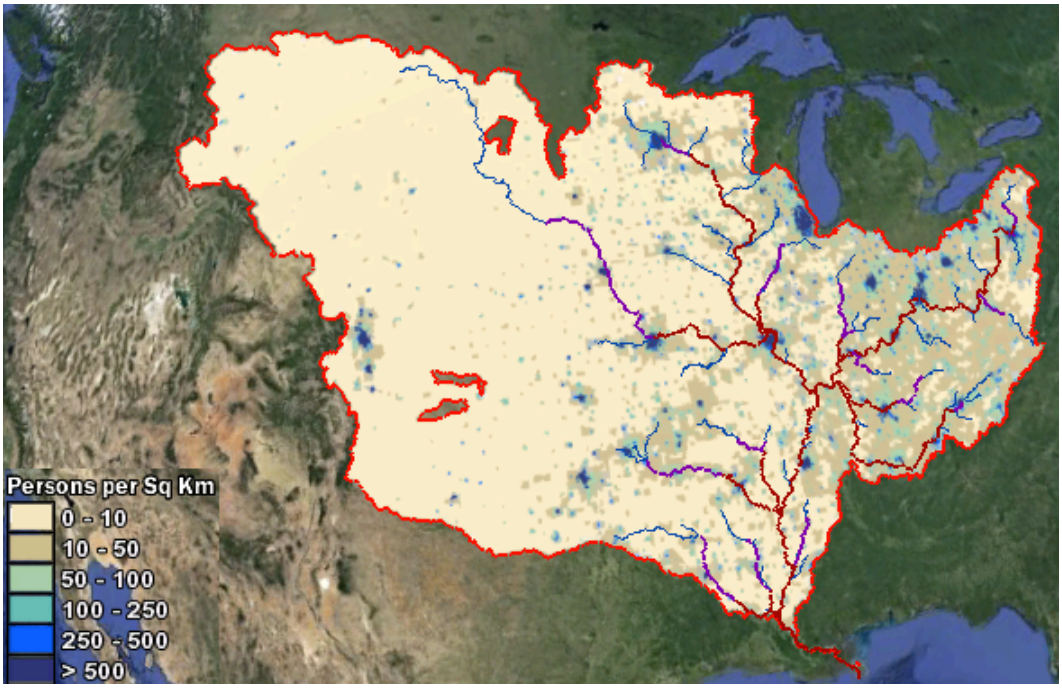

Figure 4. Population density per km^2 in 2000, retrieved from USGS and Google Earth (USGS, 2010)

2.3 Hydrological characteristics and river management

Based on physical characters, the Mississippi River can be divided into three sections, namely upper, middle and lower Mississippi. The upper Mississippi reaches from its source till the mouth of the Missouri River, the middle Mississippi reaches until the mouth of the Ohio River. At this junction the Ohio River is even larger than the Mississippi River itself. About 50% of the total annual discharge is contributed by the Ohio River (Meade, 1995). Downstream of the confluence between these two rivers the section of the lower Mississippi starts and ends in the Gulf of Mexico. At the junction of the Ohio and Mississippi River the Mississippi swells considerably to twice its upstream size. Here, the width of the river is often 2.4 km from bank to bank (Severin et al., 2015).

In 1927 the most disastrous flood in (recorded) history occurred and more than 59.600 km^2 of land in the lower Mississippi flooded (Severin et al., 2015). Over 250 people lost their lives and an enormous amount of property was damaged. Before the destructive flood in 1927 the Mississippi River Commission (MRC) only focused on dikes for flood control (Alexander et al., 2012). Afterwards, the MRC implemented a more comprehensive plan with floodways, reservoirs, spillways, cutoffs and dikes (Figure 5). Nowadays, in the Mississippi River Basin over thousands of single- and multi-purpose dams and navigation locks are used to stabilize, harness and regulate the discharge of rivers (Alexander et al., 2012). The largest floodway of the watershed is located in the lower Mississippi, the Morganza Floodway. The floodway is used to reduce the pressure on the cities New Orleans and Baton Rouge and instead mostly forested and agricultural areas are flooded.

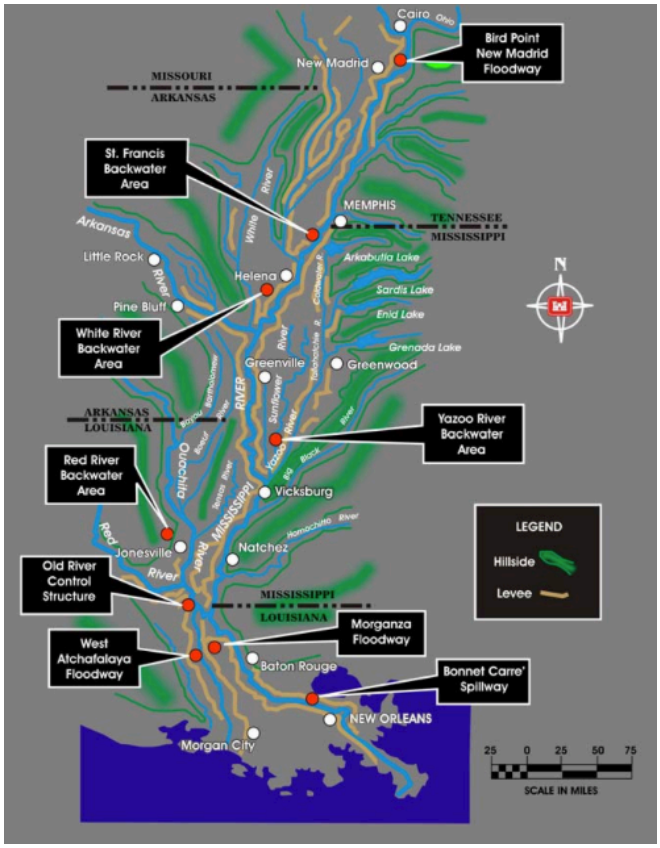

Figure 5. Overview of river management measures in the lower Mississippi (Mississippi River Commission (MRC), 2007)

The levee system of the Mississippi comprises levees, floodwalls and control structures and has a total length of 3,545 km, 2.586 km along the Mississippi River itself. The objective of the National Flood Insurance Program (NFIP) is to verify that the levee systems of the Mississippi and its tributaries provides an assurance that the leveed areas are protected against floods that occur once every 100 year (1% annual chance of exceedance) (USACE, 2014b). However, in 2014 the NFIP found that only 3 of the 25 levee systems around Vicksburg met this protection criterion.

The largest reservoir system of the Mississippi watershed is located in the Missouri River and consists of six dams, of which five were authorized by the Flood Control Act of 1944. The storage capacity is 905 km^3 and constitutes around 53% of the total storage of the Missouri River watershed. After the construction of the dams peak flood magnitudes have been reduced below each dam and reduced discharge variability (Alexander et al., 2012). In the Mississippi itself (upper Mississippi) 27 locks and dams have been built, but these were mainly realized for improving navigational routes. The impact on high discharges is low, because these events dams are overtopped (Alexander et al., 2012).

Also, since the flood in 1927 the lower Mississippi and its major tributaries are monitored. Based on data of the Global Runoff Data Centre (GRDC) the average discharge at Vicksburg between 1958 and 2010 is 17.765 m^3/s. Furthermore, in the Mississippi River large temporal variations in discharge occur. The lowest discharge measurement between 1958 and 2010 was 3.568 m^3/s in 1964 and the largest discharge was 55.501 m^3/s in 1973. Analyzing the average monthly discharge of the Mississippi river at Clinton, Keokuk, St. Louis, Chester, Thebes, the end of the Ohio River and at Vicksburg (Figure 6) in the period between 1958 and 2010 shows that the peak discharge of the Ohio River occurs in March and the peak of the Mississippi River in April-May.

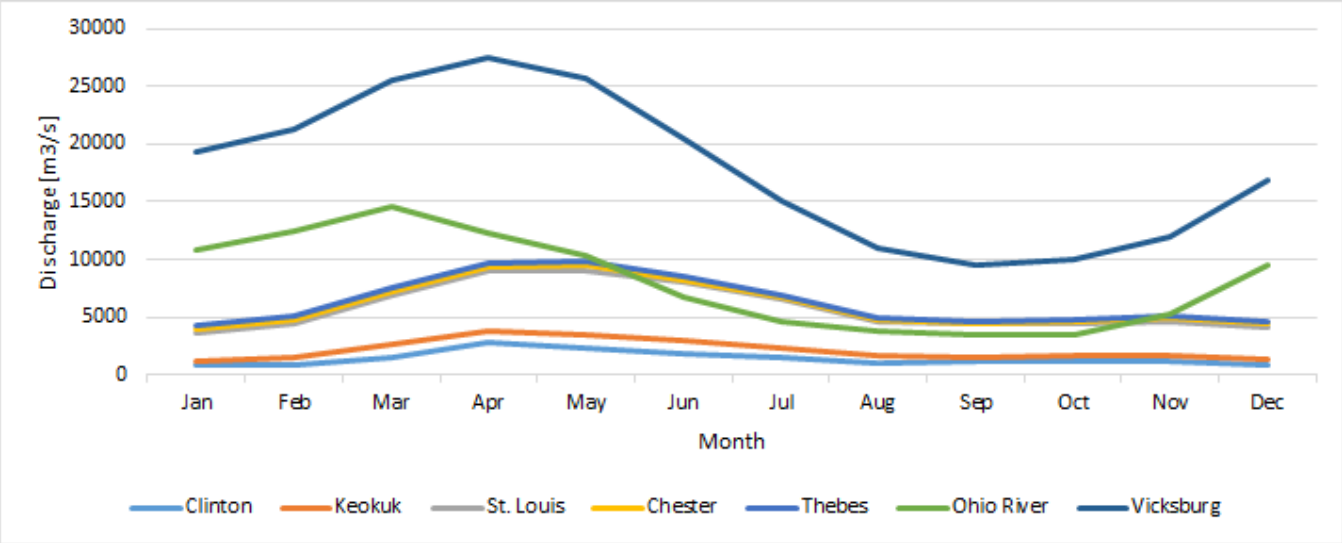

Figure 6. Average monthly discharge between 1958 and 2010 in m^3/s for several GRDC gauging stations. Clinton is the most upstream station and Vicksburg the most downstream station. The average monthly discharge of the Ohio River is based on daily data between 1958 and 2004. The location of the Ohio River gauging station is close to Thebes, just before the confluence of the Ohio River and the Mississippi River.

Furthermore, when analyzing annual maximum discharges, based on daily measured values between 1958 and 2010 at the Ohio River and the gauging stations at Thebes and Vicksburg, it is also shown that the discharges from Ohio River are larger compared to the discharge from the upper and middle Mississippi itself (Figure 7).

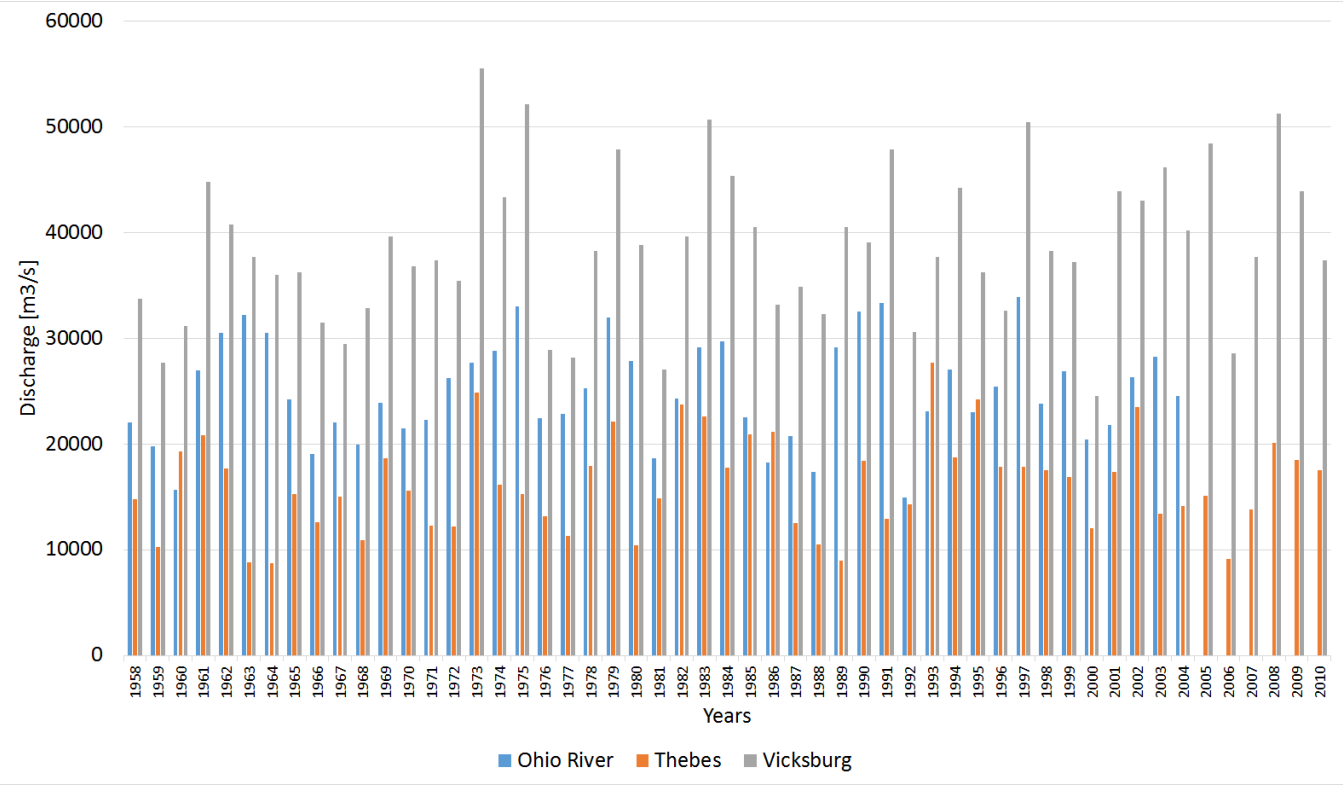

Figure 7. Annual maximum discharges between 1958 and 2010 (Ohio River– 2004) based on GRDC daily discharge data. At Thebes the total discharge is retrieved from both the upper and middle Mississippi (orange) and at Vicksburg (gray) in the lower Mississippi the discharge consists of both the discharge measured at Thebes and the discharge from the Ohio River.

3 Methods and data description

3.1 The PCR-GLOBWB model

3.1.1 Introduction to the PCR-GLOBWB model

In this study the PCR-GLOBWB model (Van Beek & Bierkens, 2008) and its extension for dynamic routing called "DynRout", as used in the framework for global river flood risk assessments by Winsemius et al. (2013), will be used to assess the impact of river regulation on river flooding. PCR-GLOBWB is developed for both global and regional hydrological studies and has already been used for several purposes.

Besides analyzing river discharges PCR-GLOBWB is used in several other studies. Wada et al. (2010) analyzed groundwater depletion on a global scale by assessing groundwater recharge with PCR-GLOBWB and groundwater abstraction estimates. Furthermore, Wada et al. (2014) analyzed the withdrawal, allocation and consumptive use of surface water and groundwater resources by coupling PCR-GLOBWB to a global water demand model. On a regional to global scale Petrescu et al. (2010) analyzed methane emission from boreal, arctic and subarctic wetlands based on the hydrological conditions. Loos et al. (2009) PCR-GLOBWB is used to calculate water fluxes, e.g. surface runoff, percolation, groundwater and river discharge, to estimate nutrient fluxes in the Rhine river basin. Also, Bierkens & Van Beek (2009) analyzed the seasonal predictability of discharge in European rivers and Sperna Weiland et al. (2010) analyzed the usefulness of climate data from twelve different Global Climate Models (GCMs) with the focus on discharge variability and extremes.

The study of Candogan et al. (2012) assessed the skill of PCR-GLOBWB in reproducing the occurrence of monthly flow extremes on a global scale for non-regulated flow, including the Mississippi River. The simulated discharge is compared with observed discharge for the period between 1958 and 2001 (Figure 8). The model is capable of producing similar trends in discharges in the Mississippi River. Based on these findings Candogan et al. (2012) concluded that this model could be used for monthly and seasonal forecasting of the occurrence of hydrological extremes.

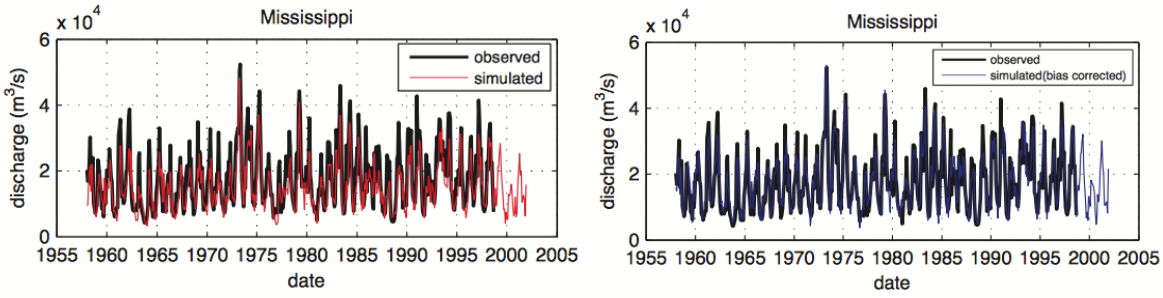

Figure 8. Discharge time series (left) and bias-corrected discharge time series of monthly flow extremes for the Mississippi River (Candogan et al., 2012). In the right figure the mean bias per month is determined and this value is subtracted from the simulated monthly discharge value. The observed discharges are retrieved from the GRDC and the simulated discharges from the PCR-GLOBWB model.

Candogan et al. (2013) looked at the contributions of initial conditions and meteorological forcing to the skill of the global seasonal streamflow forecasts. Outcomes showed that the influence of initial conditions diminishes after two months. Meteorological forcing is of higher importance, since the timing of snowmelt (The onset of ice and/or snowmelt and consequently the timing of peak flow are highly sensitive to temperature changes at the end

of the cold season) and rains in the Great Plains and the lower valley determines peak flow in the lower Mississippi.

A more comprehensive technical description of the model is given in van Beek & Bierkens (2008) and in the sections below the model concept, data input and the most important processes in this study are described. In this study PCR-GLOBWB 2.0 (Sutanudjaja et al. in prep) is used, which in comparison to the first version includes several new components, e.g. an advanced surface water routing scheme with wetland, lakes and floodplains of variable extent (Winsemius et al, 2013) and a comprehensive water demand and irrigation module (Wada et al., 2012). Lakes and reservoirs are not included during this study since errors occurred in model outcomes as these water bodies were misaligned relative to the flow direction map used.

3.1.2 Model concept

PCR-GLOBWB is a conceptual grid-based model of global terrestrial hydrology (Figure 9) and is applied on a cell-by-cell basis. In the model daily discharges and flood volumes are simulated at a spatial resolution of 30 arc-minutes. Here, meteorological forcing, consisting of the obligatory components precipitation and temperature, is applied on a daily time step and assumed to be constant over the grid cell. On the sub-grid level variability is taken into account by representing short and tall vegetation, open water, different soil types, saturated area, surface runoff, interflow and groundwater discharge.

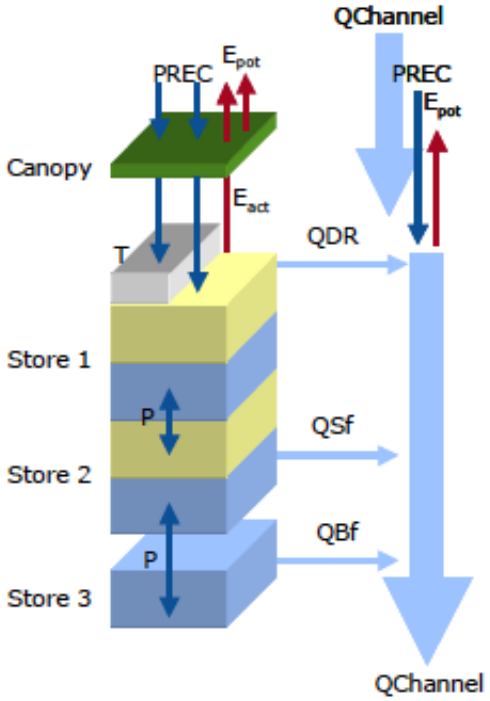

Figure 9. Model concept of PCR-GLOBWB: on the left, the soil compartment, divided in the two upper soil stores and the third groundwater store and their corresponding drainage components of direct runoff (QDR), interflow (QSf) and base flow (QBf). On the right the resulting discharge along the channel (QChannel) with lateral in- and outflow and local gains and losses are depicted (Van Beek & Bierkens, 2008).

The canopy can intercept precipitation or it can directly fall on the surface and subsequently it can infiltrate into the soil, it can evaporate to the atmosphere or it directly runs off to the channel as direct runoff (QDR). The processes of precipitation and evaporation also take place directly on open water. Furthermore, processes related

to snow, lakes, reservoirs and irrigation are also included in the model. Secondly, transport between the soil layers (store 1 and 2) and the groundwater reservoir (store 3) takes place due to percolation and capillary rise. Thirdly, the groundwater from the second soil layer can flow to channel as interflow (QSf) and from the groundwater reservoir to channel as base flow (QBf). At last, the collected water in a channel from upstream cells and lateral inflow is horizontally transported over the grid, based on the kinematic wave approximation and a drainage network. Discharge and the routing processes are described in more detail in Appendix 1. Reservoirs and lakes are normally also included in the routing scheme of the model, but due to errors and the time limit of this study they are omitted and therewith only the natural discharge is simulated.

Additionally, within each cell the maximum storage capacity in the channel is calculated based on the channel width, depth and length. When exceeding its capacity the additional volume is stored in the floodplain. The process of flooding is described in more detail in section 3.1.4.

In this study the discharge is analyzed by 1) comparing the flow pattern for the different scenarios and 2) the floodwave propagation. First, changes in the general flow pattern are compared and also variations in peak flow are analyzed by comparing the time of occurrence and the height of the peak. Floodwave propagation is analyzed by normalizing the discharge at confluence points of the Mississippi River with other rivers by dividing the discharge with the associated catchment area (Figure 10).

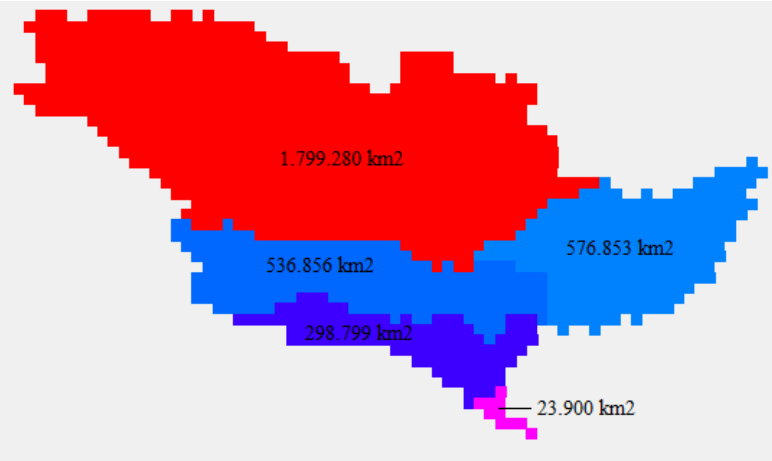

Figure 10. Catchment areas: Missouri River Basin + Upper Mississippi River Basin (red), Ohio River Basin (light blue), Arkansas – White River Basin + part of the Lower Mississippi River Basin (blue), Red River Basin + part of the Lower Mississippi River Basin (dark blue), remaining part of the Lower Mississippi River Basin (purple).

3.1.3 Meteorological input

In PCR-GLOBWB global terrestrial hydrology is simulated from 1980 until 2010 by forcing the model with daily meteorological data, which is obtained by downscaling the dataset of the Climatic Research Unit (CRU) to a daily basis using the ERA-40 and ERA-Interim reanalysis.

CRU dataset

The CRU Time Series contain long-term records of, for example, monthly time series of precipitation, daily maximum and minimum temperatures and cloud cover (ECMWF, 2003). The datasets are used for an additional correction of the reanalysis products. One of the recent released datasets is the CRU TS3.21 (CRU, 2014), which is used in the PCR-GLOBWB model at a 30 arc-min spatial resolution and cover the period between 1901 and 2012.

ERA-40 and ERA-Interim reanalysis

A reanalysis is a method that combines meteorological observations with forecast models to produce gridded datasets of climatic variables, such as precipitation, that cover the entire planet. The ERA-40 is a second-generation reanalysis and is developed by the European Centre for Medium-range Weather Forecasts (ECMWF) (NCAR, 2015). In comparison to the CRU-dataset the ERA-40 covers the period between 1957 and 2002 at a 30 arc-min spatial resolution. In PCR-GLOBWB the ERA-40 covers the period 1958-1978 and the ERA-Interim covers the period 1979-2010. The ERA-Interim is a third-generation reanalysis and is an improved version of the ERA-40. In Dee et al. (2011) the improved method is described in detail.

3.1.4 Floodplains

In PCR-GLOBWB the database HYDRO1k (USGS, 2012) is used for the elevation distribution in floodplains. The data is derived from the USGS 30 arc-seconds (approximately 1*1 km) digital elevation model of the world, GTOPO30. First, the perennial river cells are determined in the 30 arc-seconds digital elevation map based on the upstream catchment area, which is done by using the Hydro1K dataset and by determining the average drainage density (total length of water courses divided by catchment area [m^{-1}]). The average drainage density is estimated by using VMAP0 (FAO, 1997), which is a vector map of perennial water courses of the world (van Beek & Bierkens, 2008). Secondly, for each perennial river cell the cells belonging to the catchment are determined based on a local drainage direction (ldd) map (Figure 11, left). Thirdly, for all cells in the catchment the relative elevation is calculated by subtracting the surface elevation of the perennial river cell from the surface elevation of the corresponding cell. A cumulative distribution of all the relative elevations within the corresponding 30 arc-minute cell is used when the discharge volume in excess of bank-full discharge is distributed over the cells (Figure 11, middle and right). Including subcatchments partly prevents cells behind cells with a higher elevation from flooding, by eliminating the differences between elevations in upstream river cells and downstream river cells. However, unexpected flooding in cells behind cells with a higher elevation (Figure 11, left and middle – cell 2 and 3) might still occur due to depreciations in HYDRO1k elevations.

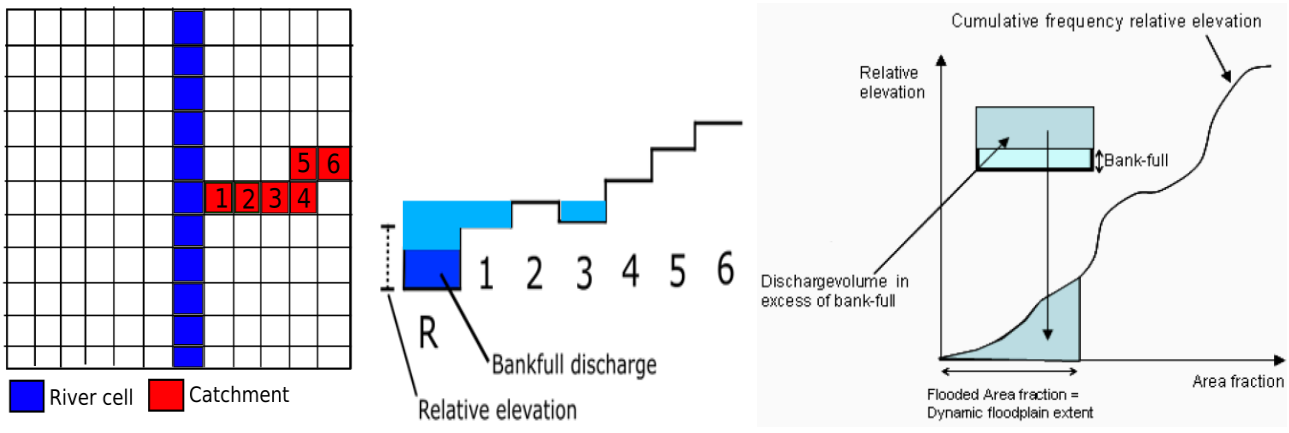

Figure 11. Flooding module in PCR-GLOBWB. 1. Determining river cells in HYRDO1K (grid of elevations of 30-arc seconds) (left), 2. Determining catchment per river cell (left), 3. Determining relative elevation between catchment cells and the corresponding river cell (middle), 4. Creating a cumulative distribution of all the relative elevations in the 30 arc-min cell (right), 5. Dividing discharge volume in excess of bankfull discharge over the HYDRO1K grid based on the cumulative distribution of relative elevations and determining the total flooded fraction of the 30 arc-min cell (middle, right).

In PCR-GLOBWB dynamic inundation is included and here floodplains are treated as regular river stretches (Winsemius et al., 2013). In the floodplains the friction, Manning's *n*, can differ from the river due to a higher resistance and an increased wetted perimeter.

PCR-GLOBWB represents flooding by giving the fraction of the cell area that is flooded and the associated inundation depth. The inundation depth is determined by dividing the total excess volume by the flooded area. In this study the differences in flooded fraction are analyzed by comparing the total flooded area (flooded fraction x cell area) along the main part of the Mississippi river (Figure 12). Furthermore, the maximum annual flooded area is analyzed to be able to see the variation over time. At last, the spatial distribution of flooded fractions is analyzed by comparing the different scenarios.

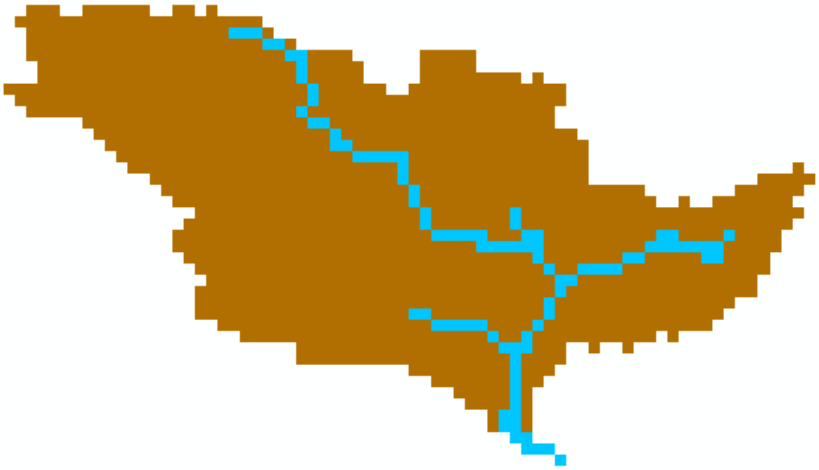

Figure 12. Main river cells (blue) that will be analyzed in terms of flooded fractions

3.1.5 Spin-up

In PCR-GLOBWB the initial conditions of all terrestrial aspects (e.g. groundwater and channel storage) are in a cold state (0.0) when running the model without spin-up. In this study a spin-up period of 20 years is used per scenario. The output files of the spin-up run are warm state files that supply the actual model run with information about initial conditions. The initial conditions in the warm state files are determined from the meteorological input, described in section 3.1.3.

3.2 Climada

The discharge, flooded fraction and inundation depths over time per cell from the PCR-GLOBWB model are written to NetCDF (Network Common Data Form) files. These factors describe the different flood events over the analyzed period and are used as input for the method used in Climada. With this method the occurring inundation depths, inundation periods and the month in a year that a flood occurs will be used in damage functions to be able to estimate the occurring economic damage per event.

3.2.1 Introduction to the Climada model

Climada is a probabilistic natural catastrophe damage model (Bresch, 2015). It is an open source assessment model to analyze the economics of climate adaptation by using the probabilistic modeling, which allows estimates of economic damage. The purpose of the model is to allow decision makers to make decisions about climate adaptation.

The model Climada is based on four elements:

1. Assets (value distribution) – Distribution of various types of insured objects and the associated values.
2. Damage functions (vulnerability) – Damage due to inundation depth or period
3. Hazards – high discharges, inundation depth extent and period of flooding
4. Adaptation measures – e.g. dikes and improved building codes

The three basic sets of data (Assets, Damage functions and Hazards) are included into the damage model. Each building block is quantified separately and combined in the process of estimating event damage. In this study only the nightlight intensity method, which determines the distribution of assets, and the impact method based on damage functions will be used from Climada. The hazard and adaptation part is already included in the PCR-GLOBWB model. The methods of distribution of assets and their values will be described below, together with the damage functions.

3.2.2 Assets

The distribution of assets per country is based on the nightlight intensity method (Ceola et al., 2014) and the value of assets is based on the Gross Domestic Product (GDP), retrieved from the World Bank (World Bank, 2015). The nightlight intensity method of Ceola et al. (2014) is used to determine human exposure to floods, based on nightlight data (NOAA, 2014) from satellites. In their study it is proved that economic losses caused by floods are correlated with nocturnal lights close to rivers. This method is mainly applicable in areas with electrical infrastructure, because in some developing countries, like Bangladesh, the estimated damage would be highly underestimated since large parts do not have access to electricity. Furthermore, there was no significant trend found between affected people and nightlights, since e.g. flood risk awareness measures are not taken into account (Ceola et al., 2014). Appendix 2 describes the process from nightlight intensity to asset values. As mentioned before, the nightlight intensity method could exclude or undervalue areas without lights. Along the Mississippi large parts consist of agricultural lands and these areas are undervalued in the nightlight intensity method. Therefore, in this study a comparison is made between the nightlight intensity method for determining urban damage and a method where the agricultural damage is determined based on the vegetation fraction. In section 3.2.3 both methods are described in more detail.

3.2.3 Damage functions

In economic damage method in Climada economic losses are determined based on depth-damage functions. Depth-damage functions relate inundation depth to a certain damage level. In this study depth-damage functions, established by the US Army Corps of Engineers, will be used to estimate damage due to flooding (Davis & Skaggs, 1992; USACE, 1985). The duration-damage functions, which are retrieved from the University of Tennessee (English et al., 2012), are mainly used for economic damage to agricultural activities and look at both the duration of the flood and the period of the flood instead of the inundation depth.

The damage for both agricultural and urban areas is determined on an annual basis and is only based on the maximum flooded fraction, maximum series of flooded days and maximum inundation depths within a year. Within a year other smaller floods might also lead to economic damages, but these are not taken into account.

Depth-Damage functions

Depth-damage relationships are frequently used in determining the expected damage to buildings. FEMA (2015) developed various credibility-weighted depth-damage functions for a variety of buildings (Figure 13), based on a historic number of claims in the USA between 1978 and 1998 for six different structure categories. In the model

the depth-damage functions can only be included to a certain extent and therefore an average of these depth-damage functions will be used to analyze the impacts in urban areas (Figure 14).

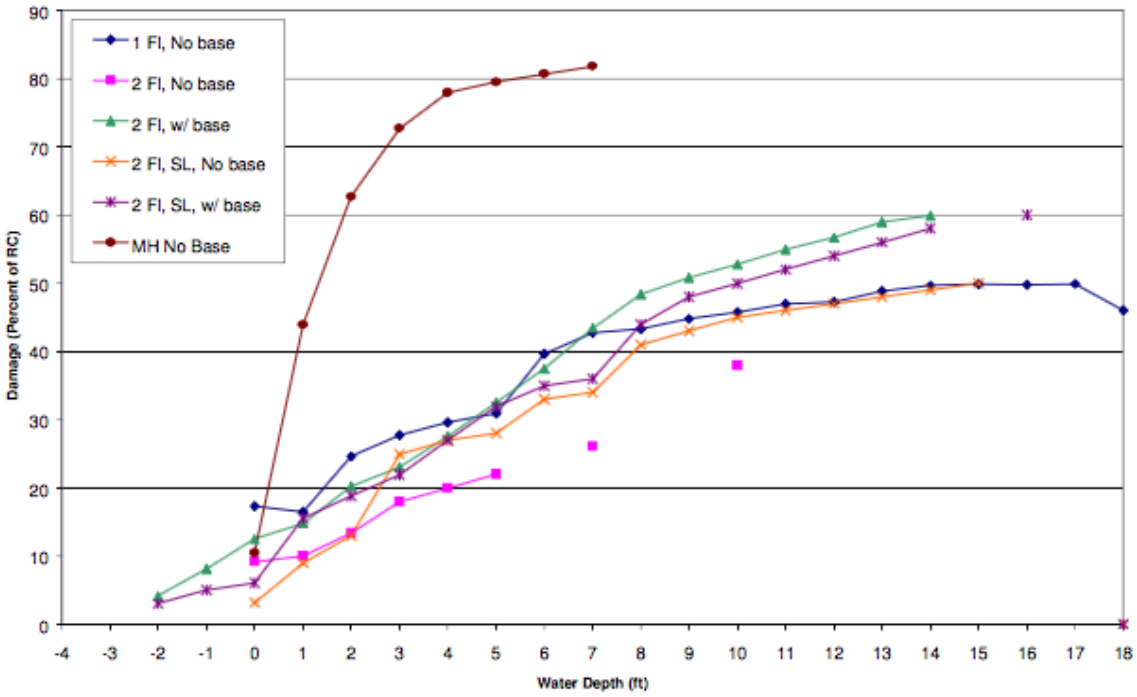

Figure 13. Credibility-weighted building depth-damage curves as of 12/31/1998 (FEMA, 2015), where RC stands for Replacement Costs.

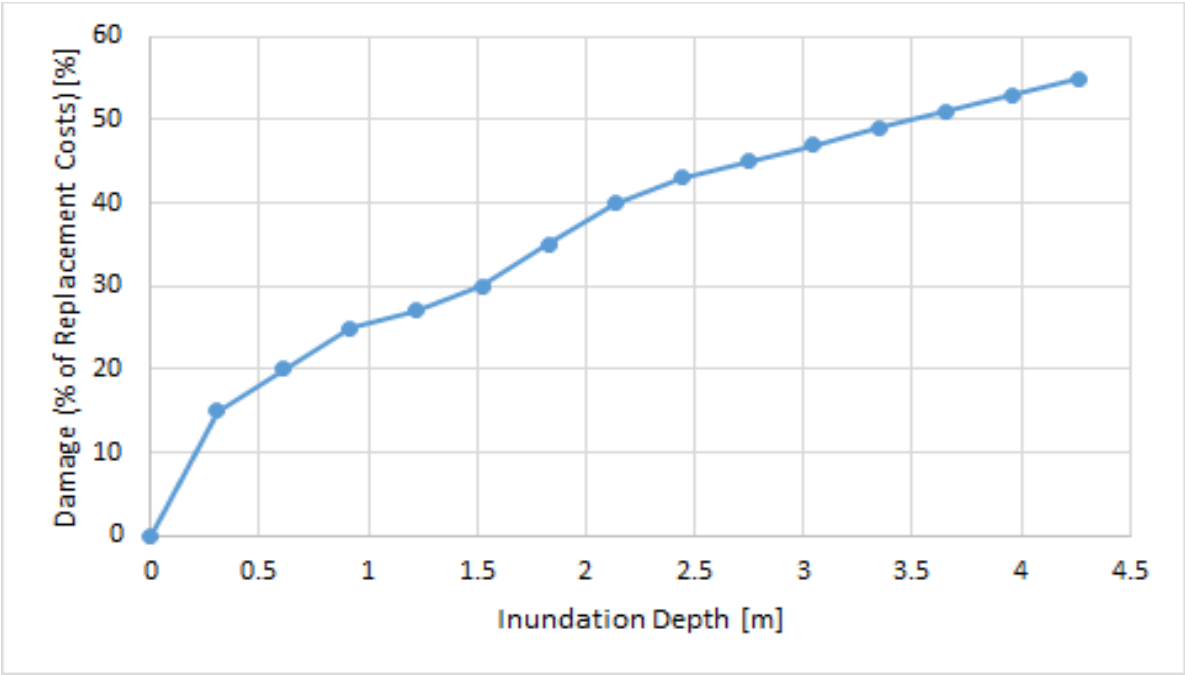

Figure 14. Average Credibility weighted building depth-damage curve as of 12/31/1998 (FEMA, 2015), edited. A conversion factor of 0.3048 is used to convert feet to meter.

Duration-Damage functions

The potential loss of agricultural areas depends on several factors, such as type of crop, time of year and physical characteristics of flood events. Throughout the year the loss potential of crops varies (Figure 15), which is due to crop stage. In harvesting periods losses are higher compared to the period of soil preparation. If an event occurs during soil preparation, there is still time left to restart the whole process and mainly production costs are lost. At the beginning of the harvest, when all the crops are fully grown, the losses are highest.

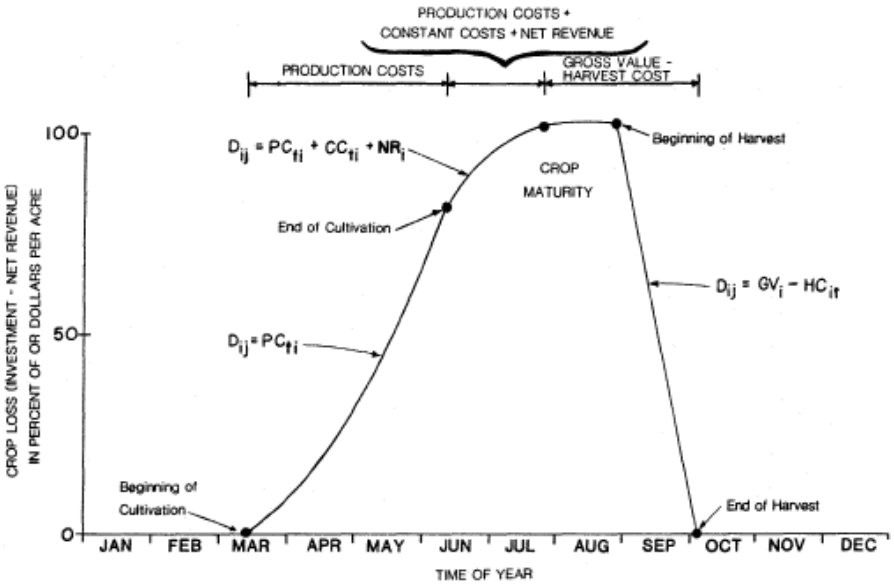

Figure 15. Conceptual representation of crop loss variation from the beginning of cultivation until the end of harvesting, where D_{ij} is the direct damage to crop (i) for event (j), PC_{ti} is the production costs at time (t) for crop (i), CC_{ti} is the constant costs at time (t) for crop (i), NR_i is net revenue for crop (i), GV_i is gross value of crop (i) at maturity and HC_{it} is harvest cost of crop (i) at time (t) (USACE, 1985).

During a flood the damage to crops depends on the duration of flooding and stage of a crop. If a crop is in its initial phase, days of flooding does not have to result in damage, but a few hours at crop maturity may result in total loss (Figure 16) (USACE, 1985). Important aspects in determining agricultural losses are the total area, yield per area, unit price value and harvest costs per area. In this study the harvest costs per area are not included since no data was available.

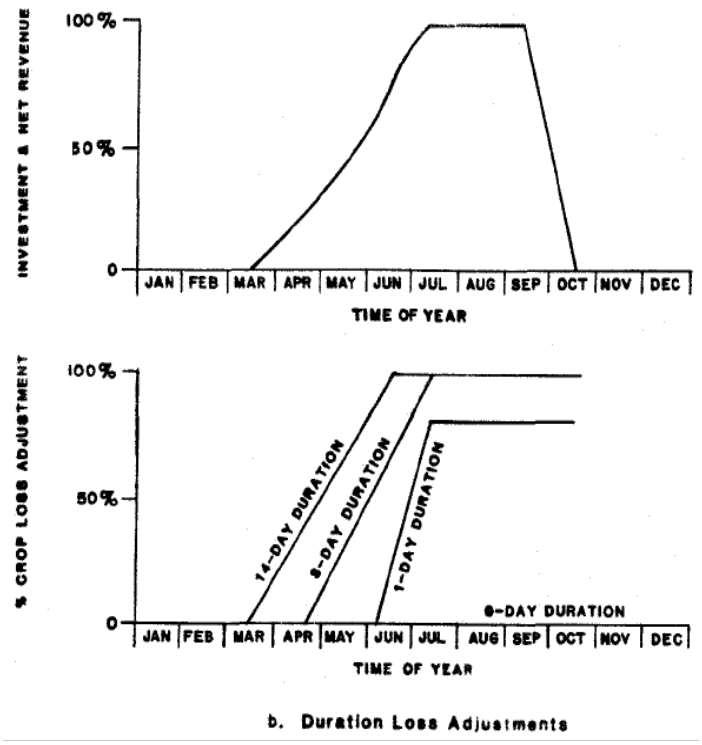

Figure 16. Conceptual graphs of the potential loss available (investment + net revenue) versus time of the year (top) and crop loss adjustments versus duration at certain time of the year (bottom), (USACE, 1985)

Soybeans

In this study the impact on soybeans is analyzed. The harvest period of soybeans is seasonal dependent, which results in different impacts in different periods in a year. The seeding starts in late April and last through June and in late September the harvest period starts and is finished by the end of November (Kowalski, 2015). English et al. (2012) analyzed the impact of flooding on soybeans by taking into account both the duration of inundation and the time of the year (Figure 17).

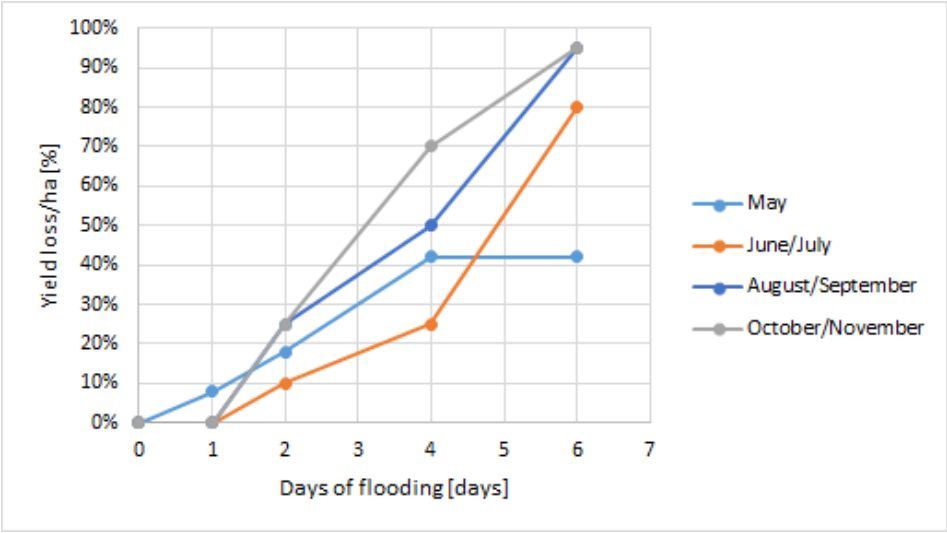

Figure 17. Estimated yield loss based on duration of flooding for soybeans in Tennessee (English et al., 2012 - table 2)

First, the number of flooded days is determined based on the 'Flooded Fraction' output of PCR-GLOBWB and the first day of flooding determines the month of flooding, which is related to the associated duration-damage relationship. In January, February, March, April and December no relationships are available and therefore it is assumed that 100% damage occurs when the total days of flooding exceeds 100 days. Between 0 and 100 days it is assumed that no damage occurs. At last, the agricultural damage is only determined per year for only the maximum series of flooded days.

The average unit price (dollars per bushel - a bushel is a measure of capacity equal to equivalent to 36.4 liters, used for dry goods and liquids.) of soybeans in the period between 2006 and 2015 is approximately $11 (USDA, 2015a), which is used in determining agricultural damage (Figure 18). The fractions of soybeans in the flooded areas are based on the cropland regions of the Monthly Irrigated and Rainfed Crop Areas (MIRCA) dataset (Portmann, 2011). The MIRCA dataset combined with the History Database of the Global Environment (HYDE) dataset and the Olson classification results in a distribution of different type of vegetation, namely non-paddy crops, paddy, pasture, rain fed crops, short natural and tall natural (Dermody et al., 2014). In this study it is assumed that the fraction of soybeans is equal to the fraction of rainfed crops, because the fraction is roughly similar compared to the research of English et al. (2012). Also, the average amount of bushels was taken over a 5-year period (2007-2011) from English et al. (2012), which is equal to 111 bushels/ha.

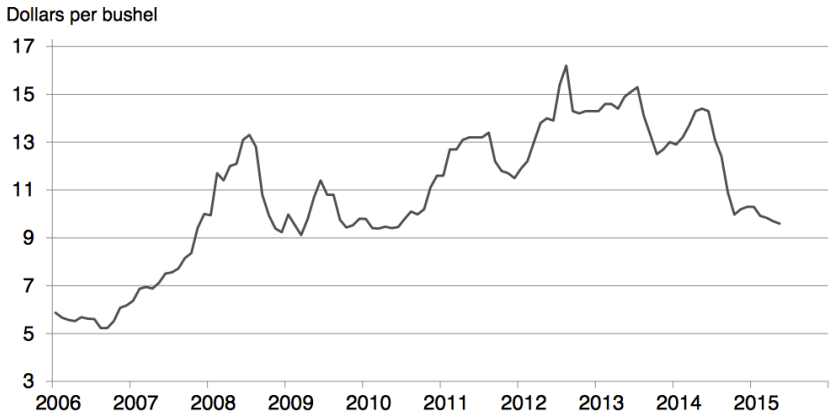

Figure 18. Monthly unit price of soybeans in the period between 2006 and 2015 (USDA, 2015a)

3.3 Scenarios and analysis

To be able to analyze the impact of river regulation on discharges and flooding in the Mississippi several scenarios will be analyzed. As mentioned before, in PCR-GLOBWB there are no dike heights incorporated. In this study dike heights and floodplains are introduced by increasing the channel depth and width of the channel (Figure 19). In the standard model the channel depth and width are calculated by using the bankfull discharge and climate indicators. Between these two factors a statistical relationship was established, based on the Global River Discharge Database (RivDis) (Vorosmarty et al., 1998). In RivDis monthly averaged discharge measurements are collected. Based on the statistical relationship the channel width, depth and length are determined with hydraulic relationships (Allen et al., 1994). In reality a cross-section of a river will not be like a rectangle as used in the standard model. However, only depth and width are included and therefore a more realistic profile like a trapezium cannot be included (Figure 20). Therefore, the capacity of the trapezium is determined in advance in PCRaster (Wesseling et al., 1996), which is the programming language of PCR-GLOBWB. In addition, a ½ trapezium profile is used, which is due to higher elevations on the east side of the Mississippi. This results in a

profile where floodplains are only present on one side. After adjusting the channel depth and width, consequently the channel capacity needs to be recalculated, which is done by multiplying the new depth and width and the length of the channel. For the trapezium profiles equation 1 and equation 2 are used.

$$Capacity\ trapezium = \left(\frac{1}{2} * (a + b) * h\right) * L \qquad (1)$$

$$Capacity\frac{1}{2}\ trapezium = \left(b * h + \frac{1}{4}(a - b) * h\right) * L \qquad (2)$$

Where, a is the new width [m], b is the standard channel width, h is the sum of the standard channel depth and the dike height [m] and L is the length of the river [m]. In the model only the capacity of the trapezium is included, but it remains a rectangular shape, therefore a new width is determined by dividing the capacity of the trapezium by the channel depth. The channel depth remains equal to the original depth plus the dike height (h).

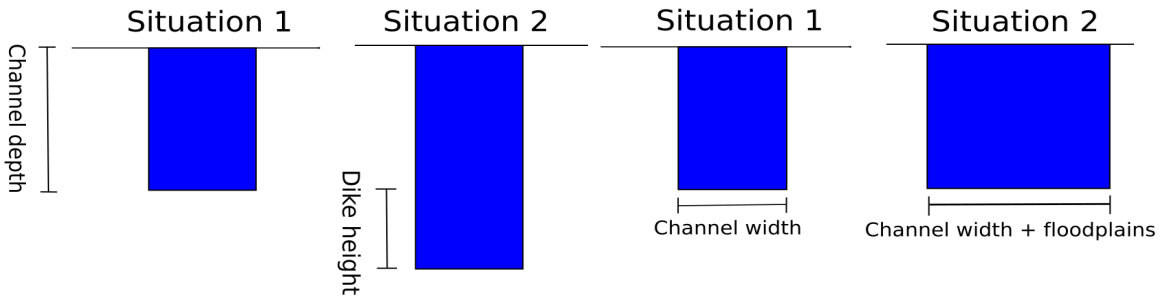

Figure 19. Schematic overview of including dike heights. The dike height is included by deepening the channel (left) and the floodplains are included by increasing the channel width (right).

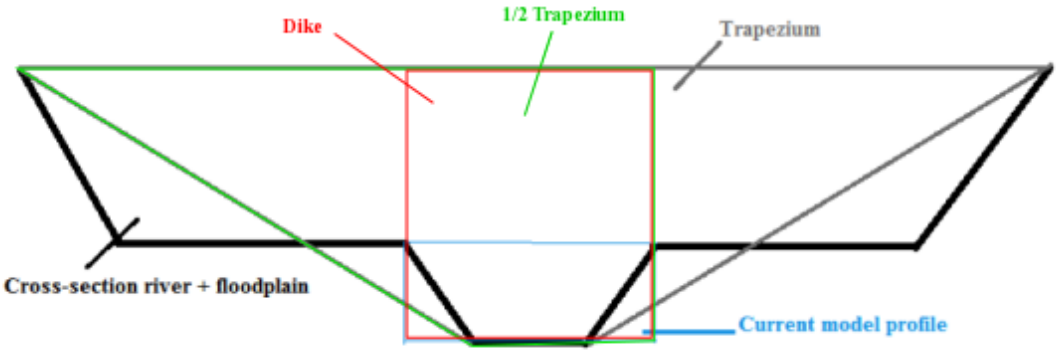

Figure 20. Schematic cross-section of a river with floodplains (black), current model profile (blue), current model profile + dike heights (red), a more realistic trapezium profile (gray) and ½ trapezium profile (green).

For all scenarios the discharge, flood wave propagation, flooded fraction, inundation depth and timing of the flood will be analyzed and compared. Furthermore, the output of the scenarios serves as the input for determining the economic impact of floods in the Mississippi. The simulated economic damage will be analyzed and compared based on total damage in years of known flood events in the Mississippi watershed (1983, 1993, 2008).

Besides analyzing the impact of changes in channel depth, width and capacity (scenario 1, 3, 4 and 5), this study also analyzes the impact of changes in the Manning coefficient (*n*). In the current parameterization the Manning coefficient is equal to 0.04 [-] for both the channel and the floodplains, which is based on earlier optimizing model runs by L. P. H. van Beek (developer PCR-GLOBWB). In the current settings the Manning coefficient in floodplains becomes important after the bankfull discharge is exceeded and flooding occurs. However, in scenario 3, 4 and 5 in this study the dikes and floodplains are included in the channel capacity, which result in a higher bankfull discharge, and thus the Manning coefficient in floodplains is, to a certain extent, neglected. Therefore, the Manning coefficient of the channel and the floodplains need to be combined, which means a larger Manning coefficient in the rivers. In this study the impact of a Manning coefficient of 0.07 [-] and 0.10 [-] in the channel is compared with the current parameterization. In Table 1 an overview of the different scenarios is given.

Table 1. Overview of parameters and a description of width and depth that will be used per scenario

Parameter	Scenario 1	Scenario 2	Scenario 3	Scenario 4	Scenario 5
Manning coefficient [-]	0.04 0.07 0.10	0.04 0.07 0.10	0.04 0.07 0.10	0.04 0.07 0.10	0.04 0.07 0.10
Flooding/ No flooding	Flooding	No Flooding	Flooding	Flooding	Flooding
Width	Original	Original	Original	+ ½ floodplains	+ floodplains
Depth	Original	Original	+ dike heights	+ dike heights	+ dike heights

3.3.1 Scenario 1 and 2: Flooding and no flooding

The first impact of river regulation is analyzed by running the model with and without flooding. Here, the model run with flooding represents the original status of the model, where flood volumes in excess of the bankfull discharge can spread out laterally over the floodplains, and the model without flooding represents a situation with overestimated dike heights, as floods never will occur. Based on this analyzes it can be shown what impact dikes along the channel can have on the simulated discharge and vice versa.

3.3.2 Scenario 3, 4, 5: Dike heights and floodplains

The main reason to analyze the Mississippi river is because of the existing National Levee Database, which provides cross-sections along the Mississippi River (Figure 21). The data is retrieved from the United States Army Corps of Engineers in a shape file format, which can be used in a Geographical Information System, such as ArcGIS.

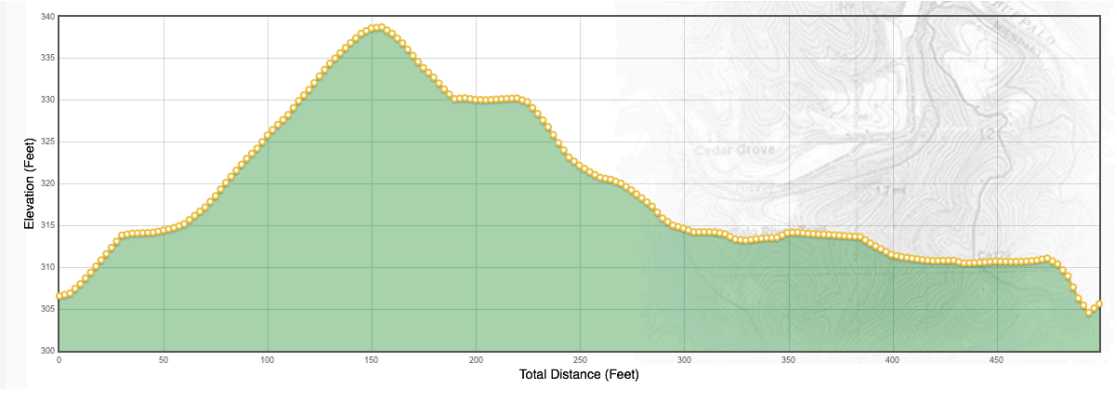

Figure 21. Example of a cross-section of a dike along the Mississippi from the National Levee Database (USACE, 2014c)

Appendix 3 describes the steps that where required to include information from the National Levee Database into PCR-GLOBWB in detail. The dike height per channel cell (30 arc-minutes from PCR-GLOBWB) is determined by subtracting the average minimum dike height from the average maximum dike height. The minimum dike height in a cell could also be chosen as critical height, but because in the National Levee Database some secondary dikes are also included the average is used. In scenario 3 only the dikes are included.

In scenario 4 and 5 the actual width of floodplains is determined in ArcGIS based on the centerline of the Mississippi River (USACE, 2014) and the distance to the cross-section. Here, the average distance in a cell is chosen as the value with which the channel width increases. The centerline was only available for the Mississippi River itself and therefore the width of the floodplains of tributaries and more upstream cells is determined by multiplying the channel width with an average factor. This factor is determined by dividing the new width (original width + width of floodplains) by the original width for the cells with a centerline and afterwards the average of all factors from the cells with a centerline was taken. At last, the capacity of the trapezium shape (scenario 5) and the ½ trapezium shape (scenario 4) is calculated in PCRaster (Figure 20). However, in PCR-GLOBWB only rectangular shape can be included and therefore a new width is determined based on the area of the trapezium shape and the channel depth (area trapezium/channel depth).

3.3.3 *Morganza Floodway*

Besides the implementation of dike heights, the impact of floodways is analyzed for the scenario with the highest NSE Coefficient or the best-fitted hydrograph. As described in section 2.3 along the Mississippi floodways can reduce the impact on cities by allowing agricultural lands to be flooded. In the model the dike height of the cell that includes the floodway will be lowered with 50% and therewith the capacity will also reduce. In this cell the flooded fraction will increase and therewith it is expected that the peak discharge in downstream (urban) areas decreases. The hydrological impact of the floodway will be analyzed for the downstream cells (Figure 22), by comparing it with the initial conditions of the associated scenario.

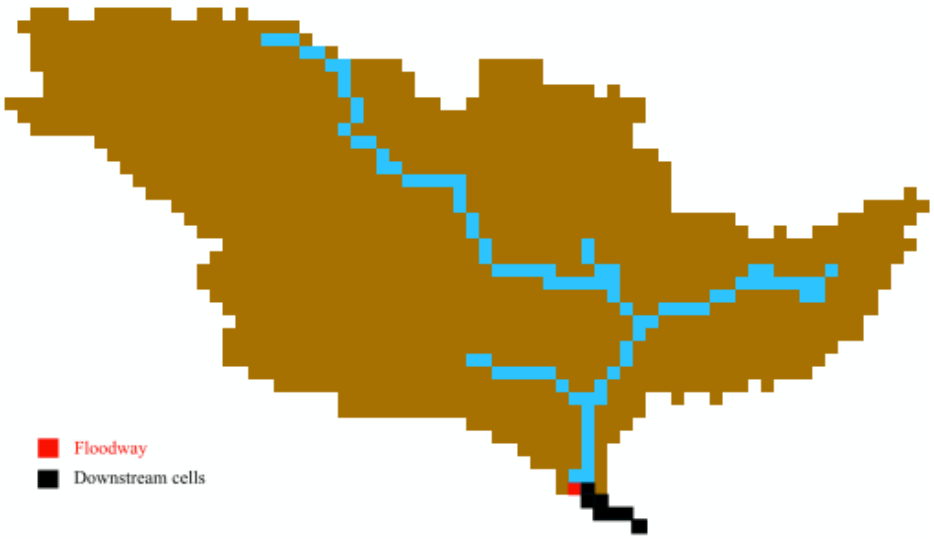

Figure 22. Location of the Morganza Floodway (red) and its downstream cells (black)

3.4 Model validation

3.4.1 River discharge

The Global Runoff Data Centre (GRDC) collects river discharges at daily intervals and in this study the data in the period between 1980 and 2010 is analyzed, which is within the boundaries of the meteorological dataset (1958-2010). This study focuses on the gauging station of Vicksburg (Figure 23), because of the largest occurring discharges.

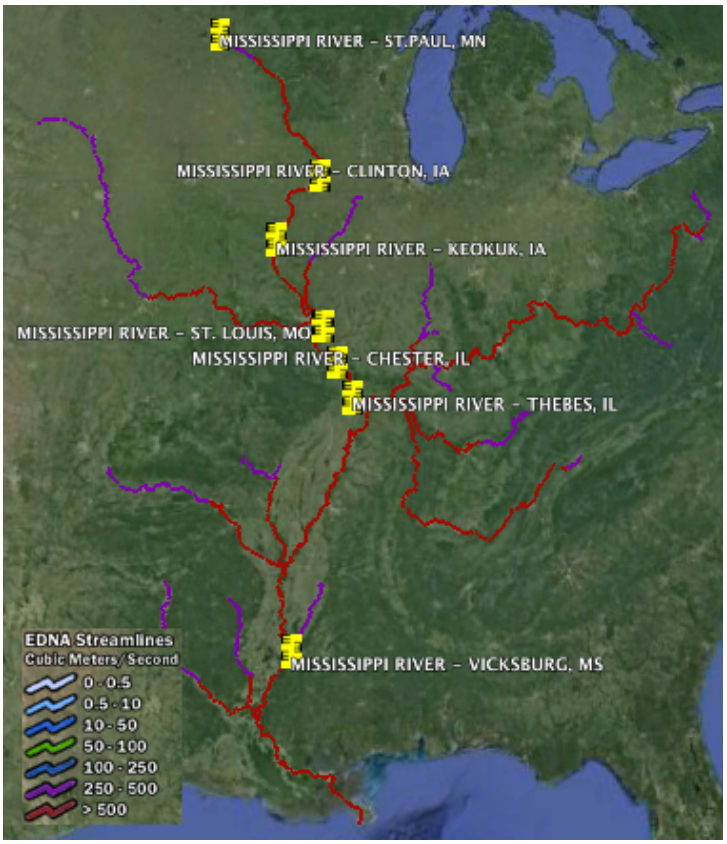

Figure 23. GRDC Stations along the Mississippi River on locations with a minimum flow of 250 m^3/s, USGS (2007). The GRDC collected river discharge data at a daily basis between 1958 and 2010, GRDC (2014)

The GRDC data is used to be able to validate the discharges at Vicksburg from PCR-GLOBWB for the different scenarios. The Nash-Sutcliffe model efficiency coefficient (NSE) (Nash & Sutcliffe, 1970) is used to compare the observed and modeled hydrographs and therewith assess the predictive power of PCR-GLOBWB, based on equation 3.

$$NSE = 1 - \frac{\sum_{t=1}^{T}(Q_o^t - Q_m^t)^2}{\sum_{t=1}^{T}(Q_o^t - \overline{Q_o})^2} \qquad (3)$$

Where Q_o^t is the observed discharge and Q_m^t is the modeled discharge in m^3/s at a given time step t in days, in a range between 1 and T and $\overline{Q_o}$ is the mean observed discharge over the range between 1 and T. The NSE varies between $-\infty$ and 1, where an NSE of 1 indicates that the observed and modeled discharges are equal and therewith the model perfectly predicts the discharge. An NSE of 0 means that the model is as accurate as the mean

of the observed discharge ($\overline{Q_o}$) and an NSE < 0 means that the mean observed discharge better predicts the discharge compared to the model.

3.4.2 Economic damage

The modeled economic damage as a result of flooding is validated for the known flood events in 1983, 1993 and 2008, based on literature and existing international damage databases. The observed economic damage is retrieved from the National Oceanic and Atmospheric Administration (NOAA) (Trotter et al., 1998) and the EM-DAT database (The International Disaster Database from the Centre for Research on the Epidemiology of Disasters (CRED)) (CRED, 2015), which both generally describe the flood events and the resulting damages. In Table 2 an overview is given of the observed data.

Table 2. Economic damages during flood events in the Mississippi Watershed in US Dollars, retrieved from Trotter et al. (1998) and CRED (2015)

Year	NOAA	EM-DAT
1983	$15.7 million: Mainly river industries, docking facilities and agriculture. Days in flood: 99	Total Damage: $400.000.000 Events: 2 Deaths: 10 Affected: 0
1993	$15 to $20 Billion: 50 thousand homes were damaged or destroyed and 54 thousand people were evacuated. Mainly Upper Mississippi	Total Damage: $12.290.000.000 Events: 5 Deaths: 98 Affected: 43700
2008	-	Total Damage: $10.002.000.000 Events: 4 Deaths: 44 Injured: 148 Affected: 11.032.500

4 Results

The hydrological analysis of the outcomes of PCR-GLOBWB is described in section 4.1 and the resulting economic damage, based on the different impact methods, is analyzed in section 4.2. The impact of scenario 2 is only analyzed in section 4.1 – Hydrological impacts of flood regulation, since this only shows the impact of the flood module. In all other sections and subsections scenario 2 is not included.

4.1 Hydrological impacts of flood regulation

The PCR-GLOBWB model is first run for the first and second scenario, respectively the original settings with and without flooding. To be able to see the difference between with and without the flooding module the hydrographs are shown for a wet year (1983 - left) and a dry year (1999 - right) (Figure 24).

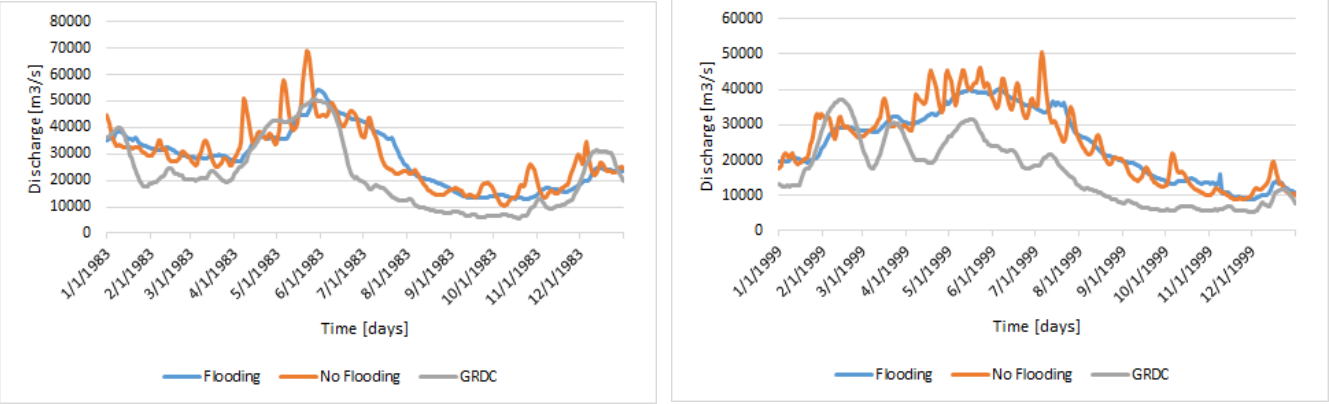

Figure 24. Influence of the flooding module in PCR-GLOBWB in a wet (1983 – left) and a dry year (1999 – right) and a comparison with the observed discharge from the GRDC at Vicksburg.

Including the flooding module in PCR-GLOBWB has resulted in more similar results compared to the observed values (Figure 24). Fewer steep peaks occur and discharges are more gradually increasing and decreasing over time. Furthermore, especially in the wet year where the discharge increases gradually, the simulated discharge follows the observed pattern and also the height of the peaks is correctly simulated. In years with multiple peaks close after one another the model follows the first peak correctly, but has no time to decrease before the second peak occurs. The differences in reproducing floods and droughts with PCR-GLOBWB is also concluded by Candogan et al. (2012).

4.1.1 *Discharge*

Changes in channel capacity and channel depth and width have resulted in variations in discharge and the way flood waves propagate downstream. An increase in capacity results in higher peak discharges (Figure 25), which might be due to less flooding in upstream cells and a higher capacity of the cell itself. However, with an increased Manning coefficient (Figure 25 - middle and bottom) only small changes in discharge are noticeable. In all scenarios the timing that the flood occurs remains almost equal to the original settings and the observed time from the GRDC. Between the scenarios the time of the peak only varies a few days.

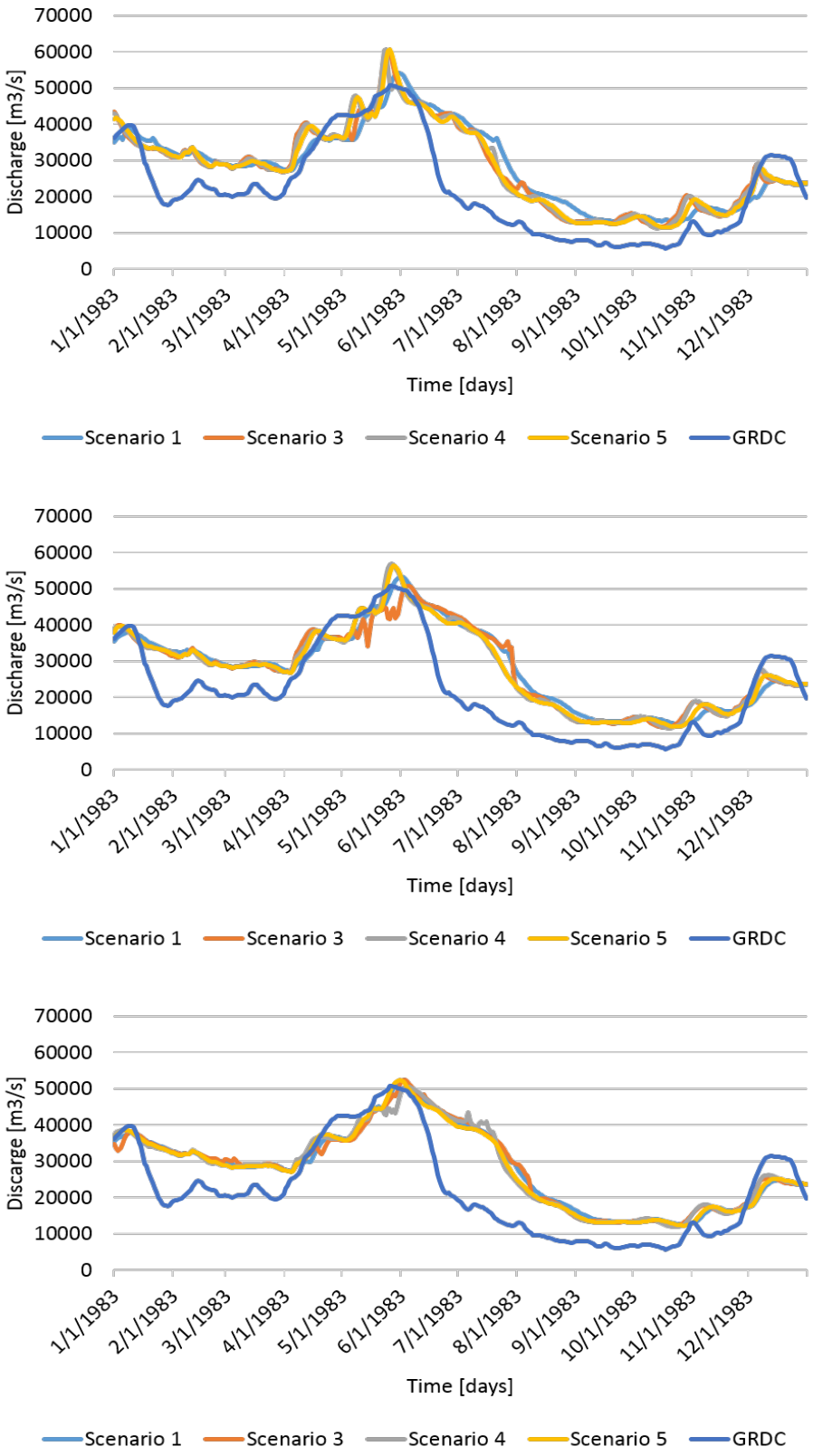

Figure 25. Hydrographs at Vicksburg in 1983 for the different scenarios for a Manning coefficient of 0.04 (top), 0.07 (middle) and 0.10 (bottom). Besides the simulated discharge the observed discharge from the GRDC is shown.

Changes in discharge with an increasing Manning coefficient follow from an increased wetted perimeter. When increasing the depth and width of the channel the wetted perimeter also increases and therewith the influence of the roughness coefficient increases. Changes in discharge are mainly noticeable during peak flows (Figure 25). Based on Table 3 it can be noted that the discharge is inversely proportional to the roughness coefficients, which results in lower discharges as the roughness coefficient increases. In the first scenario changes due to the Manning coefficient are small. Compared with the original settings the peak discharge slightly decreases as the Manning coefficient increases (0.07 and 0.10). However, as the dimensions of the channel increase, the influence of the roughness coefficient also increases. The model supports the expected results, except in scenario 3 (*) where only dikes are involved. Here, an unexpected difference occurs as the discharge with a roughness coefficient of 0.07 results in a larger decrease in discharge compared to decrease with a roughness coefficient of 0.10.

Table 3. The influence of the Manning's roughness coefficient on discharge and time shift of the peak discharge at Vicksburg for the different scenarios

Year: 1983	**Scenario 1: Original**		**Scenario 3: Dikes**		**Scenario 4: Dikes + ½ floodplains**		**Scenario 5: Dikes + floodplains**	
Manning coefficient [-]	0.07	0.10	0.07	0.10	0.07	0.10	0.07	0.10
Peak discharge [m^3/s] (manning 0.04)	54.089		60.492		60.629		60.525	
Change in peak discharge [m^3/s]	-728	-1.883	-9.644*	-7.989	-3.664	-10.035	-4.193	-8.236
Peak shift over time [days]	+1	+1	+11	+8	+ 3	+10	+2	+5

4.1.2 Flood wave propagation

In general, discharge increases in the downstream direction as the drainage area increases. Due to frictional resistance of the channel mechanical energy is lost and therewith the height of the peak reduces. However, this could only be analyzed by dividing the discharge per location with the associated drainage area, Table 4, which results in the normalized discharge (Figure 26). The different scenarios are analyzed with a Manning coefficient of 0.10, since this resulted in the best-fitted peak discharge.

Table 4. Analyzed locations and the area of the associated catchments

	Catchment location 1	**Catchment location 2**	**Catchment location 3**	**Catchment location 4**	**Catchment location 5**
Area [km^2]	1.799.280	576.853	536.856	298.799	23.990
River Basins	Missouri + Upper Mississippi River Basin	Ohio River Basin	Arkansas - White River Basin + part of the Lower Mississippi River Basin	Red River Basin + part of the Lower Mississippi River Basin	Lower Mississippi River Basin

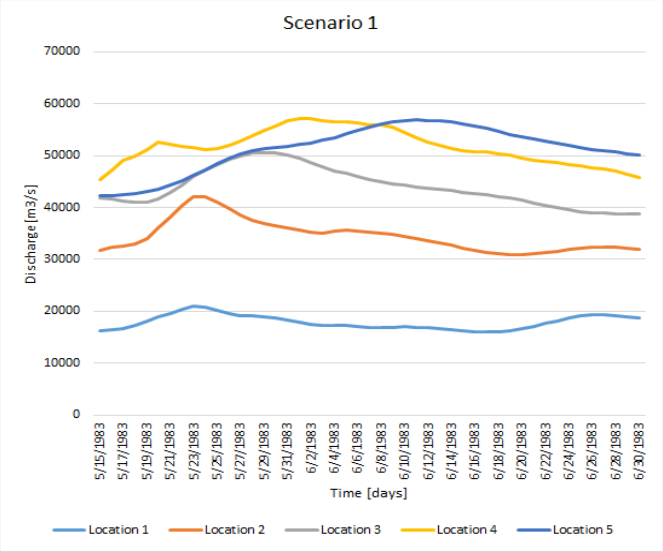
Scenario 1
Discharge [m3/s]
Time [days]
Location 1
Location 2
Location 3
Location 4
Location 5

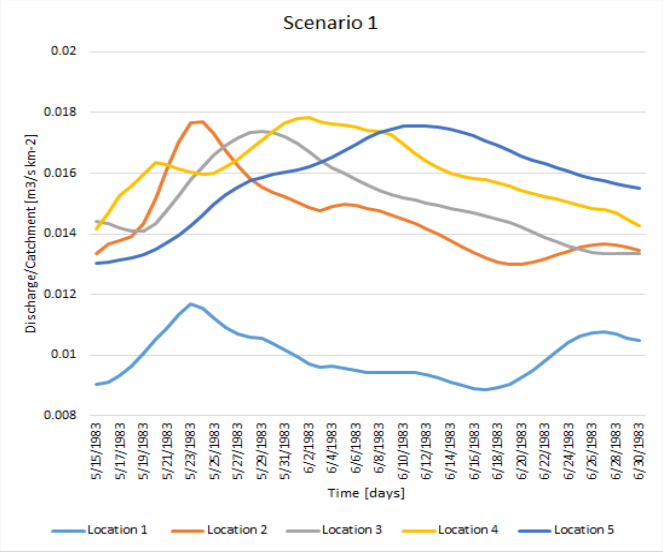
Scenario 1
Discharge/Catchment [m3/s km-2]
Time [days]
Location 1
Location 2
Location 3
Location 4
Location 5

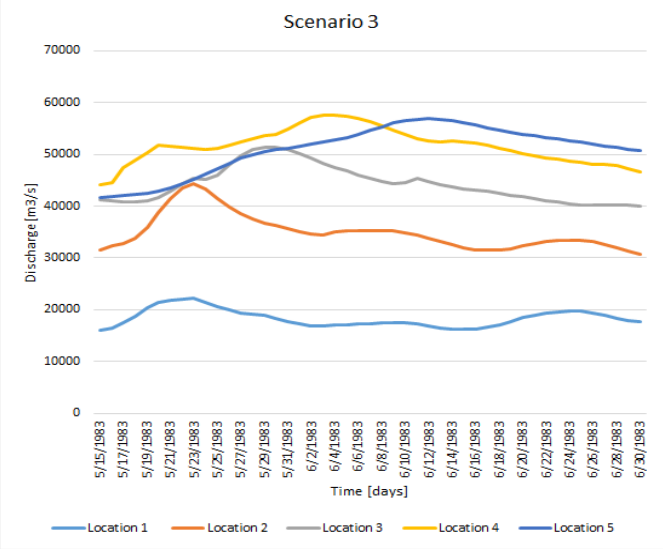
Scenario 3
Discharge [m3/s]
Time [days]
Location 1
Location 2
Location 3
Location 4
Location 5

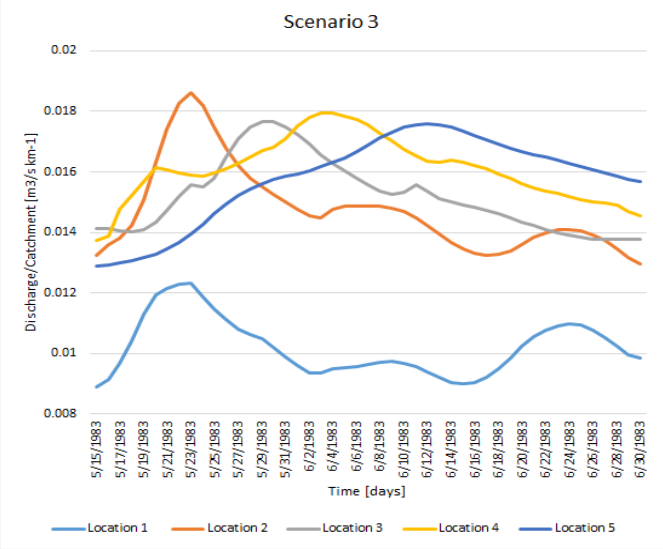
Scenario 3
Discharge/Catchment [m3/s km-1]
Time [days]
Location 1
Location 2
Location 3
Location 4
Location 5

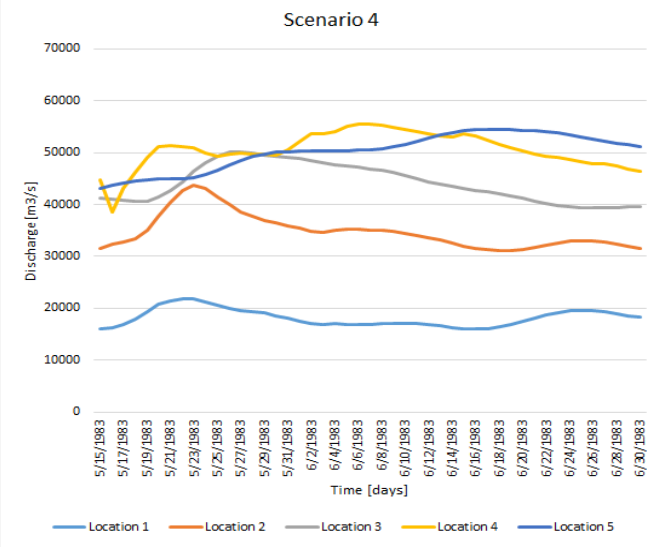
Scenario 4
Discharge [m3/s]
Time [days]
Location 1
Location 2
Location 3
Location 4
Location 5

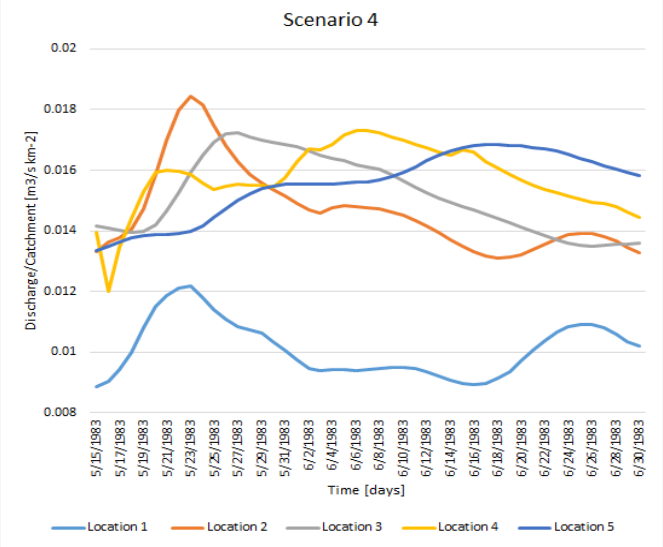
Scenario 4
Discharge/Catchment [m3/s km-2]
Time [days]
Location 1
Location 2
Location 3
Location 4
Location 5

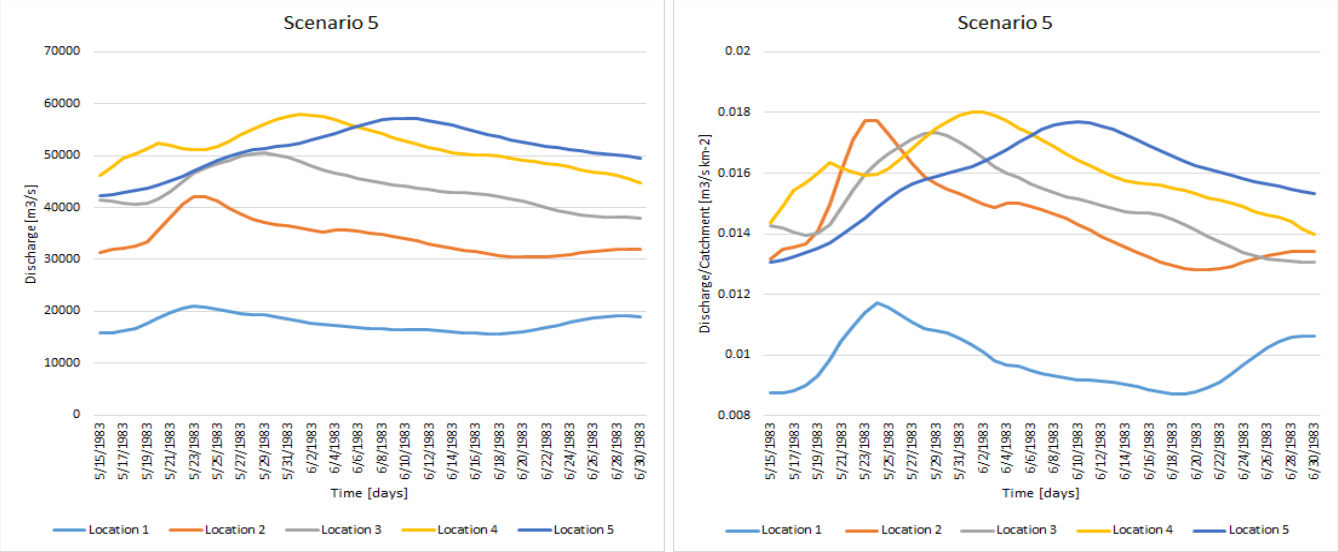

Figure 26. The floodwave in 1983 between May 15th and June 30th for the different scenarios, with a Manning coefficient of 0.10. Normal discharges are presented left and normalized discharges are presented right.

As expected, comparing the hydrographs show that the flood wave is indeed increasing in the downstream direction and that the peak is more equally temporarily distributed. The normalized discharge shows more information about the propagation of the floodwave. At location 1 it is noticeable that the normalized discharge is low compared to the other locations. This is could be explained since the discharge is relatively low and the size of the associated catchment is relatively large. The largest increase is seen at location 2, which is at the confluence with the Ohio River. In section 2.3 it was already shown that the impact of the Ohio River on the discharge was large.

Furthermore, at location 4 the peak is increasing instead of decreasing, which could be explained by the lateral inflow from tributaries and the spatial distribution of precipitation. In 1983 at Red River Landing (confluence of the Mississippi River and the Red River – location 4) one of the highest records was measured (NOAA, 2011) and this could explain the increase at location 4. Due to the variations in the spatial and temporal distribution of precipitation in the different catchments and therewith in runoff processes, variations in floodwave propagation might arise. However, comparing the normalized discharge between location 2 and 3 and location 4 and 5 shows the expected attenuation of the floodwave.

The impact of changing channel dimensions on flood wave propagation is minimal. The main differences are noticeable in the height of the peaks and the time of occurrence. In scenario 3 the peak first increases, but after the width of the channel increases (scenario 4 and 5), the impact of the Manning coefficient also increases and therewith the peak decreases.

Besides the channel dimensions the influence of flooding could also impact the propagation speed of the floodwave, due to storage and different roughness coefficients in floodplains. However, in scenario 1 and 3 the roughness coefficient in the floodplains is kept equal to the roughness coefficient of the channel and in scenario 4 and 5 the floodplains and the channel are combined, which result in one Manning coefficient and therewith flood wave propagation is not influenced by changing roughness coefficients but could be influenced by storage in the floodplains.

4.1.3 Flood characteristics

Flooded fractions are analyzed by comparing the total flooded area in the main part of the Mississippi River (Figure 12 in section 3.1.4). Comparing the model output of the original model with the output of scenario 3 (only dikes included) shows constant flooding over time in scenario 1 and in scenario 3 the inclusion of dikes has resulted in flood events instead of constant flooding Figure 27.

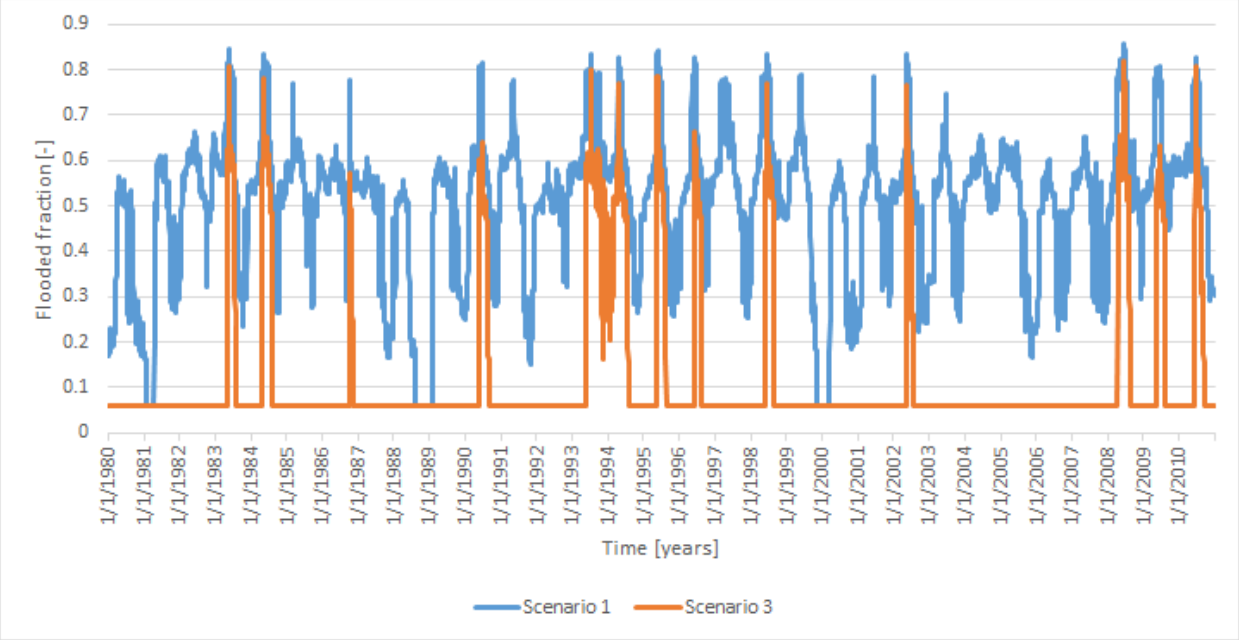

Figure 27. Flooded fractions in the period between 1980 and 2010 for a cell in the lower Mississippi for scenario 1 and scenario 3. The open water fraction is still included and therefore a constant flooded fraction of approximately 0.08 is noticeable in the bottom figure.

Increasing channel dimensions and changes in the roughness coefficient result in a different spatial distribution of floods. In Table 5 the total flooded area and the total flooded area in the main river cells is given, which shows a decrease in flooded area as the channel dimensions increase and an a increase in flooded area as the roughness coefficient increases. A correction is added for the number of cells flooded, indicated by (…), since some cells might not actually be flooded. This results from the subtraction of the open water fraction from the simulated flooded fraction.

Furthermore, the largest differences occur in the main channel, which is logical since changes are only made in these cells. Analyzing the annual maximum flooded areas in the period between 1980 and 2010 for the different scenarios with a roughness coefficient of 0.10 shows flooding on an annual basis (Figure 28). In scenario 1 there is an annual occurring flooded area of at least 30.000 km^2, which is relatively high compared to the other scenarios. However, even in the scenarios with larger channel dimensions flooding is still occurring in most of the years, which is not as expected. Large flooded areas are even simulated in 1999, which is known as a dry year.

Including floodplains and dikes in the channel capacity has especially a large impact on the main river cells (Figure 29). Flooded fractions in the main river cells are reducing with increasing regulation measures. A remarkable similarity between the different scenarios is that the most downstream cells and the cells outside the main river cells are all constantly flooded. In the most downstream cells the width of the floodplains is relatively small compared to upstream cells. This is as expected since no floodplains are located in the more dense urban

areas. Also, dike heights are lower compared to upstream cells. In the method used secondary dikes are also included in the downstream areas and therewith the mean dike height decreases. These factors strongly reduce the channel capacity in the downstream areas, which results in more and earlier flooding. In this study the channel dimensions are not adjusted besides the main method. Flooding in the cells outside the main channel is not further analyzed, but could also result from underestimated channel dimensions. These errors will have a large impact on the economic damage methods. Constant flooding results in the maximum agricultural damage possible and also in errors in determining the month of flooding. Also, due to the errors both urban and agricultural damage will occur in cells that might not be flooded in reality.

Table 5. Analysis of flooded area during the peak discharge in 1983 for the different scenarios

1983	**Scenario 1**			**Scenario 3**			**Scenario 4**			**Scenario 5**		
Manning Coefficient [-]	0.04	0.07	0.10	0.04	0.07	0.10	0.04	0.07	0.10	0.04	0.07	0.10
Flooded area [km^2]	159.190	166.860	170.310	133.480	148.530	154.520	129.660	134.540	144.560	123.640	129.530	131.600
Number of cells flooded [-] (fractions > 0.00001)	1316 (1239)	1334 (1281)	1342 (1291)	1303 (1200)	1319 (1240)	1322 (1253)	1301 (1159)	1309 (1221)	1316 (1236)	1293 (1191)	1306 (1216)	1307 (1219)
Flooded area (main river) [km^2]	42.250	48.397	50.882	16.538	30.063	35.374	12.716	16.074	25.421	6.695	11.069	12.461
Number of cells flooded (main river) [-] (fractions > 0.00001)	75 (52)	84 (72)	91 (80)	62 (13)	69 (31)	71 (42)	50 (8)	52 (12)	59 (25)	48 (4)	49 (7)	49 (8)

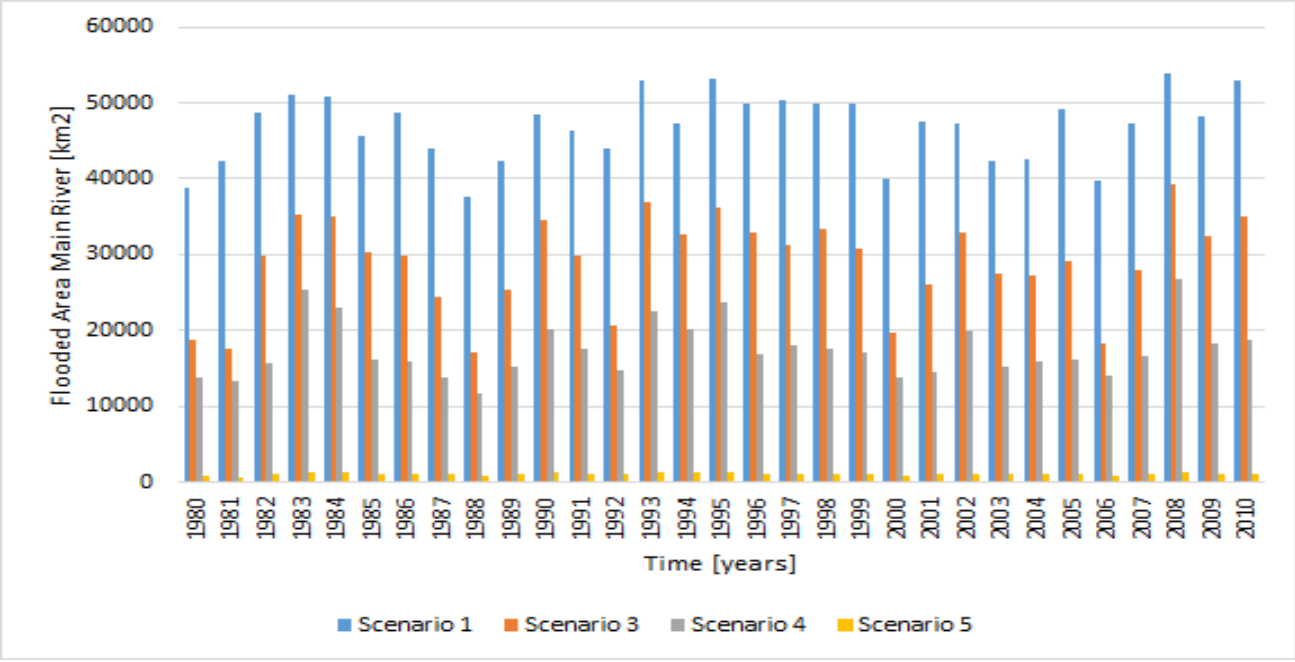

Figure 28. Annual maximum flooded area of the main river cells in the period between 1980 and 2010

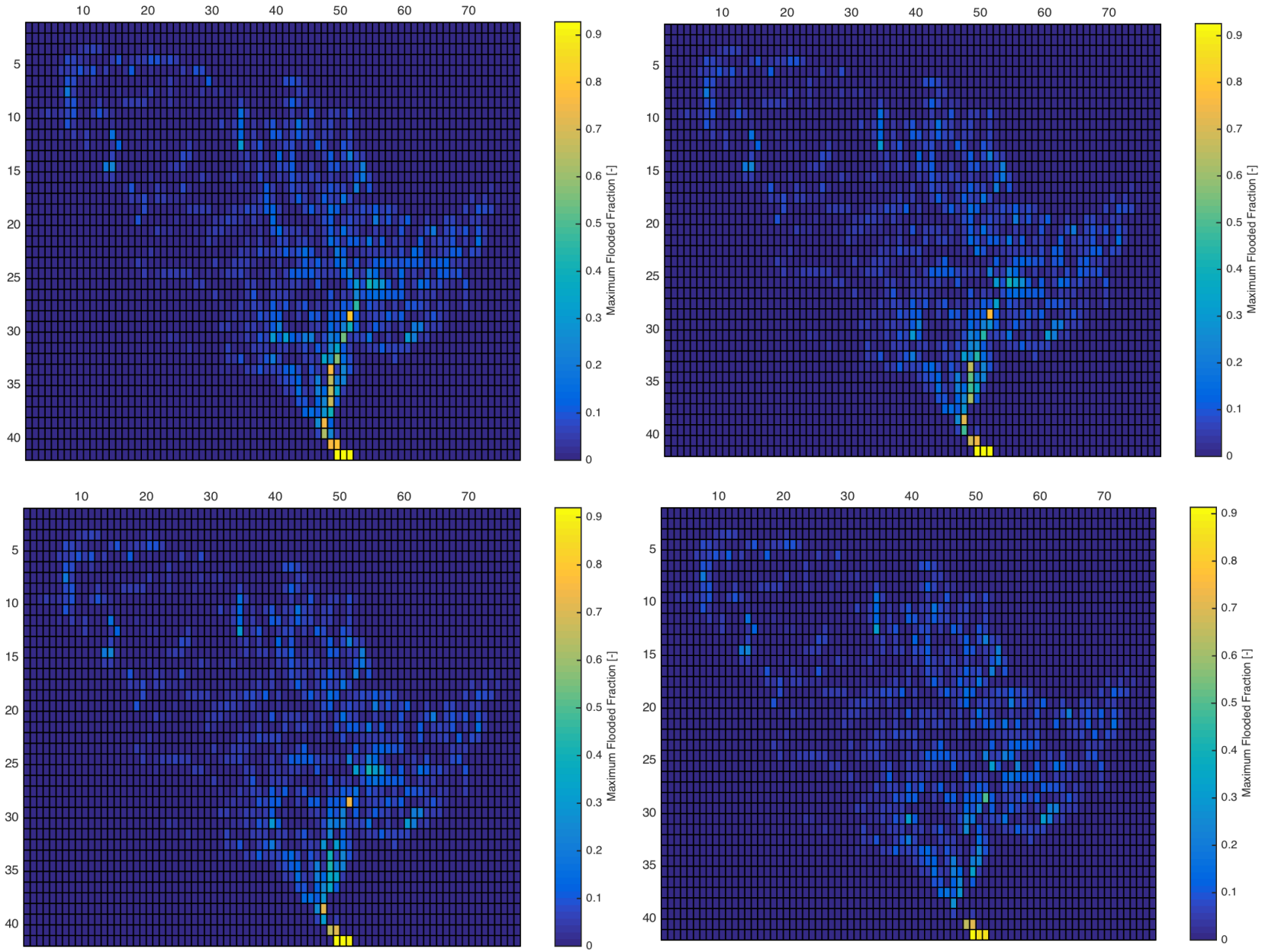

Figure 29. Spatial distribution of flooded fractions during the peak discharge in 1983 for the different scenarios (Manning = 0.10), scenario 1: top left, scenario 3: top right, scenario 4: bottom left, scenario 5: bottom right.

4.1.4 Validation of discharge

The simulated discharge for the different scenarios in the period between 1980 and 2010 is validated based on the Nash-Sutcliffe model efficiency coefficient and the observed data of the GRDC (Figure 30). These figures show that the influence of changing the channel dimensions and the Manning coefficient is small. Furthermore, the capability of the model in simulating discharge at the downstream location (at Vicksburg) is compared with the capability in simulating discharge at a more upstream location (at Chester). Large differences are shown between the downstream and upstream location. Based on the calculated Nash-Sutcliffe model efficiency coefficient it can be concluded that the observed mean discharge is a better predictor for upstream discharges than the model itself. Nevertheless, at the downstream location an average score of approximately 0.8 is a remarkably high difference in model performance.

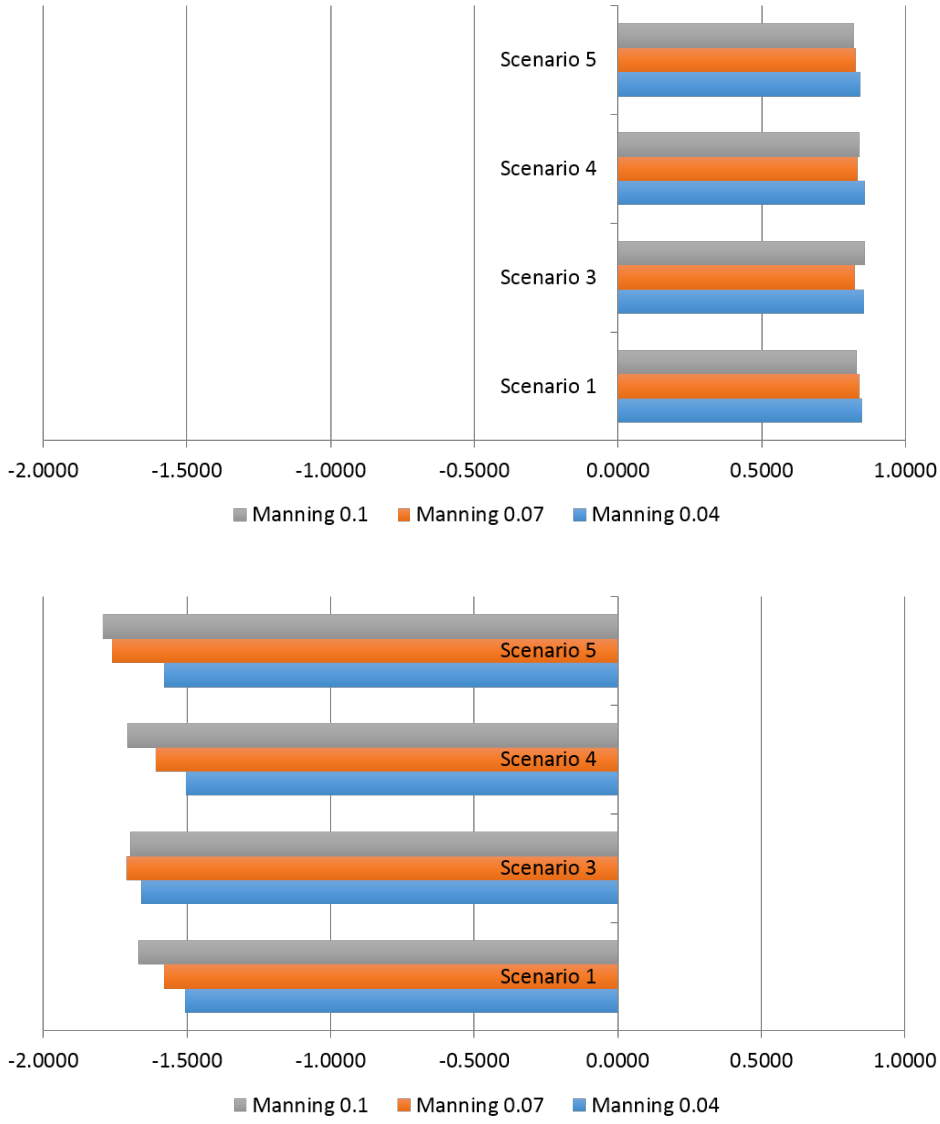

Figure 30. Nash-Sutcliffe model efficiency coefficient at Vicksburg (top) and Chester (bottom), based on the simulated discharge from PCR-GLOBWB and the observed discharge from the GRDC.

4.1.5 Effect of the Morganza Floodway

The effect of the Morganza Floodway on downstream areas is analyzed for the different scenarios, Table 6. It is shown that with this method the floodway has a large impact on the flooded fraction of the cell itself, but a small or even no impact on flooded fractions in downstream areas In the scenarios 1, 3 and 4 both discharge and flooded fractions are increasing instead of decreasing after including the floodway. In scenario 4 the largest differences in discharge occur. Here, the largest difference is around 500 m^3/s, which is still relatively small (0.9% of 55.000 m^3/s). Only in scenario 5 the floodway slightly reduces the discharge in downstream areas, but flooded fractions only reduce in the second downstream cell but in the other cells it increases. The largest impact, in scenario 5, could be explained by comparing the flooded fractions in the case with and without the floodway. Here, it is shown that in scenario 5 the largest difference (0.5764) between the flooded fractions occurs, compared to 0.0531, 0.1491 and 0.2867 in scenario 1, 3 and 4. This implies that more water can be stored in the cell of the floodway and therewith the impact increases. The negative impact in the other scenarios could result from the 50% reduction of channel capacity, which might be larger compared to the extra storage created by manually forcing of flooding.

Table 6. Effects of the Morganza Floodway on the flooded fraction and peak discharge at the location of the floodway itself and the three downstream cells in 1983 for the different scenarios. Italic flooded fractions indicate are open water fractions, which is the case when no flooding occurs.

1983	**Scenario 1**		**Scenario 3**		**Scenario 4**		**Scenario 5**	
Peak discharge [m^3/s]	Floodway	56.877	Floodway	56.793	Floodway	55.022	Floodway	57.178
	1	56.963	1	56.998	1	55.023	1	57.180
	2	56.956	2	56.861	2	54.663	2	56.984
	3	57.086	3	56.858	3	54.605	3	57.107
Peak discharge with floodway [m^3/s]	Floodway	56.885	Floodway	56.808	Floodway	55.450	Floodway	57.018
	1	56.974	1	57.005	1	55.490	1	57.067
	2	56.963	2	56.873	2	55.217	2	56.923
	3	57.094	3	56.872	3	55.195	3	57.038
Flooded fraction [-]	Floodway	0.7014	Floodway	0.5537	Floodway	0.4108	Floodway	*0.1990*
	1	0.3101	1	*0.0711*	1	*0.0777*	1	*0.0974*
	2	0.8355	2	0.7504	2	0.7302	2	0.6130
	3	0.8652	3	0.8051	3	0.7891	3	0.7948
Flooded fraction with floodway [-]	Floodway	0.7545	Floodway	0.7028	Floodway	0.6975	Floodway	0.6954
	1	0.3101	1	*0.0711*	1	*0.0777*	1	*0.0974*
	2	0.8356	2	0.7506	2	0.7339	2	0.7291
	3	0.8652	3	0.8052	3	0.7926	3	0.7945

4.2 Economic damage

After the output of the PCR-GLOBWB model is generated it is translated to economic damage by using a depth-damage relationship and a duration-damage relationship. The depth-damage relationship is used for damage to urban areas and is based on nightlight distribution, GDP, annual maximum inundation depths and annual maximum flooded fractions. The duration-damage relationship is used for agricultural areas and is based on the vegetation fractions, average price per bushel, bushels per ha, annual maximum flooded fractions, month of flooding and the duration of flooding.

4.2.1 Urban Damage

The combination of nightlight distribution and GDP (Figure 31 - left), the maximum annual inundation depths (Appendix 4 - Figure 45) and annual maximum flooded fractions, section 4.1.3, determine urban damage due to flooding.

Comparing inundation depths between the scenarios indicates that maximum inundation depths are decreasing in the main river or flooding even diminishes. In the cells outside the main river unexpected values occur, e.g. an inundation depth of approximately 16 m in all scenarios in the northwestern part of the watershed. In section 4.1.3 it was already shown that flooded fractions are also diminishing with increasing regulation measures. Due to both decreasing inundation depths and flooded fractions the simulated damage decreases per scenario (Figure 32). However, GDP strongly influence simulated damage, which results in increasing damage over time (Appendix 2 - Figure 44). These results are not as expected since damage is expected to occur during known historical flood events (1983, 1993 and 2008), but not during the entire period. This is strongly related to the findings in section 4.1.3, which explained the constant flooded fractions over the entire period in the most downstream cells and the cells outside the main channel.

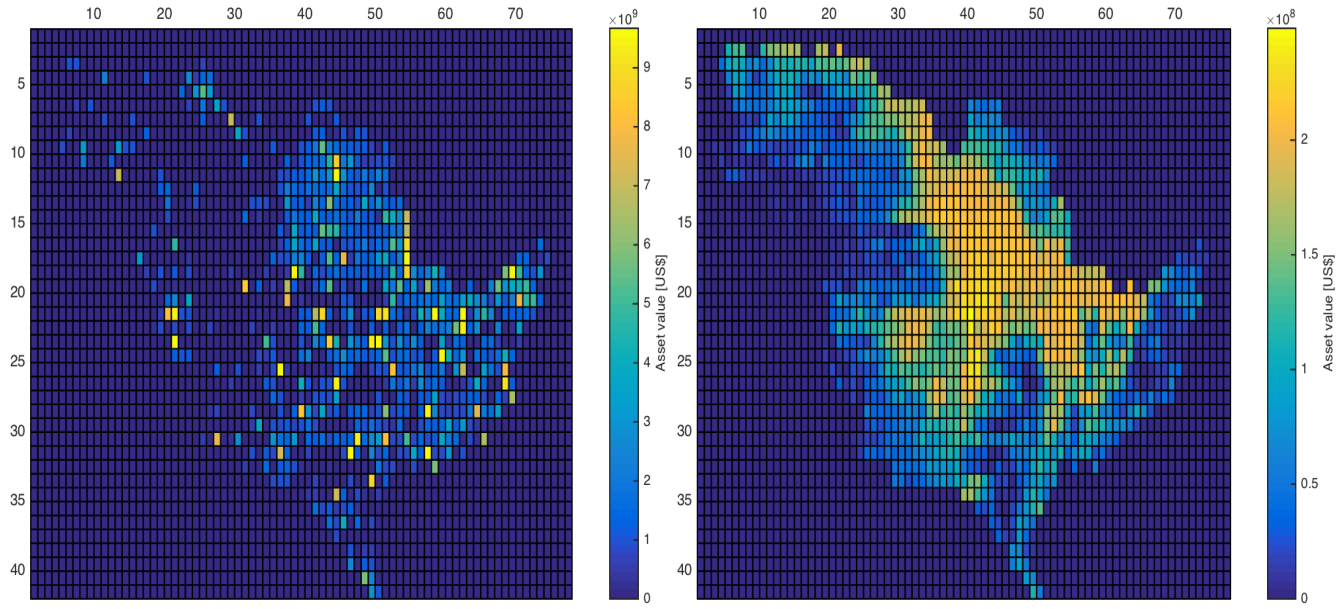

Figure 31. Distribution of urban assets with values based on the GDP in 1983 (left - *10^9) and agricultural assets (right - *10^8), which is equal over the entire simulated period.

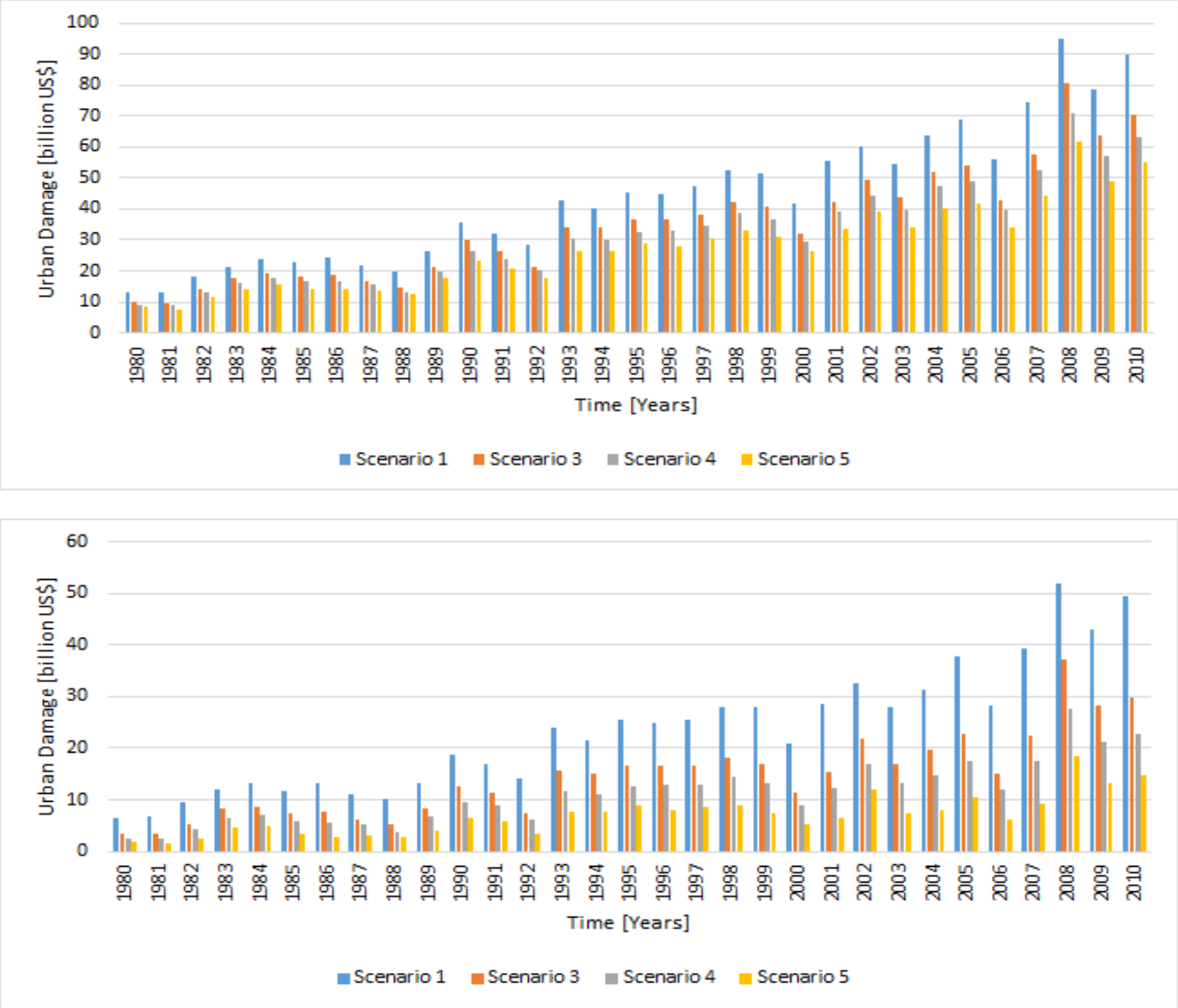

Figure 32. Annual maximum occurring urban damages in the period between 1980 and 2010 for the entire watershed (top) and the main river (bottom)

4.2.2 Agricultural Damage

The combination of vegetation fractions, average price per bushel, bushels per ha, annual maximum flooded fraction, month of flooding and the duration of flooding determines agricultural damage due to flooding. Here, vegetation fraction, average price per bushel and bushels per ha are equal for each scenario and year (Figure 31 - right). However, annual maximum flooded fraction, section 4.1.3, month of flooding (Table 7) and the duration of flooding (Appendix 4 - Figure 46) differ.

Most of the flooding already starts in the January, which is mainly the result of constant flooding in cells outside the main river cells. This is strongly related to the findings in section 4.1.3, which described a possible cause of large flooding in January. Early flooding of cells could result from underestimated original channel dimensions and therewith it results in an overestimation of the simulated economic damage.

Besides January it can be noticed that flooding mainly starts in the period between March and May. This is not as expected since the floodwave propagated downstream in the period between May and June, section 4.1.2. This could imply that flooding already starts with lower peak discharges or due to other unknown processes.

Table 7. First month of flooding per cell for the year 1983

	Jan	Feb	Mar	Apr	May	Jun	Jul	Aug	Sep	Oct	Nov	Dec
Scenario 1	1157	16	26	20	37	13	12	2	2	2	0	0
Scenario 3	1227	13	26	31	29	8	9	2	2	2	0	0
Scenario 4	1075	14	25	24	36	17	10	1	3	2	0	0
Scenario 5	1110	13	26	18	25	8	2	2	2	2	0	0

Due to constant simulated flooding, >100 days, when starting in the months without a duration-damage relationship, section 3.2.3, it is assumed that 100% of the yield is lost and therewith higher economic damages are simulated (Figure 33), compared to a situation where flooding starts within the expected months. As mentioned before, this is mainly due to early flooding of the cells outside the main river cells. Due to both decreasing inundation times and flooded fractions the simulated damage decreases per scenario. However, over the entire simulated period damages occur and these results are not as expected since damage is only expected to occur during known historical flood events (1983, 1993 and 2008). This is again strongly related to the unexpected findings in section 4.1.3, which described constant flooded fractions over the entire period in the most downstream cells and the cells outside the main channel.

Figure 33. Annual maximum occurring agricultural damages in the period between 1980 and 2010 for the entire watershed (top) and the main river (bottom)

4.2.3 Differences in agricultural and urban damage

Between the agricultural and urban method there are several differences. Besides analyzing inundation depths instead of month of flooding and duration of flooding other differences influence the difference in outcome. The urban method applies the depth-damage relationship on the value distribution, based on night light intensity and GDP in the year of flooding. With this method all GDP within the watershed (-agricultural percentage) is taken into account, whereas the agricultural method only considers the vegetation fraction to which soybeans belong, rainfed crops. The agriculture part of GDP lies between 1-1.5% of total GDP (Appendix 2 - Figure 44). The value of assets, on which both damage functions are applied largely differ (Figure 31) and therefore large differences arise in modeled economic damages. Due to the large differences in the value of assets it would be more profitable in all scenarios to decrease the pressure of flooding in urban areas by manually forcing flooding in agricultural areas.

The spatial distribution of agricultural assets is more widely spread over the watershed, compared to urban assets that are occurring within a limited amount of cells (Figure 34). This also results in a different spatial distribution of the simulated agricultural and urban damage (Figure 34). Again, agricultural damage is more widely spread and also occurs in more upstream areas (northwest), compared to urban damage. The agricultural damage also remains almost constant over time, which results from constant flooding in cells outside the main river cells and a constant unit price per bushel for soybeans. Urban damage changes over time, which is due to changes in asset values (=changing GDP). However, when an average value for GDP would be used in this method it would also result in damage that is more constant over time. In terms of US $ there is also a large difference noticeable. Urban damage is expressed in billions of dollar, compared to millions in case of agricultural damage. The exact differences between agricultural and urban damage during peak discharges in 1983, 1999 and 2008 are shown in Table 8 in section 4.2.4.

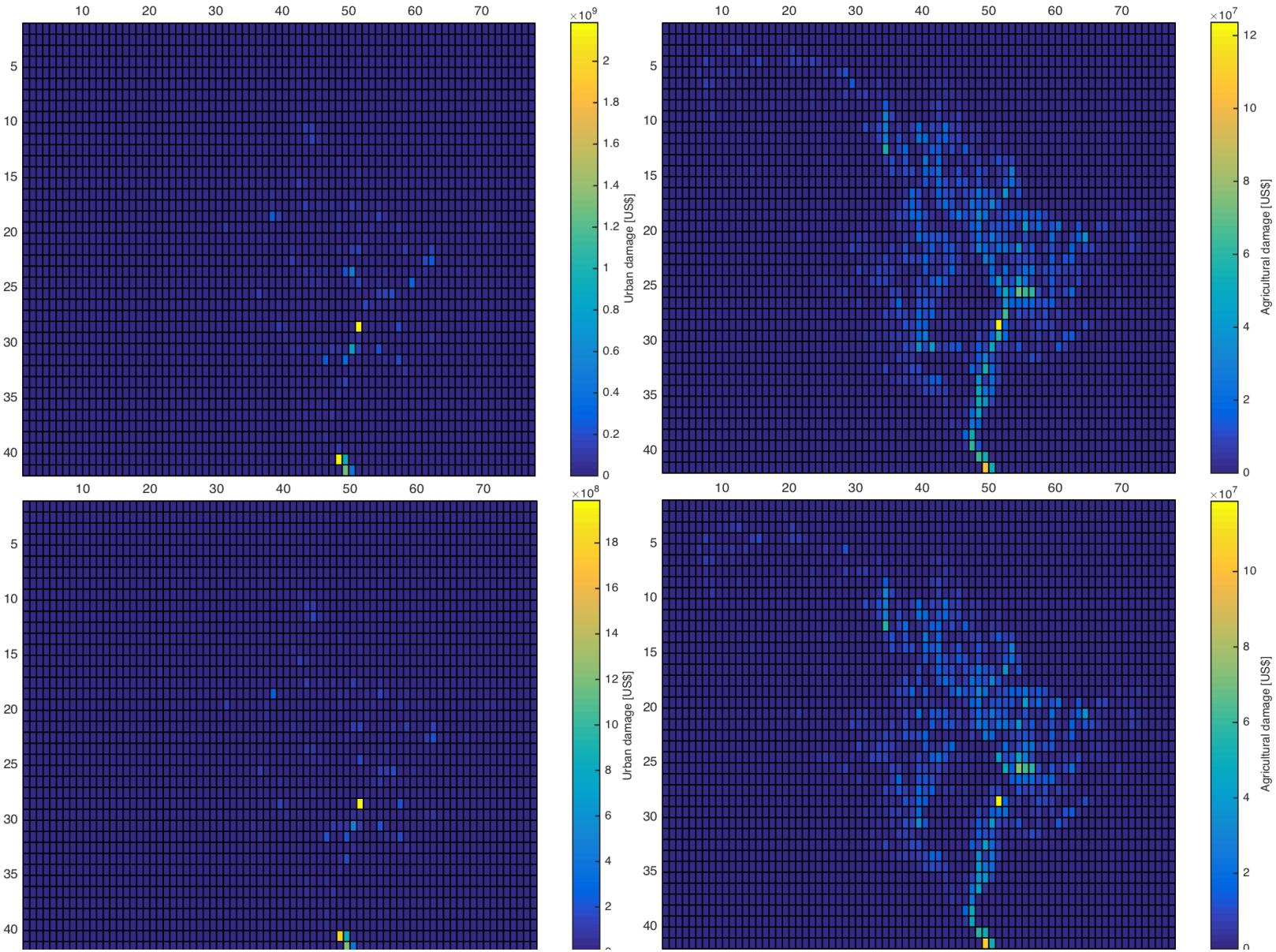
Urban damage [US$]
Agricultural damage [US$]
Urban damage [US$]
Agricultural damage [US$]

4.2.4 Validation of economic damage

Based on the comparison between the observed and simulated economic damage, Table 8, it can be concluded that large differences occur between observed and simulated damages. In scenario 5 simulated urban damages are exceeding the observed damages from EM-DAT with a factor 35 in 1983, 2.2 in 1993 and 6.2 in 2008. These factors are increasing in the scenarios with less regulation measures, scenario 1, 3 and 4.

On the other hand agricultural damage is overestimated in 1983 and underestimated in 1993 and 2008. Compared to the observed damages from EM-DAT the simulated agricultural damage in 1983 is a factor 17 higher in scenario 1. For 1993 and 2008 the simulated damages are underestimated with a factor 1.7 in 1993 and 1.38 in 2008. In scenario 3, 4 and 5 the overestimation in 1983 slightly decreases and the underestimation in 1993 and 2008 increases.

Furthermore, a remarkable difference is noticeable between the simulated damages for the entire watershed and the simulated damages in the main river cells. It is expected that the largest simulated damages would occur in the main river cells, which is not the case. The simulated urban damage improves when comparing it with the observed damage. The agricultural damage becomes more underestimated in the years 1993 and 2008, but the results in 1983 improve. However, due to the aforementioned uncertainties in the hydrological model it could be questioned if these results are useable.

Table 8. Economic damages during large flood events in the Mississippi Watershed

	Scenario 1			**Scenario 3**			**Scenario 4**			**Scenario 5**		
Year	**1983**	**1993**	**2008**	**1983**	**1993**	**2008**	**1983**	**1993**	**2008**	**1983**	**1993**	**2008**
NOAA [billion $]	0.016	15-20	-	0.016	15-20	-	0.016	15-20	-	0.016	15-20	-
EM-DAT [billion $]	0.400	12.29	10	0.400	12.29	10	0.400	12.29	10	0.400	12.29	10
Modeled Urban Damage [billion $]	22	43	95	18	34	81	16	30	71	14	27	62
Modeled Urban Damage (main river) [billion $]	12	24	52	8	16	37	6	12	28	5	8	19
Modeled Agricultural Damage [billion $]	6.896	6.980	7.225	6.193	6.269	6.404	5.805	5.84	5.945	5.379	5.452	5.5256
Modeled Agricultural Damage (main river) [billion $]	1.825	1.859	1.971	1.122	1.148	1.150	0.734	0.737	0.702	0.308	0.331	0.271

5 Discussion

5.1 Model setup and assumptions

5.1.1 PCR-GLOBWB

The main point of discussion in the PCR-GLOBWB model when analyzing a specific catchment area is the resolution of the model. When modeling an area with a resolution of 30 arc-min it is not possible to include full analysis of all ongoing processes. However, the model was developed for global analyses and therewith the computational time increases considerably with higher resolutions. The aim of this study was to mainly look at the potential impact of including river regulation in global modeling and therefore a single catchment was chosen to analyze this impact.

The model is used with default parameter settings, which was provided by the developer of the model L. P. H. van Beek. In this study no calibration is carried out and therefore the results might be improved after calibrating the model. PCR-GLOBWB also allows settings that have not been used, such as the inclusion of reservoirs and lakes. In this study the water bodies (reservoirs and lakes) are misaligned relative to the flow direction map that is used and therefore water bodies could not be included. Since the upper part of the Mississippi watershed is strongly regulated for e.g. flood regulation (Alexander et al., 2012), this could be of a major influence on simulated discharges and flooded fractions. In terms of discharge the peaks could considerably be reduced and therewith flooded fractions would reduce. Also, in PCR-GLOBWB only two values for the Manning coefficient (roughness coefficient) can be included, for the river itself and the floodplains. Including the dikes and floodplains in the channel capacity has resulted in a combination of these two values and therewith only one value of the Manning coefficient. The original settings, where a distinction was made between the river and the floodplains, could already improve the routing process, but due to method in this study this was not possible.

5.1.2 Channel Dimensions

In PCR-GLOBWB a consistent bankfull river depth and width are created based on a fitted relationship for 343 stations, excluding the territory of the USA and therewith the Mississippi. In Andreadis et al. (2013) it is also shown that, when applying this method, the Mississippi watershed has one of the larger errors (25.6%). In addition, based on this method the largest width of the channel occurs in downstream areas, since the highest discharges occur downstream. However, in the downstream area of the Mississippi watershed, at Baton Rouge (just upstream of New Orleans), the width of the channel is smaller compared to more upstream locations (Smart, 2015). Comparing the simulated width at Baton Rouge with the actual width results in a difference of (2600 m – 700 m) 1900 m. In Louisiana (the state in which Baton Rouge is located) the actual width strongly varies. The largest width is approximately 2315 m and the smallest width is approximately 518 m (Smart, 2015). The simulated width in the model thus overestimates the actual width of the channel.

The estimated depth however is more difficult to compare with depths from literature, which could be caused by backwater effects from the Gulf of Mexico and dredging for commercial navigation. The depths based on the fitted relationship are approximately 9 m at New Orleans, compared to depths of a maximum of 60 m (Klinkenberg, 2014). Further upstream, just downstream of the confluence of the Ohio River and the Mississippi River, simulated depths are around 8.5 m, compared to observed depths between 15 and 30 m.

After analyzing the database of cross-sections some remarks could be made. The database consists of a large amount of cross-sections, but due to the low resolution of the model only one mean value for dike height can be

used per grid cell. Secondly, besides the primary dikes along the river, secondary dikes were also included after selecting the cross-sections within a buffer along the Mississippi River. This has resulted in a lower mean dike height, therewith a lower capacity and earlier occurring floods. Subtracting the mean highest from the mean lowest dike height reduces the impact of secondary dikes, but dike heights would be higher if these were not included at all.

Furthermore, the width of the floodplains is an important factor in determining the capacity of the Mississippi. This width is based on the locations of the dikes and the centerline of the river. It can be questioned if this centerline is exactly in the center of the river and therewith if it is a reasonable width of the floodplain. Although, in this study it is assumed that the centerline is correct. In addition, the centerline was only available for the lower section of the Mississippi. Therefore, a method had to be developed to be able to determine the width of the floodplains in the cells without a centerline, section 3.3.2. In some cells this could have given an over- or underestimation of the width of rivers (+floodplains). In Figure 35 an example of a cell without a centerline and which is overestimated by multiplying the original width with an average factor. The width of the lower green cell is 4250 m, compared to a width of 1600 m in the downstream cell and a width of 1700 m in the upstream cell (both orange).

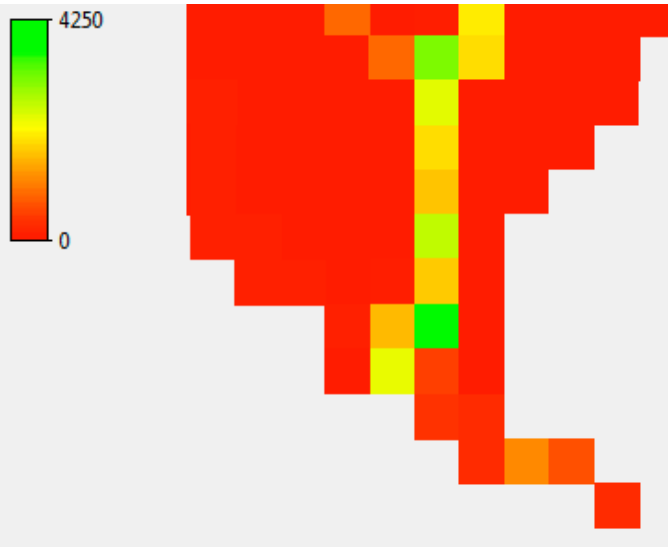

Figure 35. Overestimation of channel width, lower green cell

The impact of the floodway is analyzed by reducing the channel capacity with 50%, which is a randomly chosen percentage. This could be changed or a different method could be analyzed in following studies.

5.1.3 Flood module

In the original model the difference the relative elevation between the cells of the HYDRO1K 1*1 km and the associated river cell where the only barrier in preventing flooding. During this study it was also considered to change elevations within the HYDRO1K digital elevation map. In this way different dike heights could be applied within a 50*50 km (30 arc-min) cell and therewith a more realistic profile would be implemented. However, due to the cumulative distribution of all relative elevation heights, cells behind cells with a higher elevation could still be flooded. With this method the dikes would not be included correctly, which resulted in the channel capacity to be the only part in which dike heights and the width of floodplains could be included. As mentioned before, this resulted in a combined Manning coefficient for both the channel and the floodplains. The floodplains still have

their own Manning coefficient in the model, but this value is only used after the combined capacity of the channel and the floodplains is exceeded.

In the model flooding occurs after the capacity of both the river and the capacity between the dikes is exceeded. However, in the floodplains of the Mississippi agriculture already exists, which means that the damage to crops would already occur during lower water levels (NWF, 2011).

5.1.4 External errors in hydrological modeling

Besides the impact of the changed channel capacities and changed friction levels other included or excluded components could also influence the model results. The amount and timing of rainfall determines to a large extent the timing and intensity of discharge peaks and therewith meteorological forcing might be an even larger uncertainty in modeling flood waves. Van Beek et al. (2011) described spatiotemporal variation in station density as a cause of uncertainties, but the bias in precipitation is the largest error in hydrological models. In the Mississippi watershed withdrawals and diversions may also impact the model performance. In this study only the largest floodway is analyzed per scenario with the best-fitted hydrographs, but other diversions and withdrawals are neglected. Furthermore, the natural flows in regulated watersheds differ from the observed discharge due to the impact of reservoirs and withdrawals. In this study the reservoir operation schemes and withdrawals are not included. Therewith, the model is more sensitive to uncertainties in model parameterization affecting processes, such as the regulation of discharge by reservoirs (Candogan et al., 2012).

Other uncertainties in PCR-GLOBWB are described in more detail in Van Beek et al. (2011). Also, during the floods of e.g. 1993 dike breaches occurred (Mcconkey et al., 1994), which resulted in lower discharges and a different way of propagation in downstream areas and therewith it could have resulted in a different economic impact on both urban and agricultural areas.

5.1.5 Nightlight intensity method

The nightlight intensity method is used in Climada to determine the distribution of assets in a certain country. Due to the lower resolution of PCR-GLOBWB the data had to be resampled. In the resampling process an average value per cell is defined, based on the bilinear technique in ArcGIS. Due to the lower resolution of PCR-GLOBWB certain large cities, such as New Orleans, are not represented as they should be, which result in lower allocated values and therewith lower economic damage. Furthermore, the nightlight intensity of 2013 is used for all modeled years, which could result in a less accurate value distribution in certain years. The quality of value distribution based on the nightlight data is analyzed by comparing measured and modeled GDP per state (Figure 36). This represents the lack of accuracy of nightlight data. The largest differences are noticeable in Wisconsin, Iowa and Minnesota, which all belong to the states with the highest productivity in agriculture (USDA, 2015b). Agriculture is taken into account, since in no nightlight is present in large agricultural fields. Bickenbach et al. (2013) also shows that the relationship between nightlight and GDP data is unstable and therewith a poor proxy of regional economic activity. These findings are not just for areas where regional GDP data might be unreliable, but also in areas with high quality GDP data, such as the Mississippi area. Applying the observed GDP the simulated economic damage would still be questionable, because the main errors occur in the global hydrological model, section 4.1.3. However, there are large differences between the observed and simulated GDP and this could have a large impact after optimizing the global hydrological model. Furthermore, not all parts of GDP are prone to flooding. In Jongman et al. (2012) the maximum damage per square meter is determined. The depth-damage method is applied on these values instead of a certain part of GDP belonging to a cell based on the nightlight distribution. Here, exposure is determined by calculating the urban area in flood prone areas. This could give a

more realistic image of the values per cell and therewith a more realistic outcome of urban economic damage. This method was not applied in this study since one of the purposes of this study was to analyze if the nightlight intensity method in Climada could be an improvement in comparison to the method of Jongman et al. (2012). It can be concluded that the nightlight intensity method is less accurate, since it only takes areas with access to electricity into account, it overestimates the potential damage (not all GDP is prone to flooding) and furthermore it does not give an accurate distribution of GDP (Bickenbach et al. 2013).

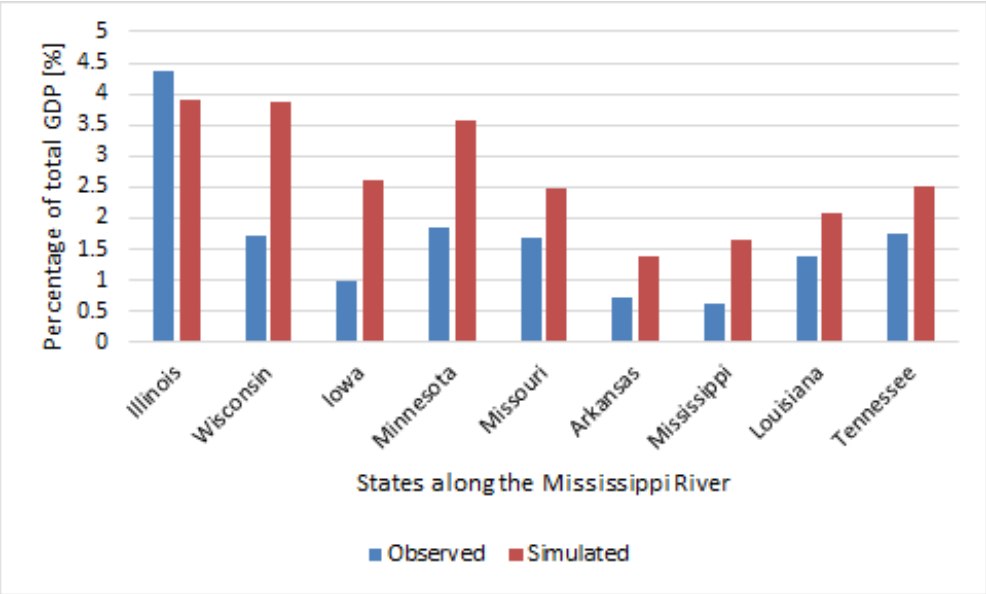

Figure 36. Simulated and observed percentages of total GDP for the different states along the Mississippi River.

The distribution of values can be based on a default non-linear or linear relationship in Climada (Appendix 2 - Figure 41). In Climada (Bresch, 2014) it is mentioned that a relation can be developed for individual cases, which is not done during this study. Therefore, the used default linear relationship does not exactly gives value distribution for North America.

5.1.6 Damage functions

The simulated economic damage in urban areas is only based on a single general depth-damage function, section 3.2.3, while these functions can strongly differ per type area. Pistrika et al. (2014) describes that it remains an open issue whether specific depth-damage function can be applied on other regions with similar climates and building conditions. Furthermore, the used depth-damage function is based on historical records of flood damages on different type of buildings and not on GDP. However, in this study and in the method in Climada the depth-damage function is applied on GDP and not on urban assets.

In determining the economic damage in the agricultural business, a duration-damage function is used for only the most common crop in the area, soybeans. Furthermore, production costs are not taken into account (USACE, 1985) and only one average price per unit is used for the entire simulated period. Also, in the months without a duration-damage function it is randomly chosen to simulate no damage until 100 days and after 100 days of flooding it is assumed that no agricultural activity can take place in the associated year and therewith 100% damage. Additionally, the maximum flooded fraction and the maximum inundation time per year are used to determine yearly agricultural damage, but these two aspects could occur at different times and therewith it could result in higher agricultural damages.

A more detailed map of different type of land use, as used in Jongman et al. (2012) could improve the estimation of economic damage due to flooding in general. Here, different types of damage functions are applied per type of land-use. Using this method would also provide a more comprehensive method to be able to make a trade-off between high pressure on urban areas and manually forcing of floods, with floodways, in areas with higher fractions of agriculture.

Also, Bremond et al. (2013) did an economic evaluation of flood damage to agriculture and found that besides flood duration and seasonality, water depth, velocity, deposits, contamination and salinity of water are important flood parameters in determining the economic damage after a flood. These flood parameters are not included in this study.

5.2 Model results

Changing the original channel dimensions, based on the National Levee Database, did not show large improvements based on the Nash-Sutcliffe model efficiency coefficient. With this method the general flow pattern over the years is analyzed by comparing the discharge per day. Changes in channel dimensions and in the Manning coefficient only have a small impact on the flow pattern and therewith no large changes in the NSE score will be noted. However, a combination of the aforementioned measures does impact peak discharges. Larger channel dimensions result in higher peak discharges compared to observed discharges and the effect of the Manning coefficient on peak discharges increases as channel dimensions increase. These changes could be noticed in hydrographs but with the NSE score these differences are not noticeable.

Besides the impact on peak discharges it also reduces the flooded area in the watershed. Where, original settings gave constant flooding over a period of 30 years, the new scenarios give more realistic floods, flood events instead of constant flooding. However, large historical floods consisted for a large part of dike breaches and in this model dikes are unbreakable. Therefore, it is hard to validate the simulated distribution of flooded areas. Furthermore, seepage under dikes is not included and this was also significant during historical floods, as it continued long after the peak discharge and caused extended periods of inundations (Jacobson, 1993).

The simulated flooded fractions are more realistic after including dikes and floodplains, since it represents flood events instead of constant flooding. However, due to e.g. the presence of secondary dike heights in the National Levee Database the capacity of downstream cells is low compared to the more upstream cells. This has resulted in higher flooded fractions in all the different scenarios and therewith also higher economic damages. A selection of the primary dike heights could improve further analysis. Due to uncertainties in channel dimensions, therewith early flooding of cells, the translation of simulated floods to economic damage is questionable.

The floodway is included in the model by reducing its capacity with 50%. However, in this manner the associated cell is constantly flooded. Van der Knijff & de Roo (2008) analyzed the impact on regulation measures for floods in the Elbe. They concluded that during a longer flood wave the impact on the peak discharge was considerably lower. Reducing the capacity with 50% result in constant flooding and this could be the reason why no impact on the peak discharge is shown between the situation with and without the floodway. In addition, it might have resulted from a larger decrease in storage capacity in the channel than an increase in storage capacity due to manually forced flooding.

The simulated flooded area and economic damage in the cells outside the main river cells is in both cases large, which is not as expected (Figure 37). In these cells no regulation measures are taken into account, but small dikes

could still be present in these areas. Therefore, in further studies it should be interesting in taking into account regulation measures for all cells instead of only the main river cells. However, datasets are mainly available for the main river sections and therewith not all information will be available. This would especially be the case in more developing regions (Jongman et al., 2012). Since, the model is developed to give an idea about potential flooding and economic damages on a global scale it should be questioned if this level of "detail" should be included. This level of detail is still lacking compared to other basin scale models. However, this is also not the main goal of this model, since it is a global hydrological model that requires data on a global basis. An example of a higher resolution model of the Mississippi River is the Noah-MP model (Cai et al., 2014). This model is using meteorological forcing at 0.125-degree spatial resolution and an hourly temporal resolution compared to the 0.5-degree spatial resolution and daily temporal resolution of the PCR-GLOBWB model. In these types of models a more realistic distribution of dike heights and floodplains could be included, but these models are computationally intensive.

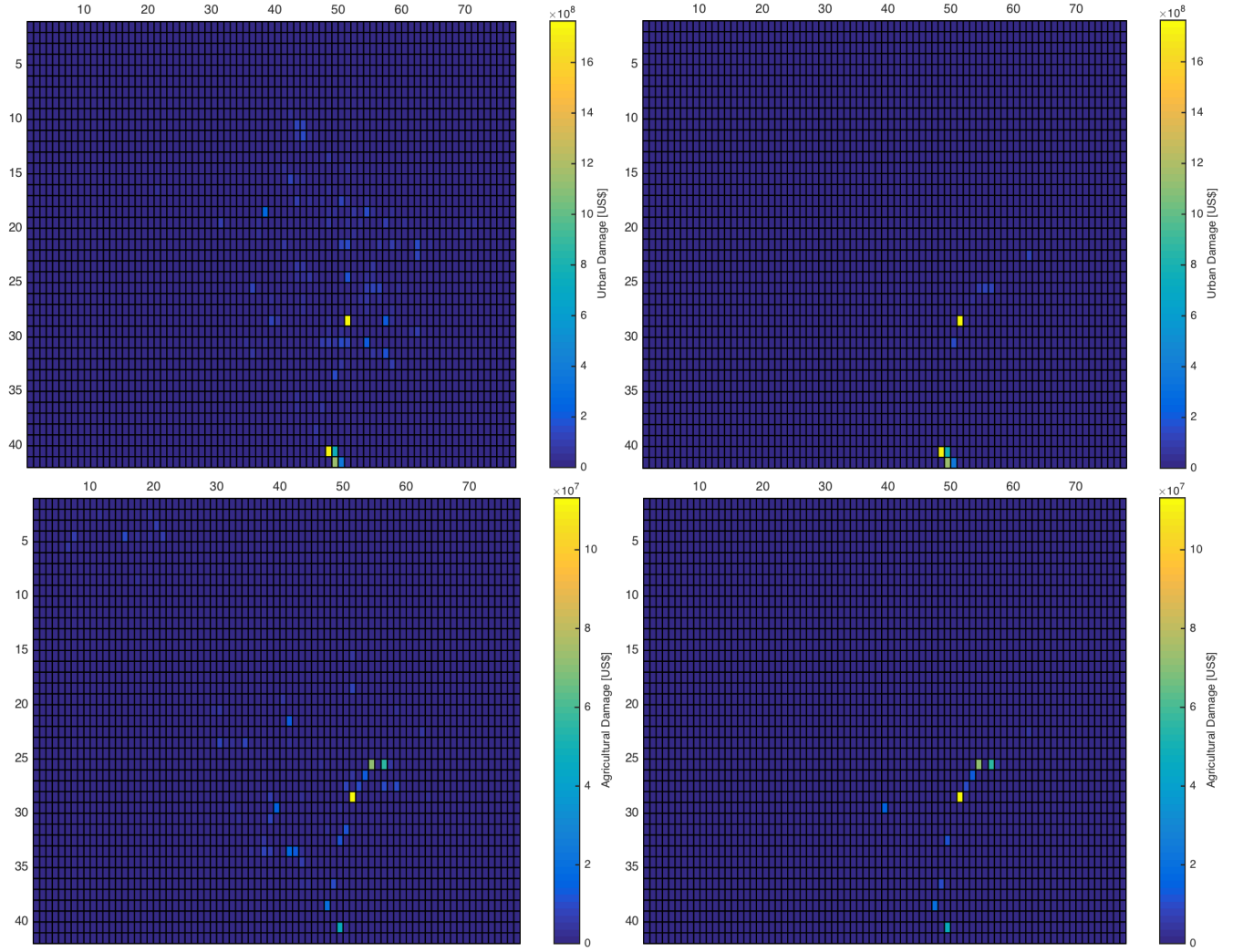

Figure 37. Spatial distribution of urban damages (top - *10^8) and agricultural damages (bottom - *10^7) for the entire watershed (left) and the main river (right)

6 Conclusion

This study has presented a first attempt at including dikes and floodways in global hydrological modeling by using the global hydrological model PCR-GLOBWB and the National Levee Dataset of the U.S. Army Corps of Engineers. Channel and floodplain dimensions are adjusted, which has influenced the characteristics of hydrographs and riverine flooding. The model has been applied on the Mississippi River to analyze the effects of river regulation on global river flood risk assessments. This allows answering of the main question and sub-questions of this study, which is done below. First, a distinction is made between two parts of the main question, namely a hydrological part and an economic part, each consisting of one overarching question and three sub-questions. This allows us to provide a complete answer to the main question, which is:

What are the impacts of river regulation on discharge and flooding in global hydrological modeling?

6.1 Hydrological impacts

The first part of the main question describes the hydrological impacts of river regulation, by answering the associated question:

1. What are the impacts of river regulation on discharge and flooding in global hydrological modeling?

1.1 How does river regulation influence discharge and flood wave propagation?

In general, after the inclusion of the dike heights along the Mississippi in the PCR-GLOBWB model, the discharge at mainly the downstream location, Vicksburg, increased considerably, which can be explained by the increased capacity. However, after increasing the Manning coefficient the peak is reduced to the height of the peak with the original settings. The impact of the Manning coefficient increases per scenario, since the depth and width are increasing and therewith the wetted perimeter. Changes in floodwave propagation are small. Only a small shift over time, a few days, is noticeable and the peaks are higher compared to the original situation.

1.2 How does river regulation influence flooding in terms of flood extent, flood depth and time of occurrence?

Furthermore, comparing the scenarios with river regulation with the original settings results in considerably less days of flooding and lower flooded fractions. Less flooded volume results in lower flooded fractions, but the inundation depths might be still equal in some cells, because the volume is divided over a smaller area.

1.3 Does the inclusion of river regulation improve the model performance in reproducing discharge (GRDC), compared to the original settings?

The Nash-Sutcliff model efficiency coefficient (NSE) does not give a complete indication of the model in modeling peak discharges, since it mainly compares daily simulated and observed discharges over a period of 30 years (in this study). Peaks only occur in small parts of this period and therefore the NSE score does not represent the differences in peak discharges, while changes in channel dimensions and Manning coefficients mainly affect the peaks. Therefore, based on the NSE score no distinction can be made between the different scenarios. However, when analyzing the height of the peaks in the hydrographs it can be noted that including dikes and floodplains result in higher peak discharges and by increasing the Manning coefficient the peak discharge decreases to a discharge similar to the observed discharge.

6.2 Economic impacts

The second part of the main question describes the economic impacts of river regulation, by answering the associated question:

2. How does river regulation influence expected damage?

2.1 What is the difference in economic damage, while including river regulation, based on the method used in Climada?

In the first part of the conclusion the impact on days of flooding and flooded fraction is already described and this is strongly related to the expected damage. In the original model flooding occurred over the entire modeled period and due to regulation measures this is reduced to a limited amount of days and lower flooded fractions. However, the translation of flooding from the PCR-GLOBWB model to urban and agricultural damage could be questioned, since flooding is constantly occurring in the downstream cells of the main river and in the cells outside the main river cells flooding constantly occurs. This has resulted in unexpected annual damages in both the agricultural and urban damage method.

2.2 What is the difference in expected damage between urban flooding (depth-damage functions) and agricultural flooding (duration-damage functions)?

The difference between these two methods is mainly noticeable in the asset values on which the damage relationships are applied. The urban damage method is applied on asset values, which are generated based on the total GDP and its distribution is based on the nightlight intensity. This compared to the agricultural damage method that only looks at soybeans. Due to these differences the depth-damage method results in economic damages that are several orders higher.

2.3 To what extent can historical economic damages (EM-DAT) be reproduced with the method used in Climada?

Comparing the modeled economic damage and the observed damages in the years of major flooding result in large differences. Estimated urban damage is largely overestimated in all scenarios, even in the scenario 5, which has the most radical regulation measures. This is again related to the fact that regulation measures are only applied on the main river cells and therewith the situation of all other cells is still equal to the original model settings. This results in constant flooding of these cells and therewith annual occurring economic damages.

Concluding, the inclusion of river regulation in global hydrological models gives a more realistic pattern of flooding events over the analyzed period. However, the inclusion of regulation measures requires further investigation, since unexpected flood events are still occurring. The combination of the nightlight intensity method with GDP is questionable since the value distribution is only focused on urban areas and not all parts of GDP are prone to flooding. The duration-damage method should be further developed by including more types of crops and by including other components, such as e.g. production costs.

6.3 Recommendations

The following recommendations can be used for any studies that want to improve upon the work presented in this thesis:

1. There differences in flooded areas and economic damages over the years is small, constantly flooded, compared to a situation where flooding only occurs in the years with more extreme weather conditions. Mainly in the areas outside the main river cells and in the most downstream cells of the main river unexpected results are shown and therefore the processes that result in flooding in these areas should be further analyzed. Firstly, an attempt should be made in improving the methods that are used for defining channel dimensions (depth, width and length), since too low channel capacities could be the cause of constant flooding over the years.
2. Use an improved database where only the main cross-sections along the Mississippi River are included, since in the current dataset secondary dikes are also included. Therewith a more representative situation could be developed.
3. Repeat the methods in PCR-GLOBWB 2.0 (5 arc-min) to get a more detailed distribution of dike heights and width of floodplains and therewith a more detailed distribution of flooding.
4. Further develop the land-use method used by Jongman et al. (2012), since with this method a distinction can be made between different type of land-use and therewith different damage functions can be applied. This combination could result in a better estimator of economic damage compared to the nightlight intensity method.
5. In the simulations in this study reservoirs and lakes are excluded, while these could have a large impact on the attenuation of peaks. A correct local drainage direction (ldd) map with reservoirs and lakes should be included to analyse the effects.

7 References

Alexander, J. S., Wilson, R. C., & Green, W. R. (2012). *A Brief History and Summary of the Effects of River Engineering and Dams on the Mississippi River System and Delta*.

Allen, P. M., Arnold, J. C., & Byars, B. W. (1994). Downstream Channel Geometry for use in Planning-Level Models. *Journal of the American Water Resources Association*, *30*(August), 663–671. doi:10.1111/j.1752-1688.1994.tb03321.x

Andreadis, K. M., Schumann, G. J. P., & Pavelsky, T. (2013). A simple global river bankfull width and depth database. *Water Resources Research*, *49*(10), 7164–7168. doi:10.1002/wrcr.20440

Bickenbach, F., Bode, E., Lange, M., & Nunnenkamp, P. (2013). Night Lights and Regional GDP, (1888). Retrieved from http://www.ifw-members.ifw-kiel.de/publications/night-lights-and-regional-gdp/KWP_1888.pdf

Bierkens, M. F. P., & Van Beek, L. P. H. (2009). Seasonal Predictability of European Discharge : NAO and Hydrological Response Time, 953–968. doi:10.1175/2009JHM1034.1

Bremond, P., Grelot, F., & Agenais, A. L. (2013). Review Article : Economic evaluation of flood damage to agriculture – review and analysis of existing methods. *Natural Hazards and Earth System Science*, *13*, 2493–2512. doi:10.5194/nhess-13-2493-2013

Bresch, D. N. (2014). *Climada module GDP entity*. Retrieved from https://github.com/davidnbresch/climada_module_GDP_entity/blob/master/docs/climada_module_GDP_entity.pdf

Bresch, D. N. (2015). *Climada Manual*.

Cai, X., Yang, Z. L., David, C. H., Niu, G. Y., & Rodell, M. (2014). Hydrological evaluation of the Noah-MP land surface model for the Mississippi River Basin. *Journal of Geophysical Research: Atmospheres*, *119*(1), 23–38. doi:10.1002/2013JD020792

Candogan Yossef, N., van Beek, L. P. H., Kwadijk, J. C. J., & Bierkens, M. F. P. (2012). Assessment of the potential forecasting skill of a global hydrological model in reproducing the occurrence of monthly flow extremes, 4233–4246. doi:10.5194/hess-16-4233-2012

Candogan Yossef, N., Winsemius, H., Weerts, A., van Beek, L. P. H., & Bierkens, M. F. P. (2013). Skill of a global seasonal streamflow forecasting system , relative roles of initial conditions and meteorological forcing, *49*(August), 4687–4699. doi:10.1002/wrcr.20350

Ceola, S., Laio, F., & Montanari, A. (2014). Satellite nighttime lights reveal increasing human exposure to floods worldwide. *Geophysical Research Letters*, 7184–7190. doi:10.1002/2014GL061859.Received

Chow, V. T., Maidment, D. R., & Mays, L. W. (1988). *Applied Hydrology* (McGraw-Hil.). New York: McGraw-Hill: New York.

Coblentz, B. (2014). Record soybean yield is valued at 1.17 billion dollar. *Mississippi State University - Office of Agricultural Communications*. Retrieved June 24, 2015, from http://msucares.com/news/print/agnews/an14/20141219soybeans.html

COMET. (2010). Streamflow Routing. Retrieved August 17, 2015, from http://stream2.cma.gov.cn/pub/comet/HydrologyFlooding/StreamflowRoutingInternationalEdition/comet/hydro/basic_int/routing/navmenu.php_tab_1_page_6.3.0.htm

CRED. (2015). The International Disaster Database. Retrieved August 28, 2015, from http://www.emdat.be/database

CRU. (2014). High-resolution gridded datasets (and derived products). Retrieved August 17, 2015, from http://www.cru.uea.ac.uk/cru/data/hrg/

Davis, S. A., & Skaggs, L. L. (1992). *Catalog of Residential Depth-Damage Functions - Used by the Army Corps of Engineers in Flood Damage Estimation*. Ft. Belvoir, Virginia, U.S.A. Retrieved from http://planning.usace.army.mil/toolbox/library/IWRServer/92-R-3.pdf

De Moel, H., Asselman, N. E. M., & Aerts, J. C. J. H. (2012). Uncertainty and sensitivity analysis of coastal flood damage estimates in the west of the Netherlands. *Natural Hazards and Earth System Science*, *12*(4), 1045–1058. doi:10.5194/nhess-12-1045-2012

Dee, D. P., Uppala, S. M., Simmons, A. J., Berrisford, P., Poli, P., Kobayashi, S., … Dee, D. P. (2011). The ERA-Interim reanalysis : configuration and performance of the data assimilation system, (April), 553–597. doi:10.1002/qj.828

Dermody, B. J., van Beek, R. P. H., Meeks, E., Klein Goldewijk, K., Scheidel, W., van der Velde, Y., … Dekker, S. C. (2014). A virtual water network of the Roman world. *Hydrology and Earth System Sciences Discussions*, *11*(6), 6561–6597. doi:10.5194/hessd-11-6561-2014

ECMWF. (2003). ERA-40 dataset (Sep 1957 - Aug 2002). *The European Centre for Medium-range Weather Forecasts*. Retrieved August 9, 2015, from http://www.ecmwf.int/en/forecasts/datasets/era-40-dataset-sep-1957-aug-2002

English, B. C., Menard, J., Wilson, B., Mcclure, A., Main, C., Totty, B., … Lambert, D. (2012). *The Effects of Occasional Flooding of Tennessee Agricultural Lands: Pickwick Dam Case Study*. Knoxville. Retrieved from http://aimag.ag.utk.edu/pubs/Pickwick_v5.pdf

FAO. (1997). VMAP0, Perennial Inland Water Areas of the World. *Food and Agriculture Organization of the United Nations*. Retrieved October 25, 2015, from http://www.fao.org/geonetwork/srv/en/main.home?uuid=c0c0dfa0-88fd-11da-a88f-000d939bc5d8

FEMA. (2015). *Multi-hazard Loss Estimation Methodoly*. Washington, D.C.

Gierk, M., & de Roo, A. (2008). *The impact of retention polders , dyke-shifts and reservoirs on discharge in the Elbe river; Hydrological modelling study in the framework of the Action Plan for the Flood Protection in the Elbe River Basin of the International Commission for the Protecti*. Luxembourg. doi:10.2788/68635

Jacobson, R. B. (1993). *Geological Survey Circular*. Denver: USGS. Retrieved from https://books.google.nl/books/reader?id=ePUkAQAAIAAJ&printsec=frontcover&output=reader&pg=GBS.PP8

Jongman, B., Kreibich, H., Apel, H., Barredo, J. I., Bates, P. D., Feyen, L., … Ward, P. J. (2012). Comparative flood damage model assessment: Towards a European approach. *Natural Hazards and Earth System Science*, *12*(12), 3733–3752. doi:10.5194/nhess-12-3733-2012

Jongman, B., Ward, P. J., & Aerts, J. C. J. H. (2012). Global exposure to river and coastal flooding : Long term trends and changes. *Global Environmental Change*, *22*(4), 823–835. doi:10.1016/j.gloenvcha.2012.07.004

Kammerer, J. C. (1990). *Largest Rivers in the United States*.

Klinkenberg, D. (2014). Mississippi River Facts - River Geology. *Mississippi Valley Traveler*. Retrieved September 17, 2015, from http://mississippivalleytraveler.com/river-geology/

Kowalski, C. (2015). Soybean Planting and Harvest Seasons. *About.com*. Retrieved June 24, 2015, from http://commodities.about.com/od/profilesofcommodities/a/soybean-growing.htm

Kundzewicz, Z. W., Kanae, S., Seneviratne, S. I., Handmer, J., Nicholls, N., Peduzzi, P., … Sherstyukov, B. (2013). Flood risk and climate change: global and regional perspectives. *Hydrological Sciences Journal*, *59*(1), 1–28. doi:10.1080/02626667.2013.857411

Leopold, L. B. (1994). *A view of the river*. Cambridge: Harvard University Press.

Loos, S., Middelkoop, H., van der Perk, M., & van Beek, L. P. H. (2009). Large scale nutrient modelling using globally available datasets : A test for the Rhine basin. *Journal of Hydrology*, *369*(3-4), 403–415. doi:10.1016/j.jhydrol.2009.02.019

Luo, T., Maddocks, A., Iceland, C., Ward, P., & Winsemius, H. (2015). World's 15 Countries with the Most People Exposed to River Floods. *World Resources Institute*. Retrieved June 11, 2015, from http://www.wri.org/blog/2015/03/world's-15-countries-most-people-exposed-river-floods

Mcconkey, S., Allan, K., & Pollock, B. (1994). *1993 Mississippi River Record Stages and Levee Failures along the Illinois Border*.

Meade, R. H. (1995). *Contaminants in the Mississippi River, 1987-92*.

Merz, B., Kreibich, H., Schwarze, R., & Thieken, A. (2010). Review article " Assessment of economic flood damage ," 1697–1724. doi:10.5194/nhess-10-1697-2010

Mississippi River Commission (MRC). (2007). *The Mississippi River and Tributaries Project: Floodways*.

Nash, E., & Sutcliffe, V. (1970). River Flow Forecasting Through Conceptual Models - Part 1 - A Discussion of Principles. *Journal of Hydrology*, *10*, 282–290.

NASS. (2015). Charts and Maps. *United States Department of Agriculture - National Agriculture Statistics Service*. Retrieved July 27, 2015, from http://www.nass.usda.gov/Charts_and_Maps/Crops_County/

National Park Service. (2015). Mississippi RIver Facts. Retrieved June 17, 2015, from http://www.nps.gov/miss/riverfacts.htm

National Research Council. (2008). *Mississippi River Water Quality and the Clean Water Act*. Washington, D.C. Retrieved from http://www.nap.edu/catalog/12051/mississippi-river-water-quality-and-the-clean-water-act-progress

NCAR. (2015). Climate Data Sets. *The National Center for Atmospheric Research*. Retrieved June 19, 2015, from https://climatedataguide.ucar.edu/climate-data

New World Encyclopedia. (2014). Mississippi River. *New World Encyclopedia*. Retrieved August 20, 2015, from http://www.newworldencyclopedia.org/entry/Mississippi_River

NOAA. (2011). High Flows and Flood History on the Lower Mississippi River. *National Weather Service Weather Forecast Office*. Retrieved September 21, 2015, from http://www.srh.noaa.gov/lix/?n=ms_flood_history

NOAA. (2014). Version 4 DMSP-OLS Nighttime Lights Time Series. *National Centers For Environmental Information*. Retrieved June 25, 2015, from http://ngdc.noaa.gov/eog/dmsp/downloadV4composites.html

NWF. (2011). *Mississippi River Flooding - Natural Solutions for an Unnatural Disaster - A Blueprint for Strengthening Nature's Defenses to better Protect People and Communities along the Mississippi River*. Retrieved from http://blog.nwf.org/wp-content/blogs.dir/11/files/2011/05/05-18-11-NWF-MissRiverFloodingReport-Final.pdf

Petrescu, A. M. R., van Beek, L. P. H., van Huissteden, J., Prigent, C., Sachs, T., Corradi, C. A. R., … Dolman, A. J. (2010). Modeling regional to global CH 4 emissions of boreal and arctic wetlands, *24*, 1–12. doi:10.1029/2009GB003610

Pistrika, A., Tsakiris, G., & Nalbantis, I. (2014). Flood Depth-Damage Functions for Built Environment, 553–572. doi:10.1007/s40710-014-0038-2

Portmann, F. T. (2011). *Global estimation of monthly irrigated and rainfed crop areas on a 5 arc-minute grid*. *Frankfurt Hydrology Paper*.

Scawthorn, C., Asce, F., Flores, P., Blais, N., Seligson, H., Tate, E., … Lawrence, M. (2006). HAZUS-MH Flood Loss Estimation Methodology. II. Damage and Loss Assessment, (May). doi:10.1061/(ASCE) 11572-6988(2006)7:2(72)

Scheidegger, A. E. (1968). Horton's Law of Stream Numbers. *Water Resources Research*, *4*(3), 655 – 658.

Severin, G. T., Muller, R. A., Kesel, R. H., & Schaetzl, R. J. (2015). Mississippi River. *Encyclopedia Britannica*. Retrieved June 17, 2015, from http://www.britannica.com/place/Mississippi-River/Hydrology

Smart, E. (2015). Q. How wide is the Mississippi River at Baton Rouge? *East Baton Rouge Parish Library*. Retrieved September 28, 2015, from http://ebrpl.libanswers.com/faq/15308

Sperna Weiland, F. C., van Beek, L. P. H., Kwadijk, J. C. J., & Bierkens, M. F. P. (2010). The ability of a GCM-forced hydrological model to reproduce global discharge variability, 1595–1621. doi:10.5194/hess-14-1595-2010

Tang, Q., Gao, H., Lu, H., & Dennis, P. (2009). Remote sensing : hydrology, *33*(4), 490–509. doi:10.1177/0309133309346650

Trotter, P. S., Johnson, G. A., Ricks, R., & Smits, D. R. (1998). Floods On The Lower Mississippi: An Historical Economic Overview. *NOAA*. Retrieved August 28, 2015, from http://www.srh.noaa.gov/topics/attach/html/ssd98-9.htm

UNISDR. (2015). *Global Assessment Report on Disaster Risk Reduction - Making Development Sustainable: The Future of Disaster Risk Management*. Geneva.

USACE. (1985). *AGDAM - Agricultural Flood Damage Analysis*. Davis, CA, U.S.A.

USACE. (2014a). GIS Center Data Repository. *U.S. Army Corps of Engineers*. Retrieved June 25, 2015, from http://mvp-extstp.mvp.usace.army.mil/gis/

USACE. (2014b). *Mississippi River and Tributaries Project - Levee System Evaluation Report for the National Flood Insurance Program*. Retrieved from http://www.mvd.usace.army.mil/Portals/52/docs/MRC/LeveeSystem/MRT_levee_system_eval_report_for_NFIP.pdf

USACE. (2014c). National Levee Database. *U.S. Army Corps of Engineers*. Retrieved May 24, 2015, from http://nld.usace.army.mil/egis/f?p=471:1:

USDA. (2015a). *Agricultural Prices*. Washington, D.C. Retrieved from http://usda.mannlib.cornell.edu/usda/current/AgriPric/AgriPric-07-30-2015.pdf

USDA. (2015b). Which are the top 10 agricultural producing States? *United States Department of Agriculture - Economic Research Service*. Retrieved September 11, 2015, from http://www.ers.usda.gov/faqs.aspx#10

USGS. (2010). *Forecasting the Effects of Land-Use and Climate Change on Wildlife Communities and Habitats in the Lower Mississippi Valley*. Leetown.

USGS. (2012). HYDRO1k Documentation ReadMe. *U.S. Geological Survey*. Retrieved June 23, 2015, from https://lta.cr.usgs.gov/HYDRO1KReadMe

Van Beek, L. P. H., & Bierkens, M. F. P. (2008). *The Global Hydrological Model PCR-GLOBWB : Conceptualization , Parameterization and Verification*. Utrecht. Retrieved from http://vanbeek.geo.uu.nl/suppinfo/vanbeekbierkens2009.pdf

Van Beek, L. P. H., Wada, Y., & Bierkens, M. F. P. (2011). Global monthly water stress: 1. Water balance and water availability. *Water Resources Research*, *47*(7). doi:10.1029/2010WR009791

Van der Knijff, J., & de Roo, A. (2008). *LISFLOOD - Distributed Water Balance and Flood Simulation Model. Revised User Manual*. Luxembourg.

Vorosmarty, C. J., Fekete, B. M., & Tucker, B. A. (1998). *Global River Discharge, 1807-1991, V[ersion]. 1.1 (RivDIS)*. Oak Ridge, TN, U.S.A. doi:10.3334/ORNLDAAC/199

Wada, Y., Van Beek, L. P. H., & Bierkens, M. F. P. (2012). Nonsustainable groundwater sustaining irrigation: A global assessment. *Water Resources Research*, *48*(1). doi:10.1029/2011WR010562

Wada, Y., van Beek, L. P. H., van Kempen, C. M., Reckman, J. W. T. M., Vasak, S., & Bierkens, M. F. P. (2010). Global depletion of groundwater resources, *37*(July), 1–5. doi:10.1029/2010GL044571

Wada, Y., Wisser, D., & Bierkens, M. F. P. (2014). Global modeling of withdrawal , allocation and consumptive use of surface water and groundwater resources, 15–40. doi:10.5194/esd-5-15-2014

Wesseling, C. G., Karssenberg, D., Burrough, P. A., & Van Deursen, W. P. A. (1996). Integrating dynamic environmental models in GIS: The development of a Dynamic Modelling language. *Transactions in GIS*, *1*(1), 40–48. doi:10.1111/j.1467-9671.1996.tb00032.x

Winsemius, H. C., Van Beek, L. P. H., Jongman, B., Ward, P. J., & Bouwman, a. (2013). A framework for global river flood risk assessments. *Hydrology and Earth System Sciences*, *17*(5), 1871–1892. doi:10.5194/hess-17-1871-2013

World Bank. (2015). GDP (current US$). *The World Bank*. Retrieved June 23, 2015, from http://data.worldbank.org/indicator/NY.GDP.MKTP.CD

WRI. (2015). Aqueduct - Global Flood Analyzer. *World Resources Institute*. Retrieved October 20, 2015, from http://floods.wri.org/#/basin/3/Mississippi - Missouri

APPENDICES

Appendix 1: Discharge and Routing

In PCR-GLOBWB, river discharge is calculated by accumulating and routing specific runoff along the drainage network, by means of the kinematic wave approximation for rivers using variable time stepping (Van Beek & Bierkens, 2008). In Figure 38 a schematization of the routing of the flood wave along the drainage network is shown.

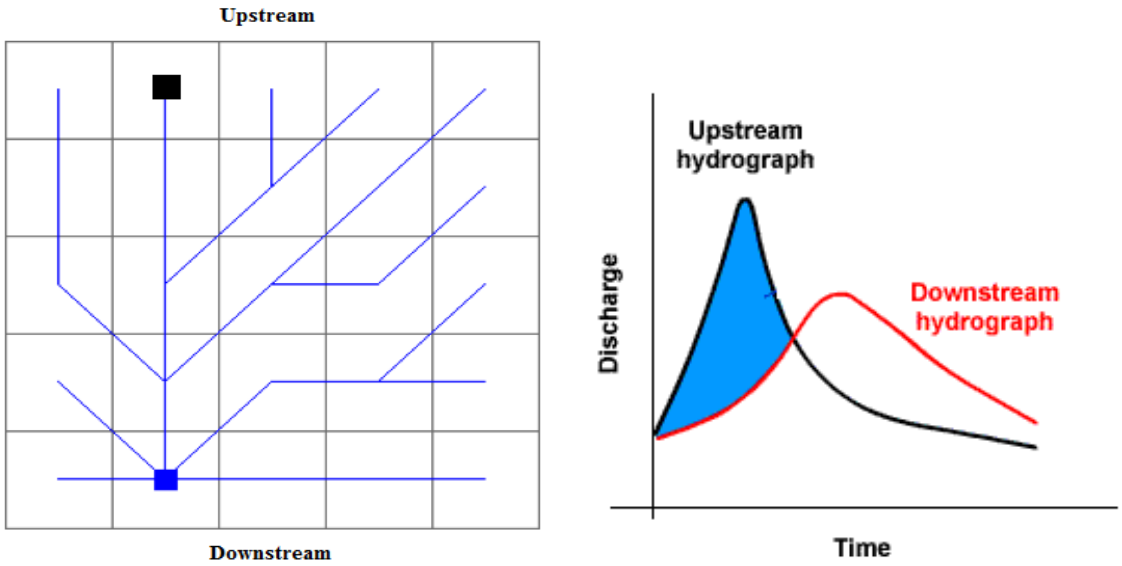

Figure 38. Drainage network (left) and associated hydrographs during peak flow (right) (COMET, 2010)

Kinematic wave approximation

Van Beek & Bierkens (2008) added an explicit numerical scheme for the routing of surface water flow based on the kinematic wave approximation of the Saint-Venant equations. The Saint-Venant equation describes shallow water flow in open channels and therefore use the principles of continuity, Equation 4, and momentum, Equation 5. In differential form, the equations are:

$$Continuity\ Equation: \quad \frac{\partial Q}{\partial x} + \frac{\partial A}{\partial t} - q = 0 \qquad (4)$$

$$Momentum: (1)\left[\frac{1}{A}\frac{\partial Q}{\partial t}\right] + (2)\left[\frac{1}{A}\frac{\partial}{\partial x}\left(\frac{Q^2}{A}\right)\right] + (3)\left[g\frac{\partial y}{\partial x}\right] - \left[g(S_0 - S_f)\right] = 0 \qquad (5)$$

Where A is the channel cross-section [m^2], Q is the streamflow through the channel [m^3/s], x is the length along the channel [m], t is the elapsed time [s], q is the inflow per length of the channel [m^2/s], y is the depth of flow [m], g is the acceleration due to gravity [m/s^2], S_0 is the bed slope of the channel [-] and S_f is the friction slope [-].

Equation 4 and 5 cannot be solved together analytically and therefore simplified cases are used, including the kinematic wave approximation. In the kinematic wave approximation the motion of the wave is considered without the influence of mass and force. Here, the continuity equation is used, while eliminating the three terms, (1) the local acceleration term, (2) the convective acceleration term and (3) the pressure force in the Momentum equation. Therewith, the kinematic wave is represented by Equation 6, where:

$$Momentum\ (Kinematic\ Wave): S_0 = S_f \qquad (6)$$

Chow et al. (1988) describes a finite difference scheme to be able to solve the Saint-Venant equations numerically by using Equation 4 and 5, where the Momentum equation can be expressed in the form:

$$A = \alpha Q^{\beta} \qquad (7)$$

The coefficients α and β are obtained from Manning's equation (Chow et al., 1988), Equation 8.

$$Manning's\ Equation: \quad Q = \frac{R^{\frac{2}{3}}\sqrt{S}}{n} A \qquad (8)$$

Where *R* is the hydraulic radius [m] (*R*=*A*/*P*, where P is the wetted perimeter [m]), *S* is the energy gradient (bed slope) [-] and *n* is Manning's coefficient [$s/m^{\frac{1}{3}}$]. When substituting *R* by *A/P* Equation 4 can be rewritten in terms of A, Equation 9.

$$A = \left(\frac{nP^{\frac{2}{3}}}{\sqrt{S}}\right)^{\frac{3}{5}} Q^{\frac{3}{5}} \qquad (9)$$

Based on Equation 6 α and β can be determined by equation 10 and 11.

$$\alpha = \left(\frac{nP^{\frac{2}{3}}}{S^{\frac{1}{2}}}\right)^{\frac{3}{5}} \qquad (10) \qquad and \qquad \beta = \frac{3}{5} \qquad (11)$$

In PCR-GLOBWB the new discharge in each cell along the channel is calculated based upon the discharge of the previous time step, the lateral inflow and the discharge of upstream cells. The model represents discharge by showing the hydrograph for each cell for the period of interest.

Appendix 2: Value distribution

In the method of determining urban damage nightlight intensity and GDP are combined. The nightlight intensity data is expressed as annual averaged digital number, with values ranging from 0-63. Here, 0 represents total darkness and 63 represents areas with the brightest areas. In Figure 39 and Figure 40 nightlights are shown for the Mississippi watershed in the original resolution, 30 arc-seconds, and the resolution of the model, 30 arc-minutes. The data in Figure 39 is resampled to 30 arc-min (Figure 40), based on bilinear interpolation in ArcGIS (Bresch, 2014).

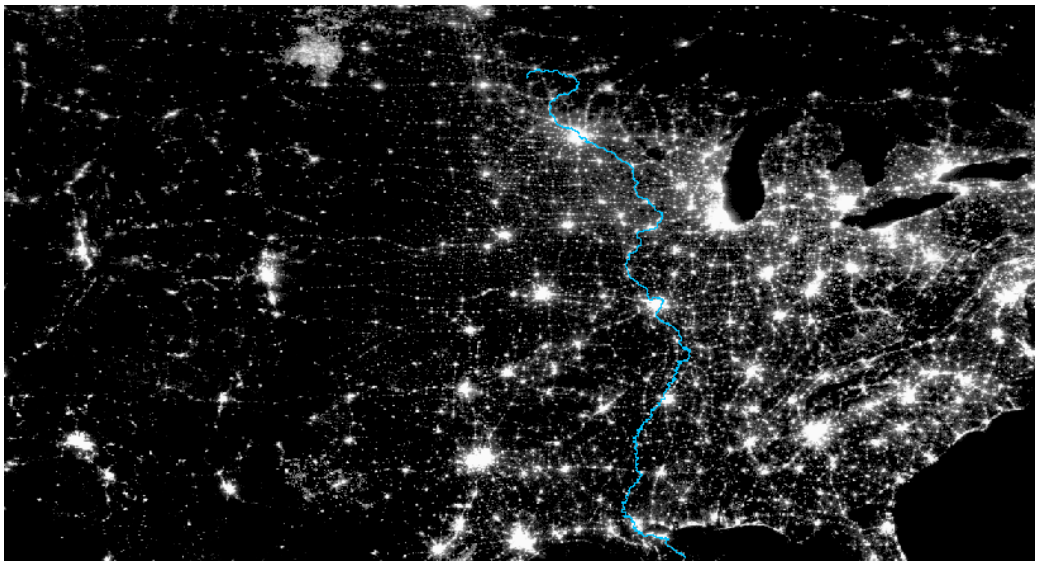

Figure 39. Nightlights in the Mississippi watershed (NOAA, 2014)

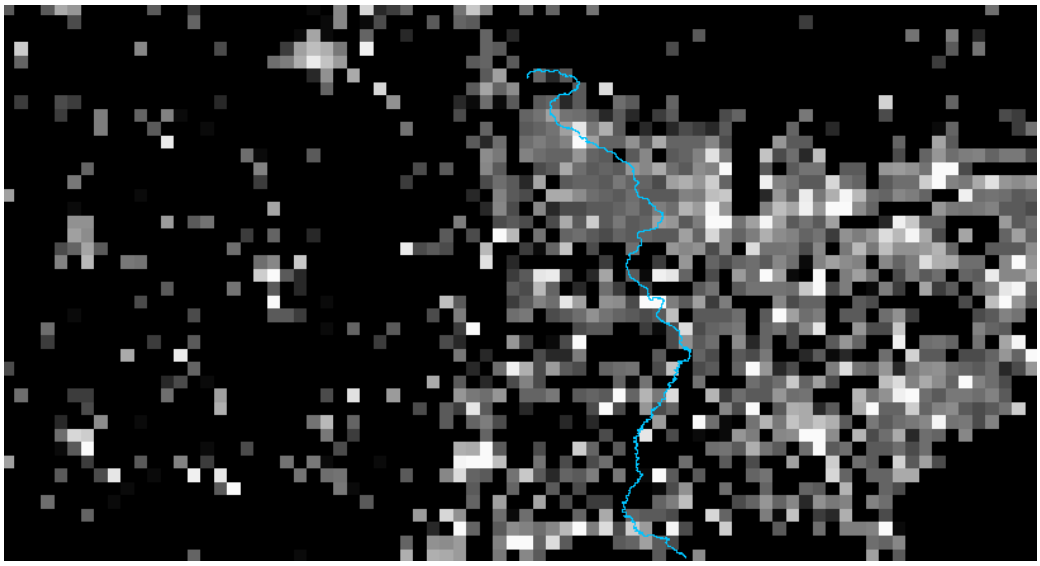

Figure 40. Nightlights in the Mississippi watershed (NOAA, 2014), resampled to 30 arc-minutes in ArcGIS.

Next, the relationship between nightlight intensities and asset values can be described in a linear or non-linear way (Bresch, 2014). In Equation 12 the nonlinear function with the standard nonlinear relationship is given and in

Figure 41 the difference is shown between a linear and nonlinear relationship. With the nonlinear relationship the new final night light value is more rapidly increasing as the original night light value increases.

$$Nonlinear: \qquad y = -0.0817x + 0.0172x^2 \qquad (12)$$

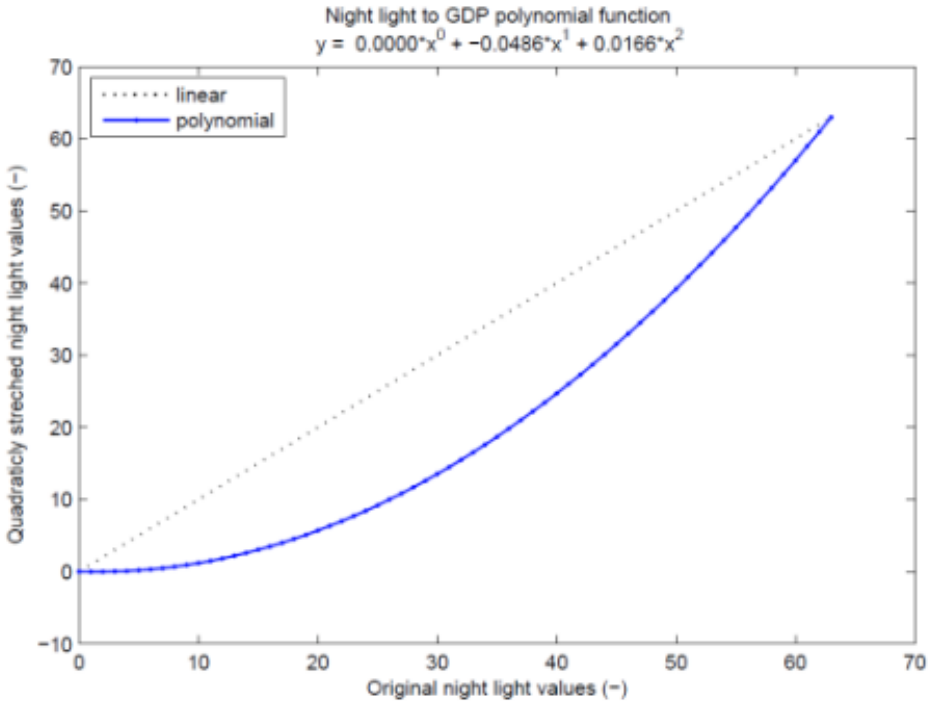

Figure 41. Second order polynomial transformation function to define the relationship between nightlight intensities and asset values (Bresch, 2014)

In Figure 42 and Figure 43 the difference in value distribution is shown for the linear and non-linear relationship.

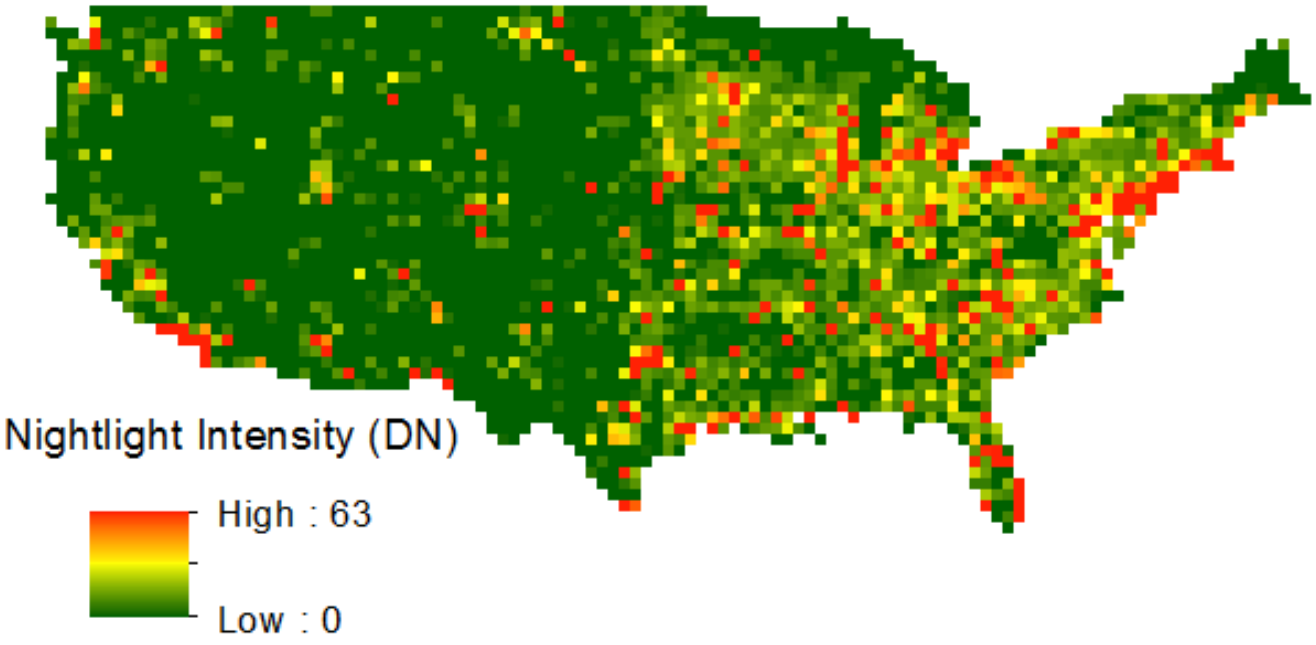

Figure 42. Linear value distribution of nightlights

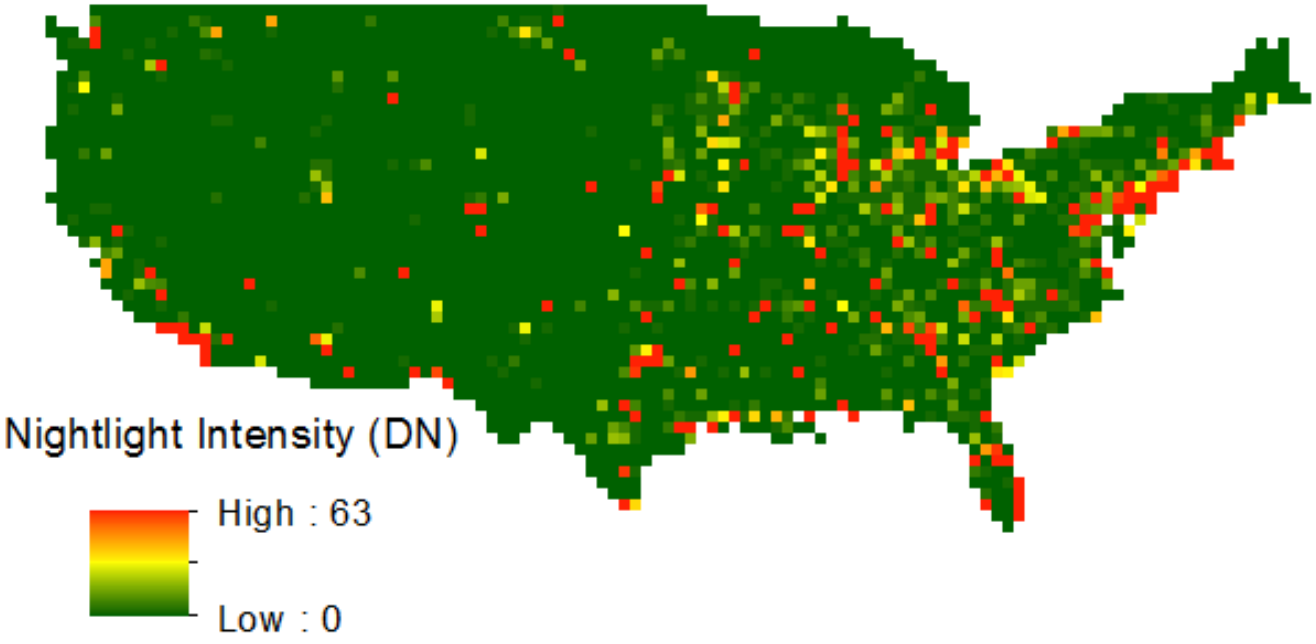

Figure 43. Non-linear value distribution of nightlights

Based on the digital numbers an asset base is created for a specific country, in this study North-America (excluding Alaska and Hawaii), which consist of centroids that have a similar resolution as the hazard event. The sum of all values that are distributed in a country is set to 100, which makes it easy to scale up the values to GDP for a given year. In Figure 44 GDP is shown for the United States in the period between 1980 and 2010.

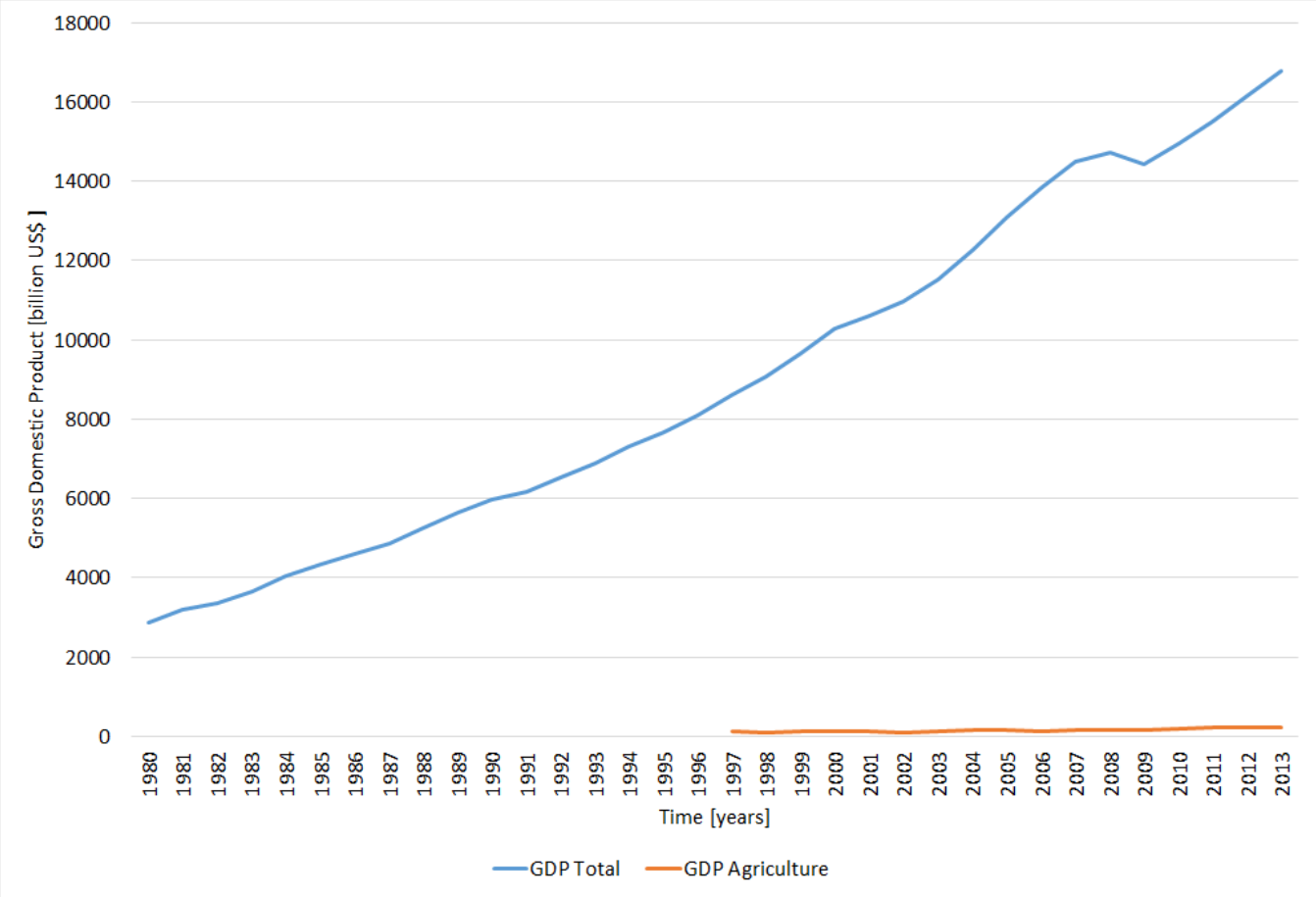

Figure 44. Gross Domestic Product of the United States between 1980 and 2010 (World Bank, 2015)

Appendix 3: Cross-sections to dike heights

- Coordinate system = GCS_WGS_1984
- Cell Size (X, Y) = 30 arc-minutes (In ArcGIS 0.5 degrees)
- Extent of files based on imported maps from PCR-GLOBWB

Step	Program	Toolbox/Action	Comments
1	ArcGIS	Add x, y coordinates	Also includes z coordinates
2	ArcGIS	Feature to points	
3	PCRaster	Streamorder: creates a map where the channel network is classified based on the local drainage direction (ldd) by using the Strahler Stream Order (Scheidegger, 1968). Smallest channels: 1, Largest channel: 5 Create mainchannel.map by only extracting streamorder 4 and 5.	
4	PCRaster	map2asc: converts .map format to .ascii format	
5	ArcGIS	ASCII to Raster	
6	ArcGIS	Raster to polygon (no simplified polygons) Edit: edit polygon based on mainchannel.map from PCRaster	
7	ArcGIS	Clip: Extract cross sections within mainchannel cells	
8	ArcGIS	Edit output step 6: remove all 0 and 0.00001 values to delete wrong cross sections	
9	ArcGIS	Summarize maximum and minimum of cross sections based on cross section number. Add summarized tables to file.	
10	ArcGIS	Remove duplicates: All cross sections consist of several points, but after determining the max and min only one point per cross section is used in further steps.	
11	ArcGIS	Add cell ID's from polygon "mainchannel" to crossection file.	
12	ArcGIS	Summarize average maximum and minimum of cross sections in mainchannel based on id numbers cells	

13	ArcGIS	Add column and determine dike height within cell based on average maximum and average minimum height per cell.	
14	ArcGIS	Point to raster: add dike heights from points to raster for 30 arc-min cells.	
15	ArcGIS	Raster calculator: Interpolate dike heights for all missing cells	Some cells still do not have a dike height
16	ArcGIS	Raster to ascii	
17	PCRaster	Asc2map: converts .ascii format to .map format	
18	PCRaster	Inversedistance: Interpolate for cells without dike height value by using a radius and a max number of cells (closest cells) on which the value is based.	Possible to interpolate first in ArcGIS and then in PCRaster, but also possible to interpolate only in PCRaster.
19		Map is ready to be imported in PCR-GLOBWB	

Appendix 4: Model results – economic damage

4.1 Urban damage – Inundation depth

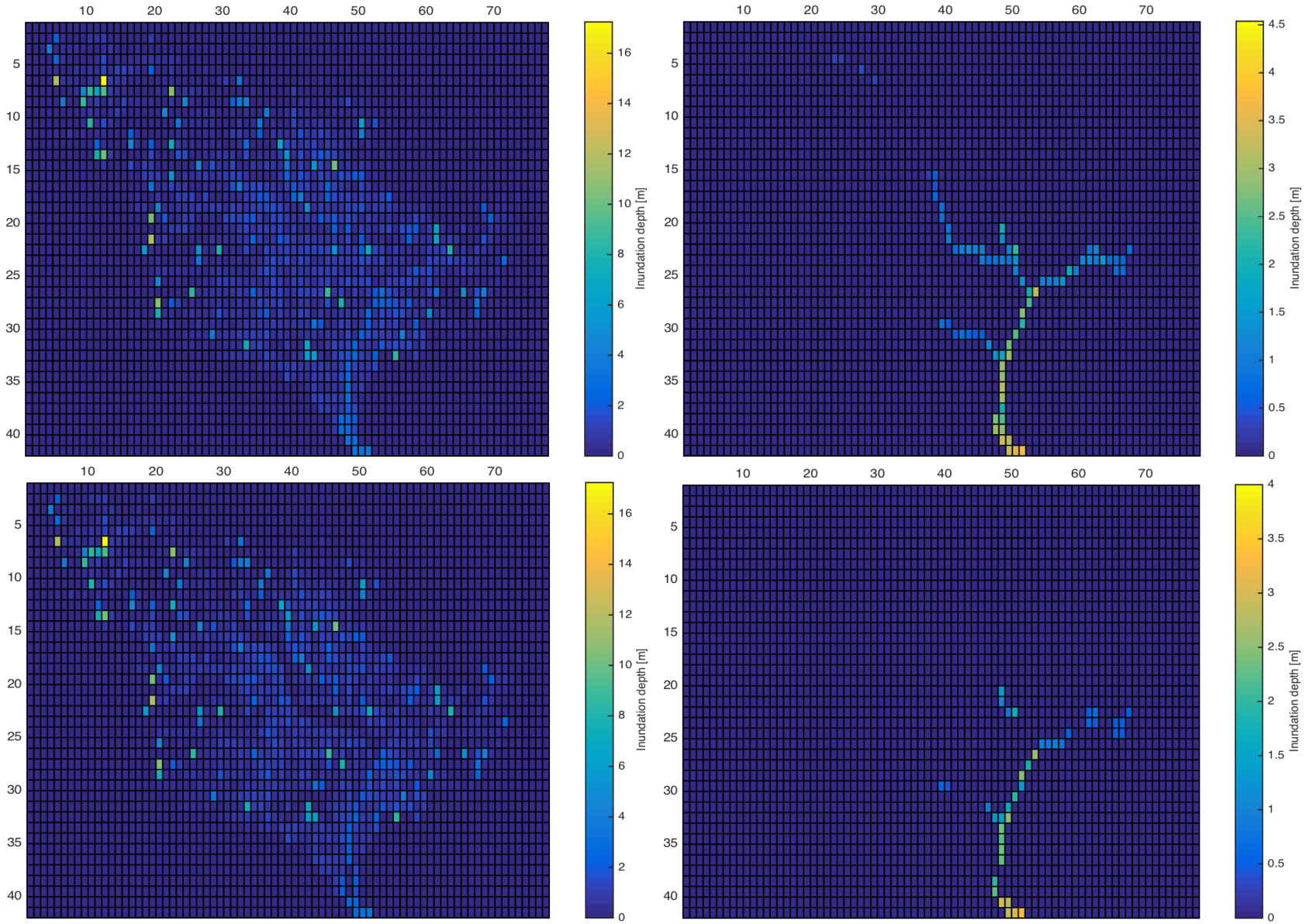

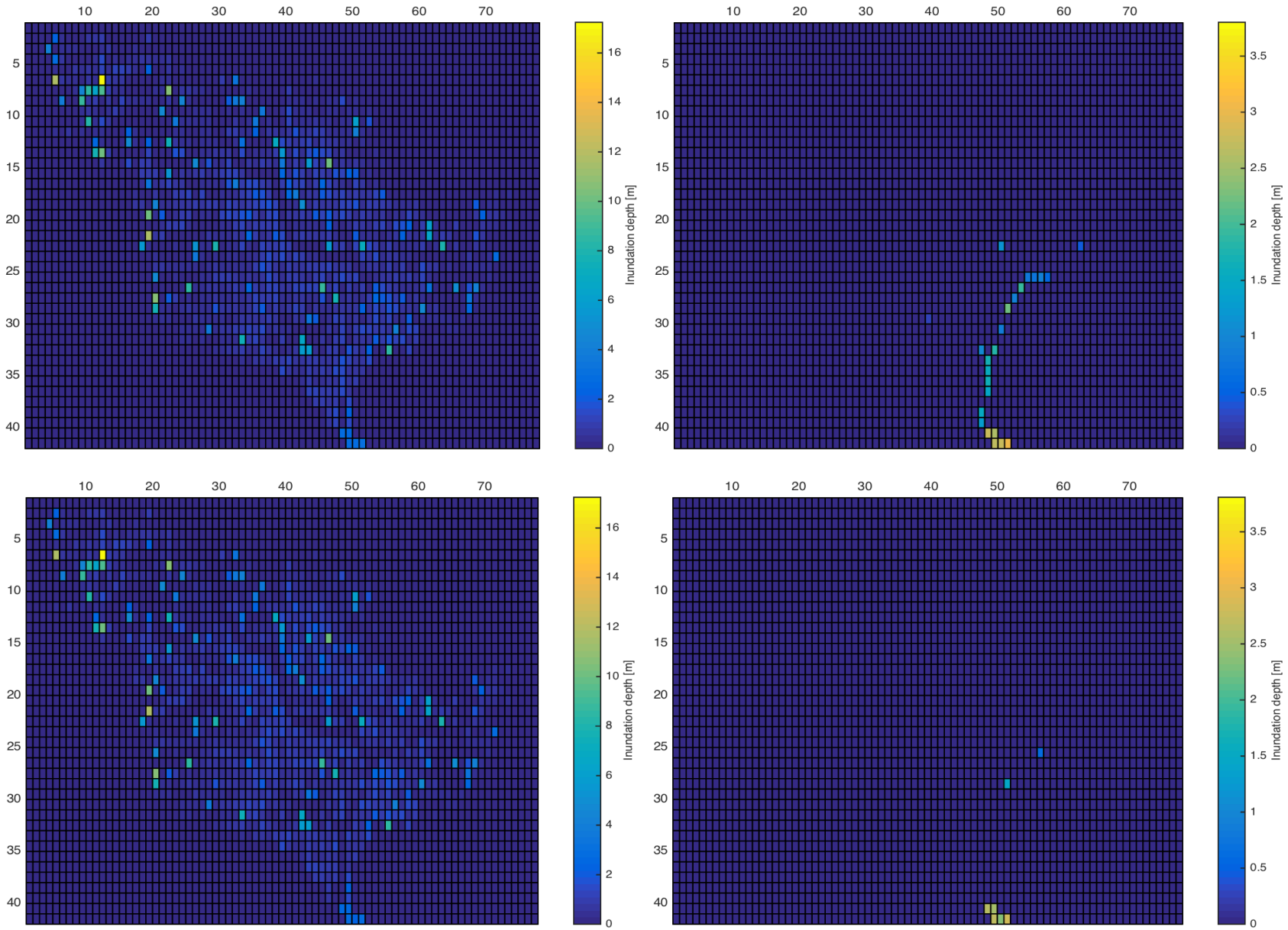

Figure 45. Inundation depths per scenario for the entire watershed (left) and for the main river (right) with a Manning coefficient of 0.10. Scenario 1 (top), scenario 3 (top-middle), scenario 4 (bottom-middle), scenario 5 (bottom).

4.2 Agricultural damage – Duration of flooding

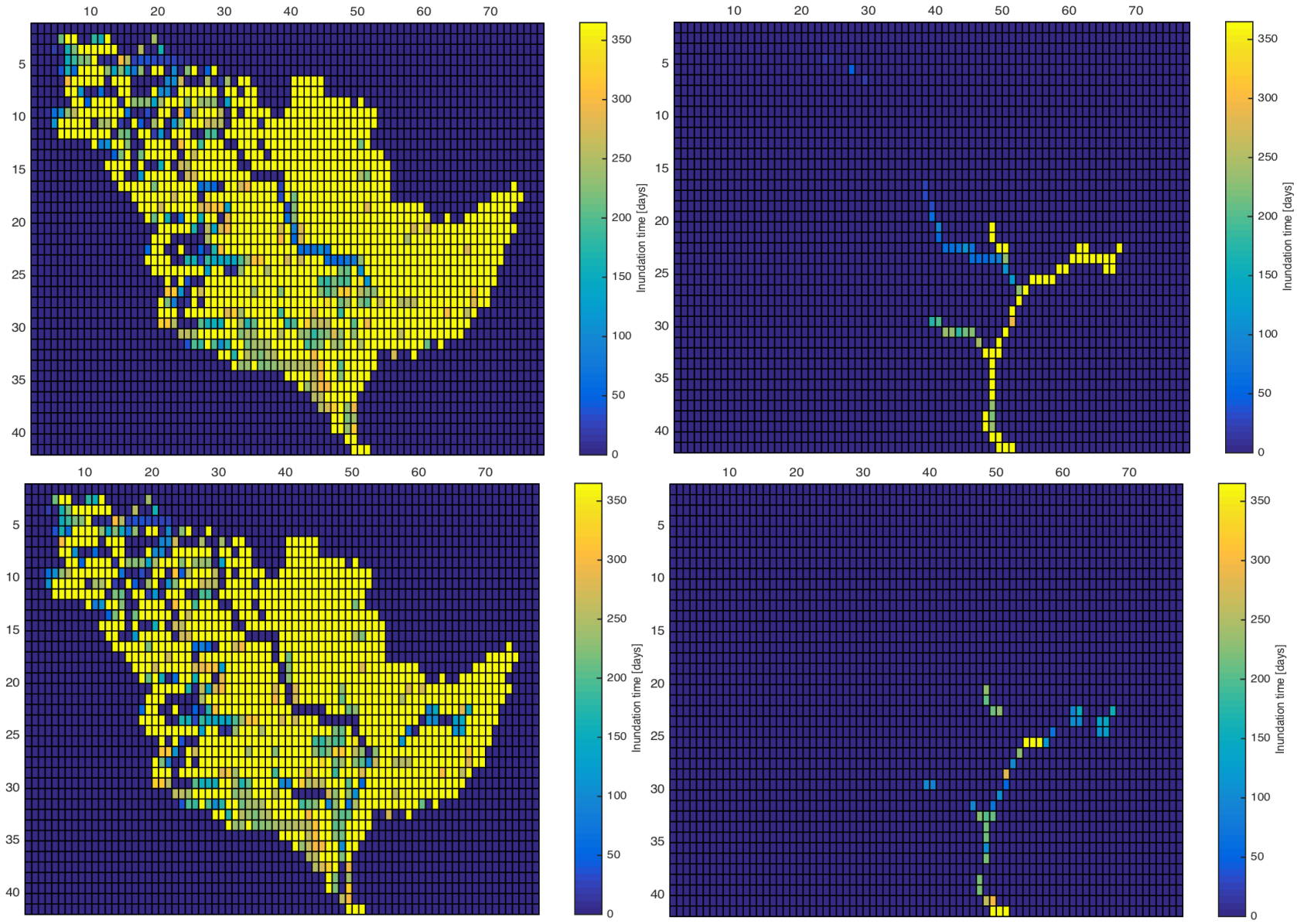

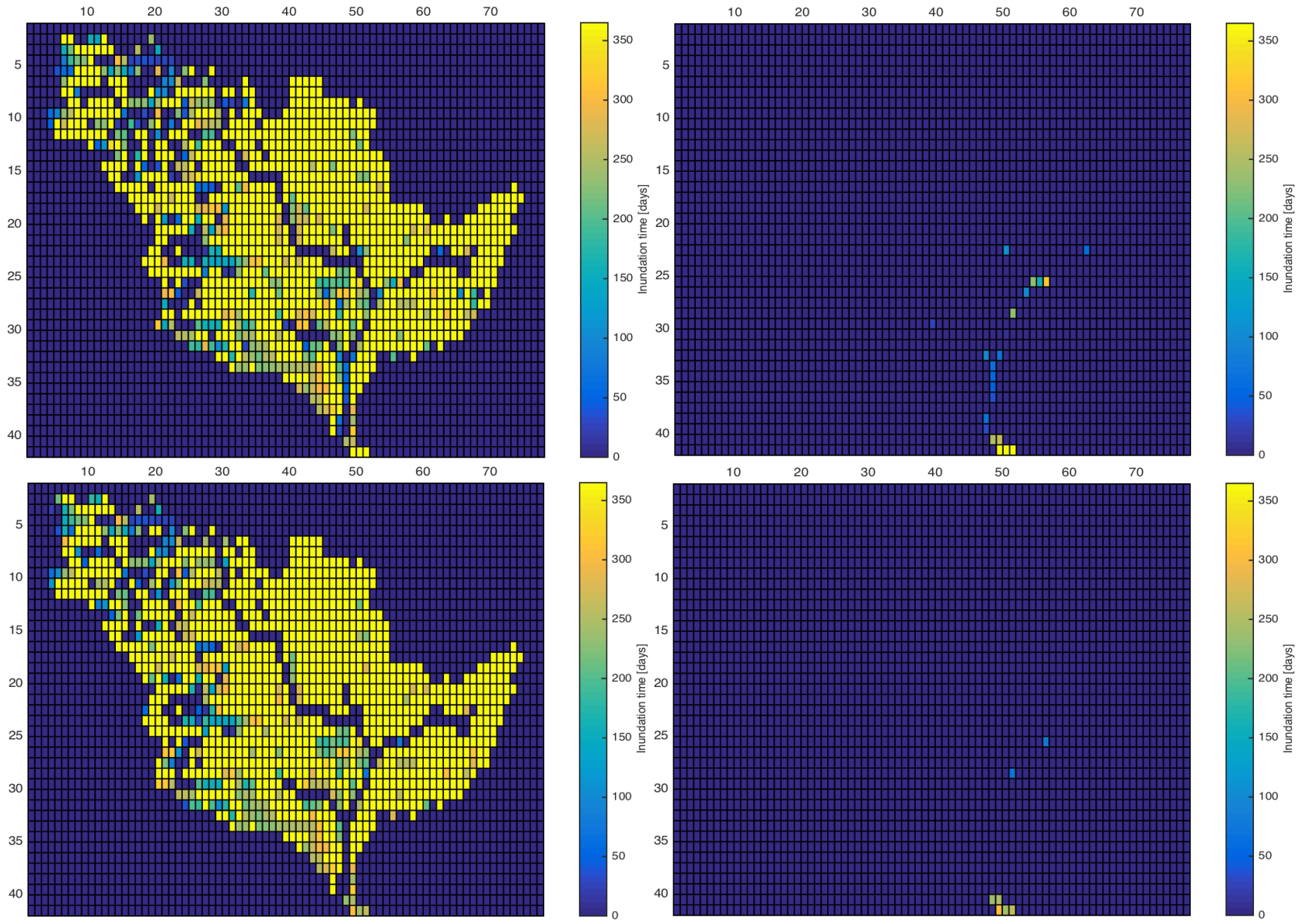

Figure 46. Inundation times per scenario for the entire watershed (left) and for the main river (right) with a Manning coefficient of 0.10. Scenario 1 (top), scenario 3 (top-middle), scenario 4 (bottom-middle), scenario 5 (bottom).